UNIVERSITY OF OKLAHOMA

GRADUATE COLLEGE

SPECTROSCOPIC STUDY OF AMINE SALTS AND POLYAMINE SALT SYSTEMS

A DISSERTATION

SUBMITTED TO THE GRADUATE FACULTY

in partial fulfillment of the requirements for the

Degree of

DOCTOR OF PHILOSOPHY

By

GUINEVERE A. GIFFIN
Norman, Oklahoma
2009

SPECTROSCOPIC STUDY OF AMINE SALTS AND POLYAMINE SALT SYSTEMS

A DISSERTATION APPROVED FOR THE
DEPARTMENT OF CHEMISTRY AND BIOCHEMISTRY

BY

_____
Dr.Roger Frech, Chair

_____
Dr. Daniel Glatzhofer

_____
Dr. Wai Tak Yip

_____
Dr. Charles Rice

_____
Dr. Lance Lobban

ACKNOWLEDGEMENTS

I would like to thank the many people who have helped me along the way in the pursuit of my degree. **Dr. Roger Frech**, my advisor, thank you for the guidance you have given me throughout my tenure at OU and for teaching me how to approach research problems. I hope you thoroughly enjoy your retirement when it comes. **Dr. Daniel Glatzhofer**, thank you and your research group for teaching me about good collaboration and for your help with the more organic portions of my research. **Dr. Wai Tak Yip**, **Dr. Charles Rice**, and **Dr. Lance Lobban**, my other committee members, thank you for the advice you have given me during my time at OU. **Dr. John Moore Furneaux**, thank you for answering my many questions about how instruments work and about how to fix them when they don't. **Dr. Ralph Wheeler**, thank you for recruiting me to come to OU, for working with me in our recent collaboration and for your support. I have to tell you that although I didn't find a softball league to play in while I was here, I did start rowing, a sport I have always wanted to try. **Dr. Scott McKay** at the University of Central Missouri, thank you for being my mentor during my undergrad days and directing me towards physical chemistry and spectroscopy. I might still be making poor attempts at organic synthesis without your candor. **Dr. Renee Cole** at the University of Central Missouri, thank you for your advice and support when I was searching for a graduate school. **Frank Yepez Castillo**, I thoroughly enjoyed our collaboration and our friendship. It was great to have a partner on so many of my projects. The current and former members of the Frech Group:

Rachel Mason, **Allison McCoy**, **Dharshani Nimali Bopege**, **Chris Burba**, **Nathalie Rocher**, **Matt Petrowsky**, **Varuni Seneviratne**, **Shawna York**, **Rebecca Sanders** and **Dilhani Jayathilaka**. Thank you for your friendship, the fun times in the office and working together in the lab. I wouldn't have made it through without you. I wish you all the best with your future endeavors. **Scott Boesch**, thank you for contributions to the amine salt projects. **Dr. Douglas Powell**, you have been very patient in answering all of my crystallography questions. **Dan Bye**, thank you for taking the time to edit my dissertation. **Dr. Janis Paul**, thank you for giving me a job that made my last year graduate school so much easier. **Jean Keil**, thank you for all of your help over the years.

To all my friends and family, both near and far, I know I haven't been the best at keeping in touch, but thank you for being there for me when I needed you. My parents, **Greg and Shirley Giffin**, you have always said there was nothing I couldn't do when I wanted to. Thank you for pushing me to be the best I can and always encouraging me to do all the things that I wanted to do. My siblings, **Bernita, Amanda and Tyrell Giffin**, I am very proud of you for all the things you have accomplished and all you will do in the future. Thank you for being the best you can at everything you do and pushing me to do the same. My grandmother, "**Nani Giffin**", I know I have been gone for a long time, but thank you for always supporting me even though I know you wish I was closer to home. **Uncle Wade and Helen Marie Giffin**, thank you for your support. I always knew that if I needed anything, you would do whatever you could. Finally, **Ariel Balderas**, my boyfriend, thank you for encouraging me to try new things and

meet new people. Also, thank you for just being there on the many days I didn't think I would ever finish and for helping to keep me sane through all the stress involved with of this last phase of earning my PhD.

TABLE OF CONTENTS

LIST OF TABLES

LIST OF FIGURES

ABSTRACT

Fundamental research is a necessary foundation for advanced technological development and application. Progress in improving application-based systems largely depends on understanding the nature of the system. A better understanding of the charge-containing species, their environment and the movement of protons through the system is necessary to improve proton-conducting membranes. This dissertation primarily focuses on investigating the moieties involved in charge transport in polymer electrolytes, in particular proton-containing species.

Vibrational spectroscopy is a particularly useful technique in interpreting the local environment present at heteroatom sites and the conformations along the backbone, and probing hydrogen bonding and coordination of salts. Connecting the vibrational spectrum of a crystal to the known structure of that crystal allows a direct correlation of the observed vibrational signatures to the structure. The power of combining crystal structures and vibrational spectra to interpret hydrogen bonding is strongly emphasized in this dissertation.

Polyamines, polyamine salts and model compounds of these polymeric systems are examined. Poly(alkylethylenimine)s are studied with respect to the effect of the sidechain length. Polymer electrolytes made from these polymers exhibited an unusual hysteresis effect with temperature cycling. Unlike PEO, these PEI-based systems show a decrease in ionic association. Cross-linked polyethylenimine hydrochloride is characterized using both vibrational and nuclear magnetic resonance spectroscopy to

determine the degree of cross-linking and identify the vibrational signatures of the membrane moieties. Amine salt model compounds are studied in both the mid and near infrared regions. The band assignments of these amine model compounds are extended into a polymeric amine salt system. In the secondary amine salt systems, vibrational spectra were correlated with crystal structures and computational results to identify the vibrational modes of the protonated amine heteroatom sites. In a crystal containing several different heteroatom sites, the vibrational signatures of each type of site is identified by comparing portions of the asymmetric unit with simple model compounds.

The degree of intermolecular coupling within the unit cell of a crystal determines the nature of factor group vibrations and can have a dramatic effect on the rule of mutual exclusion. In DMEDA:HX crystals, the rule of mutual exclusion is obeyed to different degrees in various regions of the spectrum. This suggests that the degree of adherence to the rule of mutual exclusion can be correlated to the strength of the intermolecular coupling, particularly when the crystallographic inversion center does not lie on the asymmetric unit.

A significant portion of this dissertation focuses on hydrogen-bonded groups in amine salt systems. The findings reported here can be useful in interpreting the results seen in more complex polyamine and polyamine salt systems. In particular, the ability to identify heteroatom sites from their vibrations signatures is essential. These systems may have an important role as electrolytes in energy applications, specifically proton exchange membrane fuel cells.

CHAPTER I

FUNDAMENTAL RESEARCH AND ITS CONNECTION TO ENERGY OF THE FUTURE

1.1 Energy in the 21st Century

"The world's energy system is at a crossroads. Current global trends in energy supply and consumption are patently unsustainable – environmentally, economically and socially."[1]

Recently, energy has been at the forefront of most national and international debates. This was extremely evident in the last presidential election. During a period of time when oil prices hit an all time high, energy was certainly an issue of importance. Current predictions indicate that oil demand will increase by 1% annually from 2006 to 2030.[1] However, the supply cannot indefinitely meet future demands. One possible solution to this problem is a hydrogen-based energy economy. The Hydrogen Fuel Initiative was introduced in 2003 to work towards commercialization of hydrogen fueled vehicles by 2020. The strategy behind this initiative was to accelerate research and development of hydrogen-based technologies.[2] Aside from the infrastructure and technology needed for production, delivery and storage, an efficient method to convert hydrogen into useable energy is necessary; fuel cells (described in the next section) are a good option. They may be used in a wide variety of applications and have the potential to reduce the emission of greenhouse gases. In terms of the hydrogen-fueled vehicles of the Hydrogen Fuel Initiative, those powered by fuel cells are essentially zero

emission vehicles. However, the emissions from the vehicles alone do not give the full picture. The "wells-to-wheels" emissions must be considered. "Well-to-wheels" considers the total energy usage, starting at the fuel source, moving through hydrogen production to hydrogen consumption.[2] A fuel cell powered hydrogen vehicle could show an approximately 50% reduction of carbon dioxide emissions compared to a gasoline internal combustion engine vehicle.[3] If carbon dioxide sequestration was used during the hydrogen production process, this reduction rises to approximately 95%.[3] Fuel cells typically have higher efficiencies than other conventional methods of energy conversion. Internal combustion engines are only about 20% efficient and conventional power plants are only 33-35% efficient.[2] In comparison, fuel cells can be up to 60% efficient.[2]

1.2 Fuel Cells

Fuel cells are electrochemical devices that combine hydrogen with oxygen to produce electrical energy from chemical energy.[4,5] There are several types of fuel cells, such as solid oxide, alkaline, molten carbonate, phosphoric acid,

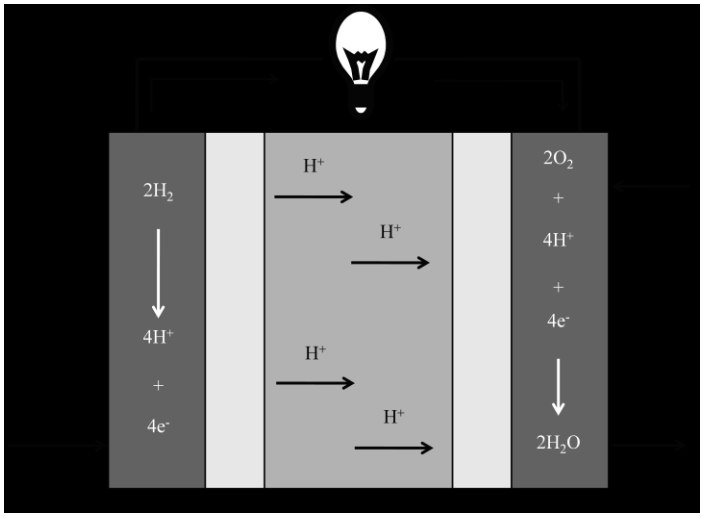

Figure 1.1 – Scheme for a typical PEMFC.

direct methanol or proton exchange membrane fuel cells (PEMFCs). Most of the discussion here will apply to PEMFCs. The scheme for a typical PEMFC is shown in Figure 1.1.[5] This fuel cell has three main components: a cathode, an anode and a proton conducting electrolyte membrane. Catalysts are an integral part of the cathode and the anode. Hydrogen gas is fed into the fuel cell at the anode, where when it comes in contact with the catalyst; the hydrogen gas is broken down into protons and electrons. The electrons are shunted via a current collector to the external circuit, providing the electrical current. The protons move through the polymer electrolyte or proton exchange membrane to a second catalyst layer, which is part of the cathode. At the cathode the protons combine with oxygen to form water and heat. The types of fuel cells differ by the fuel, the composition of the electrode and electrolyte and the charged moiety that is transported through the system. For example, alkaline fuel cells, which use pure hydrogen as fuel, have been used for space applications; solid oxide fuel cells, which are fueled by methane, are primarily used for large scale power generation.[2,5] These fuel cells are both very different from PEMFCs, which are primarily targeted at transportation and back-up power applications.[2,5] There are many problems that must be overcome before fuel cells can be implemented for practical use. In particular, there are many areas that must be addressed with respect to the membrane, such as performance, temperature-related limitations and water management.[6]

1.3 Proton Exchange Membranes

The performance of the proton exchange membrane (PEM) is integral to the

overall function of the fuel cell. There are several properties that a membrane must have in order to have to maximize efficiency, which include: 1) high proton conductivity with minimal resistive losses, 2) low electronic conductivity, 3) mechanical, chemical, thermal and electrochemical stability in various states of hydration, 4) good water management, 5) little crossover of gases from anode and cathode and vice versa, and 6) reasonable cost.[7,8] Several different types of polymer electrolytes[8] have been investigated as potential membranes, such as perfluorosulfonic acids,[9,10] sulfonated poly(arylenes)[11-16] and acid-doped polymer complexes.[17-22] All of these membranes have advantages and disadvantages, but one thing common to all PEMs is that they must have very good proton conductivity. The key to good proton conductivity is proton transport through the membrane. There are two main mechanisms of proton transport that are widely recognized. One mechanism is vehicular transport, where protons are moved through the membrane by a hydronium ion or some other mobile group.[23,24] The other mechanism of transport is the Grotthus, or hopping mechanism, which has also been considered structural diffusion.[24-26] A simplistic view of transport by the Grotthus mechanism involves a proton from a hydronium ion moving or "hopping" to an adjacent neutral water molecule. However, it is likely that protons also are bound to self-assembled clusters of water molecules, such as the Zundel ion ($H_5O_2^+$) or the Eigen ion ($H_9O_4^+$), and protons are moved from one molecule to the next during the dissociation of these clusters.[24,25,27]

1.4 Why Study Amine Salt and Simplified Membrane Systems?

The key to making a proton exchange membrane with a high conductivity is to better understand the mechanism of conductivity, *i.e.* proton transport through the membrane. There have been numerous previous studies on the mechanisms of transport,[23-31] many of which look at methods for modeling these phenomena. This work addresses one of the most basic questions of proton transport, *i.e.* can the proton containing species be identified and can their potential energy environment be deduced from their spectroscopic signatures? Spectroscopy can be a very useful tool in the investigation of PEMs because vibrational modes are sensitive to their molecular environment. However, before complex systems like a functioning PEM can be understood, the proton-containing species and the various components of the membrane itself must be identified. Fundamental studies, such as the one described here, are essential in the understanding of complex phenomena and once the phenomena are better understood, it is easier to improve the functioning system.

1.5 Brief Synopsis of the Dissertation.

The research included in this dissertation results from a number of different, but interrelated, projects. Each project is in the area of fundamental energy research and concerned with the mechanism of charge transport, but each has its own focus. Chapter II focuses on a series of polymer electrolytes that are potentially applicable to rechargeable lithium-ion batteries. Polymer electrolytes based on polyethylene oxide, PEO, have been studied extensively, but they exhibit unacceptably low room

temperature conductivities. The low room temperature conductivities are attributed to their highly crystalline nature at room temperature. Highly crystalline samples inhibit the segmental motion of the polymer, which is primarily responsible for charge transport through the electrolyte. Linear poly(ethylenimine), PEI, is the nitrogen-based structural analog of PEO. PEI also forms semi-crystalline polymer electrolytes at room temperature. However, PEI is a particularly useful polymer matrix because of the chemical versatility of the secondary amine heteroatom site. Specifically, another functional group can be substituted for the hydrogen atom of the amine site. Such a substitution can improve the conductivity by lowering the temperature of the glass transition. Vibrational spectra of the polyethylenimine-based polymer electrolytes are examined, particularly addressing the spectral changes due to the length of the sidechain. In this study, an interesting hysteresis effect seen with temperature cycling is discussed. Chapter III also focuses on polymer electrolytes, but these membranes would have application in PEMFCs. This chapter concentrates on determining both the degree of cross-linking and identifying the spectroscopic signatures of the membrane. Here, nuclear magnetic resonance, infrared and Raman spectroscopic results are combined to characterize this complex system. Chapter IV correlates the vibrational spectra of a number of secondary amine hydrohalide salts to the crystal structures. Computational results complement the vibrational analysis in understanding the various phenomena seen in the spectra. These amine salts are a good model for the polyamine salts and membranes studied in Chapters III and V. Chapter V uses the results of Chapter IV to better characterize the base polymer, polyethylenimine hydrochloride

(PEI·HCl), which was used to make the membranes in Chapter III. In this chapter, the vibrational spectra are correlated to the model compounds investigated in Chapter IV and a previously reported crystal structure.

Chapters III and V make use of model compounds and Chapter IV focuses solely on model compounds. Model compounds can be an invaluable experimental tool in the study of complex systems, particularly polymer electrolytes. At first glance, model compounds are structurally similar to small portions of the larger structure, allowing for conclusions about the complex structure to be drawn based on the results seen in the model. However, this general type of analysis can miss some of the most important uses of model compounds in polymer electrolytes. Model compounds are typically chosen so that the moieties surrounding the heteroatom are similar to those found in the larger structure. This careful selection provides a heteroatom potential energy environment that is similar in both structures, meaning that the interaction of the heteroatom with the charged particles can be more easily studied and the results applied to the extended chain. Additionally, low molecular weight model compounds may form crystals whose structures can be solved using small molecule x-ray methodologies. Crystal structures allow for direct structure property correlations. This approach has been successfully used in the past.[32-36] Finally, in multiple heteroatom model compounds, conformational changes of the backbone can be studied. These occur upon coordination of charged particles with the heteroatom sites. It has been shown previously that the changes in conformation occurring in the small molecules mimic those occurring in the extended polymer chain.[37]

Chapter VI examines a system that includes different kinds of hydrogen-bonded groups within a single unit cell. Each group has a unique spectroscopic signature in both the NH stretching and bending modes. The discovery of this crystal was an unexpected result in a research project focusing on a series of amine hydrohalide salts. Studies involving hydrogen bonding in known structures illustrate another use of model compounds, which can be used to infer the local environment of more complex hydrogen-bonded systems. Chapter VII revisits some of the amine salts examined in Chapter IV, but now is directed towards the near-infrared region of the spectra, allowing the analysis of the overtone and combination spectra. Some of the characteristic group frequencies for the near-infrared region are assigned. These assignments, particularly those of proton-containing species, are essential in order to move into more complex systems, such as functioning fuel cell membranes.

1.6 References

(1) *World Energy Outlook 2008 Executive Summary*; International Energy Agency Paris, 2008.

(2) *Hydrogen and Our Energy Future*; Department of Energy: Washington, D.C., 2007.

(3) *Handbook of Fuel Cells: Fundamentals Technology and Applications*; Vielstich, W.; Lamm, A.; Gasteiger, H. A., Eds.; Wiley: West Sussex, 2003; Vol. 3.

(4) Barbir, E. *PEM Fuel Cells: Theory and Practice*; Elsevier Academic Press: New York, 2005.

(5) Merewether, E. A. *Alternative Sources of Energy - An Introduction to Fuel Cells*; U.S. Geological Survey: Virginia, 2003.

(6) Mehta, V.; Cooper, J. S. *J. Power Sources* **2003**, *114*, 32-53.

(7) Smitha, B.; Sridhar, S.; Khan, A. A. *J. Membr. Sci.* **2005**, *259*, 10-26.

(8) Hickner, M. A.; Ghassemi, H.; Kim, Y. S.; Einsla, B. R.; McGrath, J. E. *Chem. Rev.* **2004**, *104*, 4587-4612.

(9) Basnayake, R.; Peterson, G. R.; Casadonte, D. J., Jr.; Korzeniewski, C. *J. Phys. Chem. B* **2006**, *110*, 23938-23943.

(10) Mauritz, K. A.; Moore, R. B. *Chem. Rev.* **2004**, *104*, 4535-4585.

(11) Carretta, N.; Tricoli, V.; Picchioni, F. *J. Membr. Sci.* **2000**, *166*, 189-197.

(12) Cho, C. G.; Kim, Y. S.; Yu, X.; Hill, M.; McGrath, J. E. *J. Polym. Sci., Part A: Polym. Chem.* **2006**, *44*, 6007-6014.

(13) Hofmann, M. A.; Ambler, C. M.; Maher, A. E.; Chalkova, E.; Zhou, X. Y.; Lvov, S. N.; Allcock, H. R. *Macromolecules* **2002**, *35*, 6490-6493.

(14) Lee, H.-S.; Badami, A. S.; Roy, A.; McGrath, J. E. *J. Polym. Sci., Part A: Polym. Chem.* **2007**, *45*, 4879-4890.

(15) Sankir, M.; Kim, Y. S.; Pivovar, B. S.; McGrath, J. E. *J. Membr. Sci.* **2007**, *299*, 8-18.

(16) Yang, Y.; Holdcroft, S. *Fuel Cells* **2005**, *5*, 171-186.

(17) Asensio, J. A.; Borros, S.; Gomez-Romero, P. *J. Electrochem. Soc.* **2004**, *151*, A304-A310.

(18) Bouchet, R.; Siebert, E. *Solid State Ionics* **1999**, *118*, 287-299.

(19) Kim, H.-J.; Lim, T.-H. *J. Ind. Eng. Chem.* **2004**, *10*, 1081-1085.

(20) Lobato, J.; Canizares, P.; Rodrigo, M. A.; Linares, J. J.; Aguilar, J. A. *J. Membr. Sci.* **2007**, *306*, 47-55.

(21) Lobato, J.; Canizares, P.; Rodrigo, M. A.; Linares, J. J.; Manjavacas, G. *J. Membr. Sci.* **2006**, *280*, 351-362.

(22) Xiao, L.; Zhang, H.; Jana, T.; Scanlon, E.; Chen, R.; Choe, E. W.; Ramanathan, L. S.; Yu, S.; Benicewicz, B. C. *Fuel Cells* **2005**, *5*, 287-295.

(23) Kreuer, K.-D.; Rabenau, A.; Weppner, W. *Angew. Chem. Int. Ed.* **1982**, *21*, 208-209.

(24) Eikerling, M.; Kornyshev, A. A.; Kuznetsov, A. M.; Ulstrup, J.; Walbran, S. *J. Phys. Chem. B* **2001**, *105*, 3646-3662.

(25) Weber, A. Z.; Newman, J. In *Advances in Fuel Cells*; Zhao, T. S., Kreuer, K.-D., Nguyen, T. V., Eds.; Elsevier: New York, 2007.

(26) Fimrite, J.; Struchtrup, H.; Djilali, N. *J. Electrochem. Soc.* **2005**, *152*, A1804-A1814.

(27) Spohr, E.; Commer, P.; Kornyshev, A. A. *J. Phys. Chem. B* **2002**, *106*, 10560-10569.

(28) Thampan, T.; Malhotra, S.; Tang, H.; Dattaa, R. *J. Electrochem. Soc.* **2000**, *147*, 3242-3250.

(29) Kreuer, K. D. *Solid State Ionics* **2000**, *136*, 149-160.

(30) Commer, P.; Hartnig, C.; Seeliger, D.; Spohr, E. *Mol. Sim.* **2004**, *30*, 755 - 763.

(31) Elliott, J. A.; Paddison, S. J. *PCCP* **2007**, *9*, 2602-2618.

(32) Boesch, S. E.; York, S. S.; Frech, R.; Wheeler, R. A. *PhysChemComm* **2001**.

(33) Rocher, N. M.; Frech, R.; Khan, M. *J. Phys. Chem. B* **2005**, *109*, 20697-20706.

(34) Sanders, R. A.; Frech, R.; Khan, M. A. *J. Phys. Chem. B* **2003**, *107*, 8310-8315.

(35) Sanders, R. A.; Frech, R.; Khan, M. A. *J. Phys. Chem. B* **2004**, *108*, 12729-12735.

(36) York, S. S.; Boesch, S. E.; Wheeler, R. A.; Frech, R. *PhysChemComm* **2002**, *5*, 99-111.

(37) Rhodes, C. P.; Frech, R. *Macromolecules* **2001**, *34*, 2660-2666.

CHAPTER II

SPECTROSCOPIC INVESTIGATION OF POLYMER ELECTROLYTES BASED ON POLY(N-METHYLETHYLENIMINE), POLY(N-ETHYLETHYLENIMINE), AND POLY(N-BUTYLETHYLENIMINE)

Portions of this chapter have appeared in R. Frech, G. A. Giffin, F. Yepez Castillo, D. T. Glatzhofer, J. Eisenblätter, "Spectroscopic studies of polymer electrolytes based on poly(N-ethylethylenimine) and poly(N-methylethylenimine)", *Electrochim. Acta* **50(19)**, 3963-3968 (2005).

2.1 Introduction

Polymer electrolytes based on polyethylene oxide have been studied extensively for application in rechargeable batteries. However, these electrolytes exhibit unacceptably low room temperature conductivities, primarily due to their crystalline nature at room temperature. Linear poly(ethylenimine), LPEI, the nitrogen-based structural analog, is a useful polymer matrix because the hydrogen atom on the secondary amine can be substituted by some other functional group, thus improving the conductivity by lowering the glass transition temperature. The substitution of a methyl group to form poly(N-methylethylenimine), PMEI, on the nitrogen atoms reduces the crystallinity, as is evident in the depression of the glass transition, T_g, from LPEI (T_g = -23˚C)[1] to PMEI (T_g = -91˚C)[2]. The elimination of the hydrogen-bonding network in

LPEI primarily accounts for the decrease in T_g. The synthesis of poly(N-ethylethylenimine), PEEI, and poly(N-butylethylenimine), PBEI, allows for an evaluation of the effect of alkyl side chain length on the thermal and spectroscopic properties of the N-alkyl substituted members of the ethylenimine-based family of polymer electrolytes.

2.2 Experimental Methods

2.2.1 Polymer Synthesis

Linear PMEI[2,3] and PEEI[4] were prepared as previously reported. The resulting polymers had an average molecular weight of about 115,000 and 142,000 Da, respectively. Linear PBEI was prepared following the same method as PEEI, except butanal was substituted for acetaldehyde in the first step of the reaction. The average molecular weight of PBEI was about 198,000 Da. All of these polymers were made by Frank Yepez Castillo, of Dr. Daniel T. Glatzhofer's group.

2.2.1 Preparation of Polymer Electrolytes

Lithium trifluoromethane sulfonate, $LiCF_3SO_3$, described here as lithium triflate, was obtained from Aldrich and dried under vacuum for at 120 °C for 48 hours. Polymer electrolytes were prepared by dissolving weighed amounts of lithium triflate and the host polymer in dry methanol. The solutions were stirred for approximately 12 hours before being cast as films. All sample preparation and manipulation steps were carried out in a dry argon glove box ($\leq$ 1 ppm H_2O). Sample compositions are reported

as a nitrogen:cation molar ratio.

2.2.3 Differential Scanning Calorimetry

Thermal data were measured with a Mettler DSC 820 calorimeter. Samples between 20 and 25 mg were sealed in a 40 μL aluminum pan, and data were collected under a dry nitrogen purge. The samples were cycled from 25°C to 150°C in the first heating cycle to evaporate any residual methanol from the polymer electrolyte preparation. The samples were then cycled from -150°C to 50°C three times. All heating and cooling rates were 5°C/min. Data were collected during the heating and cooling stages. The glass transition temperatures were remarkably consistent in all three cycles: *e.g.* for neat PEEI T_g = -80°C (cycle 1), -80°C (cycle 2), -80°C (cycle 3).

2.2.4 FTIR Spectroscopy

FTIR spectra were collected on a Bruker IFS66V system under vacuum at a 1 wavenumber spectral resolution. Samples were cast from solution directly onto zinc selenide windows and the solvent was allowed to evaporate for at least 6 hours. The removal of solvent was confirmed by IR spectroscopy. Temperature dependent spectra were collected at 10°C intervals and the samples were heated at approximately 10°C/hour. The samples were cooled to room temperature between each heating cycle where they remained for 14 hours. Two-dimensional correlation spectra were obtained from processing the temperature dependent data using OPUS software. Dr. Christopher

Burba, former member of Dr. Frech's group and currently at Northeastern State University, helped with the processing of this data.

2.3 Results and Discussion

2.3.1 Glass Transition Temperatures (T_g)

Glass transitions are reported for PMEI, PEEI and PBEI polymers and $LiCF_3SO_3$ polymer-salt complexes in Table 2.1. There was no evidence for melting transitions in any of the samples. The glass transition temperatures are reported as midpoints of the thermal event. It should be noted that slightly higher values were reported in a previous study for PMEI:$LiCF_3SO_3$ polymer-salt complexes.[2] In all polymer systems the T_g increases as the salt concentration increases. This occurs because the segmental motion of the polymer is reduced as lithium ions coordinate to the polymer backbone. The T_g also increases as the length of the alkyl side chain increases. This could be accounted for by decreased main chain mobility. Chains with low energy barriers to bond rotation have low T_gs. Bulky groups that are present in either the backbone or the sidechain provide a steric hindrance to rotation and therefore result in an increased T_g.[5] All spectroscopic measurements were made at temperatures well above the glass transition temperature.

Table 2.1 – Glass transition temperature (ºC) of PMEI, PEEI and PBEI polymer electrolytes. Composition represents N:Li ratio.

Composition	***PMEI***	***PEEI***	***PBEI***
Pure	-93	-80	-50
20:1	-79	-77	-44
10:1	-60	-41	-18
5:1	-14	-4	5

2.3.2 Room Temperature Vibrational Spectroscopy

The three polymers studied here can be used to show changes in the system, particularly in the backbone and ionic association regions, as the side chain length increases. Figure 2.1 shows spectra of the polymers and polymer complexes from 1000 to 1140 cm^{-1}. Peak frequencies and mode assignments are found in Table 2. This region in the pure polymer contains many mixed modes, with contributions from CH_3 wagging, CH_2 twisting and rocking, and CC and CN stretching motions. These mode contributions were determined using computational results obtained for PMEI and model compounds.[2,6,7] There are two prominent bands in pure PMEI at 1030 and 1117 cm^{-1}. These correspond to bands at 1058 and 1098 cm^{-1} in PEEI and 1084 and 1133 cm^{-1} in PBEI. These bands contain contributions from both the side chains and the backbone. The changes in the peak frequencies are accounted for by the additional CH_2 groups found in the sidechains of PEEI and PBEI, which couple with the CH_2 groups in the backbone. There is a distinct and significant shift in the 1117 cm^{-1} band to 1097 cm^{-1} upon coordination with the Li^+ cation in the PMEI. A similar type of shift is not

seen in the PEEI and PBEI complexes. This trend could perhaps be accounted for by the additional electron-donating ability of the longer sidechains. Upon coordination, some electron density located on the nitrogen atom is drawn into the coordinative bond with the lithium cation. This would result in electron density being pulled from both the backbone and the sidechain. The longer sidechain could allow less electron density to be pulled from the backbone, therefore resulting in a smaller shift. Unlike the backbone and sidechain bands, which are affected differently by coordination in each system, the intensity of the symmetric SO_3 stretching frequency, $\nu_s(SO_3)$, from the triflate anion at 1040 cm^{-1} increases as the salt concentration increases. At the highest salt concentration, the 5:1 spectra, the symmetric SO_3 stretching band is the most prominent feature in the spectra of all three electrolyte systems, as seen in Figure 2.1.

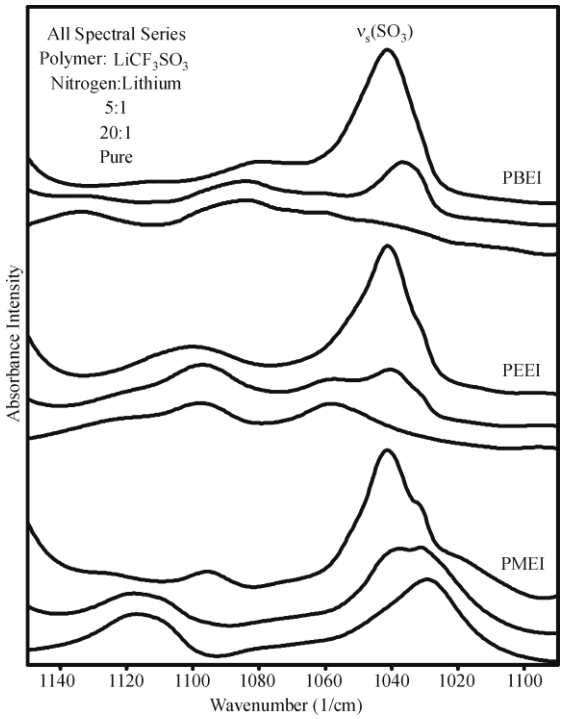

Figure 2.1 – Infrared spectra of PMEI, PEEI, and PBEI and their respective with $LiCF_3SO_3$ (N:Li = 20:1 and 5:1). Spectral region 1140 to 1000 cm^{-1}.

Figure 2.2 shows spectra of the same polymer series over the region from 1000 to 700 cm^{-1}. Bands in this region of the spectrum contain contributions primarily from

Table 2.2 – Vibrational frequencies (cm^{-1}) of PMEI, PEEI, and PBEI and 5:1 complexes of these polymers with LiTf. (sh) = shoulder. (br) = broad.

Assignment	PMEI		PEEI		PBEI	
	Pure	5:1 LiTf	Pure	5:1 LiTf	Pure	5:1 LiTf
Polymer Bands						
$\rho(CH_2)$					733	735
$\rho(CH_2)$, ν(C-N)	771(sh), 787	782	763, 790	790	769, 795	797
$\rho(CH_2)$	807(sh)	804	803	806		
$\rho(CH_2)$, ν(C-N)		825, 845	842			
ν(C-N)	866, 893	869			881, 897	881(sh), 900
$\rho(CH_2)$, ν(C-C)		903		913		
$\rho(CH_2)$, ν(C-N)	940	938, 948			943	949
$\rho(CH_2)$		983	970, 989, 996	977, 997	974	
$\rho(CH_2)$, ν(C-N), $\omega(CH_3)$	1030	1016(sh), 1032(sh)				
$\rho(CH_2)$, ν(C-N), $\omega(CH_3)$, ν(C-C)			1058		1061	
$\rho(CH_2)$, ν(C-C)	1075(sh)				1084	1080
$\omega(CH_3)$		1097	1098	1100		
$\tau(CH_2)$, ν(C-N), $\omega(CH_3)$, $\rho(CH_2)$	1117		1121		1133	
$\tau(CH_2)$, $\omega(CH_3)$	1149(sh)	1127(sh)	1166		1160(sh)	
$\omega(CH_3)$						
$\tau(CH_2)$, $\omega(CH_3)$	1231, 1255(sh)		1201, 1249		1215, 1263(sh), 1272	
$\tau(CH_2)$	1294		1293		1303	
$\omega(CH_2)$	1332(sh), 1357, 1364	1356, 1363(s)	1332, 1348, 1369, 1382	1352, 1379	1338, 1361, 1377	1338, 1364, 1337
$\delta_s(CH_3)$	1422	1431			1436(sh)	1436(sh),
$\delta_{as}(CH_3)$	1458(sh), 1465	1458(sh), 1470	1453(sh), 1466	1455(sh), 1470	1460(br)	1448, 1464
ν(C-H)	2718(sh), 2771, 2803, 2839, 2949, 2975(sh)	2783(sh), 2813, 2852, 2963	2725(sh), 2752(sh), 2809, 2870, 2931, 2966	2725(sh), 2829, 2849(sh), 2871(sh), 2936, 2969	2744(sh), 2808, 2861(sh), 2871, 2930, 2956	2813, 2862, 2871, 2932, 2958
Triflate Bands						
$\delta_s(SO_3)$		639		640		640
$\delta_s(CF_3)$		758		758		762
$\nu_s(SO_3)$		1040		1041, 1032(sh)		1041
$\nu_{as}(CF_3)$		1161		1164		1170
$\nu_s(CF_3)$		1227		1227		1229
$\nu_{as}(SO_3)$		1255, 1299		1251, 1302		1252, 1297

CN stretching and CH_2 rocking motions.[2,6,7] The most striking difference between the three different polymers is the presence of the band at 733 cm^{-1} in PBEI. The butyl side chain in PBEI contains three methylene units, which when coupled would result in a strong CH_2 rocking band. This band is not present in PMEI. There is a weak feature present in this region in PEEI; however, the intensity is low, most likely because there is only a single CH_2 in the side chain of PEEI. More methylene units coupled together do not always result in a larger intensity. The intensity of a band depends on the manner in which the derivatives of the dipole moments of each coupled mode add together. If they add constructively, then the band will have a larger intensity. This appears to be the case with the 766 cm^{-1} band.

All three polymers have a broad band or group of bands around 790 cm^{-1}. These bands are particularly sensitive to Li^+ ion coordination as is shown by the shifts that occur in these bands with increasing salt concentration. In both PMEI:$LiCF_3SO_3$ and PEEI:$LiCF_3SO_3$, the CF_3 symmetric deformation, $\delta_3(CF_3)$, is found at 758 cm^{-1}. In comparison, this band is found in PBEI as a broad band with a lower frequency

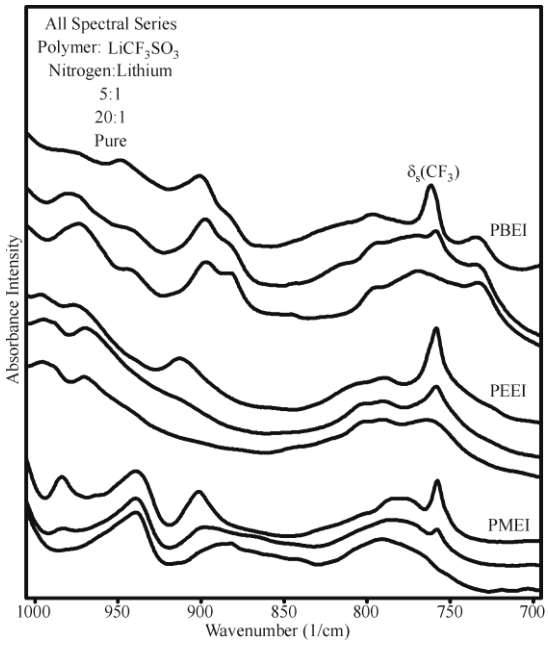

Figure 2.2 – Infrared spectra of PMEI, PEEI, and PBEI and their respective complexes with $LiCF_3SO_3$ (N:Li = 20:1 and 5:1). Spectral region 1000 to 700 cm^{-1}.

shoulder and a band center at 762 cm^{-1}. The $\delta_s(CF_3)$ frequency is sensitive to the degree of ionic association of the triflate ion. Bands at 753, 758 and 762 cm^{-1} have been assigned to "free" ions, contact ion pairs and aggregates, respectively.[8] The band frequency and shape of PBEI would suggest that both contact ion pairs and aggregates exist in the 5:1 PBEI:$LiCF_3SO_3$ system. In comparison, contact ion pairs exist as the predominant species in both PMEI and PEEI polymer:$LiCF_3SO_3$ complexes.

2.3.3 Temperature Dependent Vibrational Spectroscopy

A very unexpected and interesting hysteresis effect was seen upon heating 10:1 PMEI:$LiCF_3SO_3$ and PEEI:$LiCF_3SO_3$ complexes. Figure 2.3 shows the effects of successive heating and cooling cycles applied to the PEEI system. During the first cycle, the intensity of the band at 1040 cm^{-1} decreases while the intensity of the 1032 cm^{-1} increases. Both of these bands are assigned to the symmetric stretching motion of the triflate SO_3, $\nu_s(SO_3)$, but they differ in the degree of ionic

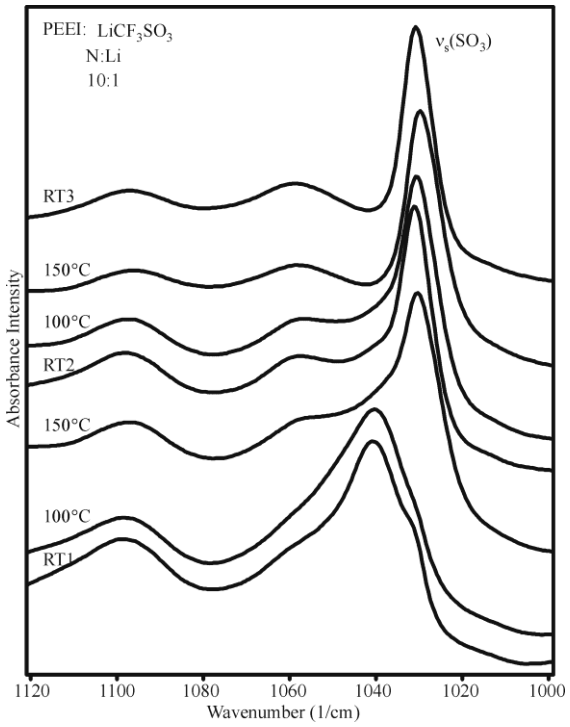

Figure 2.3 – Temperature-dependent spectra of 10:1 PEEI:$LiCF_3SO_3$ complex. RT1 in the initial room temperature spectrum, RT2 is the spectrum after the first heating cycle to 150 ºC and cooling, RT3 is the spectrum after the second heating cycle to 150 ºC and cooling.

association. The 1040 cm^{-1} band is assigned to the contact ion pair and the 1032 cm^{-1} band to the "free" triflate ion.[8,9] With this decrease in ionic association, *i.e.* contact ion pair to "free" ion, it is interesting to note that none of the polymer bands show intensity changes or frequency shifts with the temperature cycling. This trend is surprising because changes in ionic association are usually accompanied by changes in some of the polymer bands containing contributions from the motion of the heteroatom that is coordinated to the cation.[10,11] It would appear that there is an increase in the intensity of the 1058 cm^{-1} band in the PEEI:$LiCF_3SO_3$. However, this apparent intensity increase is really the result of the triflate ion's shift to lower frequency. In the RT1 spectrum in Figure 2.3, the 1058 cm^{-1} band can be seen as a high frequency shoulder on the multi-structured 1040 cm^{-1} feature. However, as the 1040 cm^{-1} band decreases in intensity, the PEEI band is uncovered and easily discernable. The intensity of the "free" triflate band at 1032 cm^{-1}, which increased during the first heating cycle, is maintained through the second heating and cooling cycle. It is possible that the system was not given sufficient time at room temperature to allow the system to come back to thermodynamic equilibrium and the ionic association to shift back to contact ion pairs. However, the PMEI:$LiCF_3SO_3$ system was remeasured after remaining at room temperature for 7 weeks. This spectrum showed no discernible change, implying that triflate ions remained as "free" ions.

This shift from contact ion pairs to "free" ions with increased temperature is quite unexpected in polymer electrolyte systems. In poly(propylene oxide) and poly(ethylene oxide) systems, the opposite trend is observed,[12-14] and in some

poly(propylene oxide) electrolyte systems the salt has even been seen to precipitate out with increased temperature.[4,15] The antisymmetric stretching triflate band, $\nu_{as}(SO_3)$, can also be used to confirm the shift from a triflate environment of contact ion pair to "free" ion. This band, shown in Figure 2.4, is a doubly degenerate mode. In the initial room temperature measurement, RT1, the degree of ionic association is sufficient for the degeneracy of this band to be broken and two prominent features are seen at 1231 and 1300 cm^{-1}, a separation of 69 cm^{-1}. As the sample is cycled, the splitting between the two bands decreases. After the first heating and cooling cycle, the bands now appear at 1259 and 1276 cm^{-1}, a 17 cm^{-1} split. In this second room temperature spectrum, there remains a high frequency shoulder on the 1276 cm^{-1} band, but this feature disappears after the next heating and cooling cycle. After the final cycle, the separation has decreased to only 14 cm^{-1}, with the band peaks at 1262 and 1276 cm^{-1}. This decrease in the separation between this degenerate mode implicates a decrease in the ionic association between the cation and the anion, supporting the shift to "free" triflate anions seen in the $\nu_s(SO_3)$ band. Additionally, the separation in the

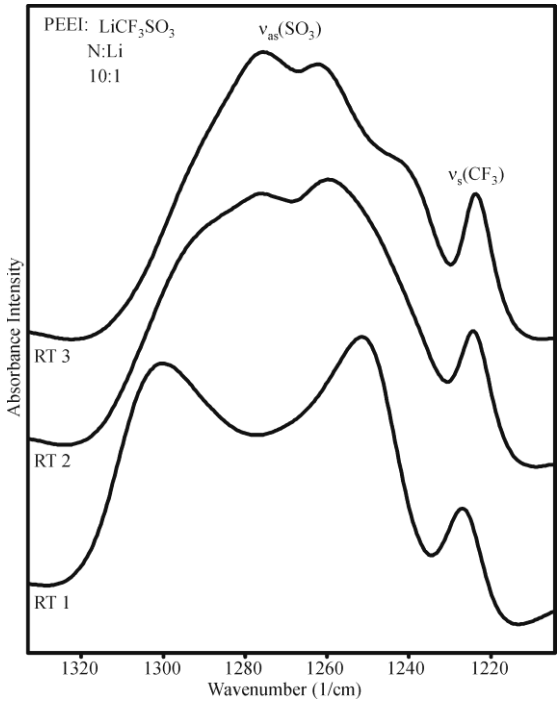

Figure 2.4 – The room temperature spectra before and after each of the heating cycles to 150 ºC are shown in the antisymmetric SO_3 stretching region, $\nu_{as}(SO_3)$.

peaks drops dramatically between the first and second room temperature spectra; this drastic change is mirrored in the large intensity changes in the $\nu_s(SO_3)$ band during the first heating cycle. There is a shoulder that appears in the final room temperature spectrum that cannot be explained, but could originate in a small population of triflate ions whose degeneracies have been broken by interactions with Li^+ ions.

2.3.4 Two-Dimensional Correlation Spectroscopy

The temperature-dependent data presented above is surprising, particularly in the fact that there is a shift in the ionic association without a corresponding shift in the polymer backbone modes sensitive to cation-polymer coordination. To further investigate this phenomenon, the temperature-dependent spectra were transformed into two-dimensional correlation spectra. This technique was first developed in 1990,[16] and then revisited in subsequent publications,[17,18] by Noda. An abbreviated summary of this technique will be provided.

Two-dimensional correlation spectroscopy was originally developed for nuclear magnetic resonance (NMR) spectroscopy, but mimicking the procedures used for NMR is not possible with conventional optical spectrometers. Noda's technique is based on the concept that the application of the pulse series

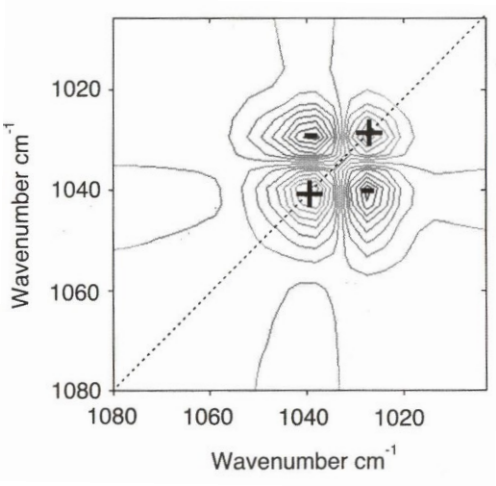

Figure 2.5 – Synchronous correlation spectrum of 10:1 PMEI :$LiCF_3SO_3$ in region containing $\nu_s(SO_3)$.

used in NMR can be simply viewed as an external perturbation.[18] In vibrational spectroscopy, an external perturbation such as temperature induces changes in the system that can be seen in the vibrational spectra. The two-dimensional correlation spectrum can be obtained by collecting sequential "dynamic spectra," spectra that have been subject to the external perturbation, and subjecting those spectra to a mathematical correlation analysis. A synchronous correlation spectrum is used to show simultaneous intensity changes measured at frequency one and two over the entire perturbation range.[18]

The synchronous spectrum for a 10:1 PMEI:$LiCF_3SO_3$ complex in the $\nu_s(SO_3)$ spectral region is shown in Figure 2.5. The positive correlation peaks correspond to the "free" ion band at 1032 cm^{-1} and the contact ion pair at 1041 cm^{-1}. The off-diagonal negative cross-peaks show that the increasing intensity of the "free" ion band and the decreasing intensity of the contact ion pair band occur simultaneously, such that the intensity of one band grows at the expense of the other band. Figure 2.6 shows an expanded view of the above synchronous spectrum. This spectrum shows no positive correlation peaks

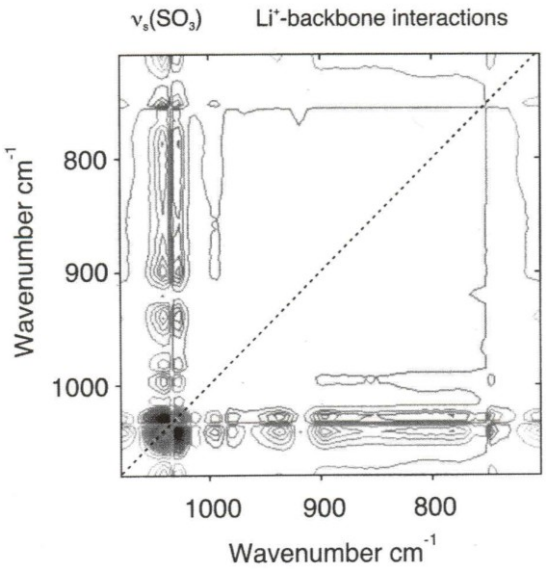

Figure 2.6 – Synchronous correlation spectrum of 10:1 PMEI :$LiCF_3SO_3$ in region from 1080 to 700 cm^{-1} containing $\nu_s(SO_3)$ and bands sensitive to polymer-cation coordination.

along the diagonal, which indicates that there are no significant changes in the bands that are particularly sensitive to polymer-cation coordination between 1000 to 700 cm^{-1}. The only cross-peaks that exist are attributed to small changes along the baseline that are correlated to the shifts in the $\nu_s(SO_3)$ region.

2.4 Summary and Conclusions

The differences in the spectra of pure PMEI, PEEI and PBEI occur because of the differences in the length of the side chain. These variances are most easily observed in the regions of the spectrum containing CH_2 rocking modes. The rocking motions tend to be highly coupled with the other modes in the region and, as such, appear as changes in several bands throughout the lower frequency region of the spectrum. The spectra of the polymer salt complexes show mostly only small changes with increasing salt concentration. However, there is one striking difference: the shift in the ionic association as indicated by the $\delta_s(CF_3)$ band. In the PBEI:$LiCF_3SO_3$ complexes there are both contact ion pairs and aggregates present, while in the PEEI and PMEI complexes ionic association is predominantly contact ion pair. It is expected that changing the length of the side chain would have a minimal effect on the cation coordination to the polymer backbone, and this appears to hold for the shorter side chains. However, a substantial increase in the side chain does cause a change in the nitrogen-lithium environment.

The ionic association shifts in a very unexpected way with increasing temperature. In contrast to polyether systems, a decrease in the ionic association is seen

with temperature cycling, shifting from contact ion pairs to "free" triflate ions. It is particularly surprising that the cation-anion interaction is decoupled from the host polymer. Despite evidence in the one-dimensional spectra of interaction of the lithium with the backbone, the two-dimensional spectra show no evidence of a change in the backbone bands that can be correlated to the shift in ionic association. Further evidence of the lithium interaction with the host polymer is seen in the dramatic increase of T_g with increased salt concentration; all spectroscopic measurements were made far above T_g.

2.5 References

(1) Saegusa, T.; Ikeda, H.; Fujii, H. *Macromolecules* **1972**, *5*, 108.

(2) Sanders, R. A.; Snow, A. G.; Frech, R.; Glatzhofer, D. T. *Electrochim. Acta* **2003**, *48*, 2247-2253.

(3) Tanaka, R.; Ueoka, I.; Takaki, Y.; Kataoka, K.; Saito, S. *Macromolecules* **1983**, *16*, 849-53.

(4) Frech, R.; Giffin, G. A.; Castillo, F. Y.; Glatzhofer, D. T.; Eisenblaetter, J. **2005**, *50*, 3963-3968.

(5) Painter, P. C.; Coleman, M. M. *Fundamentals of Polymer Science*; 2nd ed.; Technomic Publishing Company: Lancaster, PA, 1997.

(6) Sanders, R. A.; Frech, R.; Khan, M. A. *J. Phys. Chem. B* **2003**, *107*, 8310-8315.

(7) Sanders, R. A.; Frech, R.; Khan, M. A. *J. Phys. Chem. B* **2004**, *108*, 12729-12735.

(8) Huang, W.; Frech, R.; Wheeler, R. A. *J. Phys. Chem.* **1994**, *98*, 100-10.

(9) Petersen, G.; Jacobsson, P.; Torell, L. M. *Electrochim. Acta* **1992**, *37*, 1495-7.

(10) Dissanayake, M. A. K. L.; Frech, R. *Macromolecules* **1995**, *28*, 5312-19.

(11) Seneviratne, V.; Frech, R.; Furneaux, J. E. *Electrochim. Acta* **2003**, *48*, 2221-2226.

(12) Kakihana, M.; Schantz, S.; Torell, L. M. *J. Chem. Phys.* **1990**, *92*, 6271-7.

(13) Kakihana, M.; Schantz, S.; Torell, L. M.; Stevens, J. R. *Solid State Ionics* **1990**, *40-41*, 641-4.

(14) Sandner, B.; Tuebke, J.; Wartewig, S.; Shashkov, S. *Solid State Ionics* **1996**, *83*, 87-97.

(15) Greenbaum, S. G.; Pak, Y. S.; Wintersgill, M. C.; Fontanella, J. J. *Solid State Ionics* **1988**, *31*, 241-5.

(16) Noda, I. *Appl. Spectrosc.* **1990**, *44*, 550-561.

(17) Noda, I. *Appl. Spectrosc.* **1993**, *47*, 1329-36.

(18) Noda, I.; Dowrey, A. E.; Marcott, C.; Story, G. M.; Ozaki, Y. *Appl. Spectrosc.* **2000**, *54*, 236A-248A.

CHAPTER III

SPECTROSCOPIC INVESTIGATION OF CROSS-LINKED POLY(ETHYLENIMINE) HYDROCHLORIDE

Portions of this chapter have appeared in G. A. Giffin, F. Yepez Castillo, R. Frech, D. T. Glatzhofer, C. M. Burba. "Spectroscopic Investigation of Proton-Conducting, Cross-linked Linear Poly(ethylenimine) Hydrochloride Membranes" *Polymer*, **50(1)**, 171-176 (2009).

3.1 Introduction

Recent interest in fuel cell technologies has prompted research in the area of solid polymer electrolytes for use as proton-conducting membranes. Membrane development has focused on finding systems that have good mechanical properties, electrochemical stability at operating conditions, cost effectiveness and high proton conductivity.[1,2] Several different types of membranes currently are being investigated including perfluorosulfonic acids,[3,4] sulfonated poly(arylenes)[5-10] and acid-doped polymer complexes.[11-16] A cross-linked poly(ethylenimine) hydrochloride/phosphoric acid system has been presented as a potential membrane alternative with good conductivity, mechanical integrity and thermal stability up to 150ºC.[18] The degree of cross-linking in the system has a large effect on the physical properties of the film, as well as its spectroscopic signature. However, determination of the degree of cross-linking and a thorough spectroscopic investigation of the cross-linked network

previously has not been explored. The presence of the phosphoric acid further complicates an already intricate network; therefore, two things have been done to simplify the system: 1) The cross-linked network was examined without phosphoric acid to remove any interaction of phosphate species present with the polymer and to eliminate bands from the spectra that were the result of phosphate modes. 2) Small molecules were used to model small sections of the complex network, allowing the spectroscopic signature of various parts of the network to be identified. Here, 3-(dimethylamino)-acrolein was used to model β-aminoacrolein branching groups, one possible reaction product of the cross-linker with the base polymer.

3.2 Experimental Methods

3.2.1 Synthesis of Membranes

Linear poly(ethylenimine)·hydrochloride (PEI·HCl) was prepared by acidic hydrolysis of poly(2-ethyl-2-oxazoline) (Aldrich, average M_w ca. 500,000).[19,20] Cross-linked membranes were made as previously described by Glatzhofer *et al*;[18] the synthesis is briefly summarized as follows. PEI·HCl was dissolved in water (~0.6 M) and 1,1,3,3-tetramethoxypropane (Aldrich) was added while stirring, generating malonaldehyde *in situ*. The solutions were stirred for approximately 15 minutes. The solutions were cast onto a silicone rubber substrate and covered. After two days, the samples were uncovered and placed in an oven at ~ 40ºC to facilitate evaporation of residual water and formation of a free-standing film. Samples for infrared measurements were cast from solution, as prepared above, on ZnSe windows

approximately 1.5 hours after mixing to form thin films. Approximately 12-24 hours after preparation, the cast films were dried under vacuum. Raman and solution-state NMR samples were prepared by placing solution in a sealed glass tube approximately 15 minutes after mixing to form a gel.

3.2.2 Sample Characterization

Samples were characterized using infrared, Raman, NMR and impedance spectroscopy. Infrared spectra were collected using a Bruker IFS 66v spectrometer with a KBr beam splitter; 64 scans at a spectral resolution of 1 cm^{-1} were averaged for each spectrum. Spectra of cast thin films were measured at 11 mbar, while those of the liquid model compound, 3-(dimethylamino)-acrolein (DMAA) (Aldrich, 90%), were measured under a dry air purge. Raman spectra were collected on a Bruker Equinox 55 FRA 106/S with a Nd:YAG laser (1064 nm) and a CCD detector. Solution-state NMR experiments were carried out using a Varian Mercury-300 spectrometer (300.1 MHz ^{1}H). Water was suppressed from the spectra by pre-saturation using the PRESAT pulse sequence as supplied by Varian, Inc. The spectra were collected after 48 scans and were referenced to d_4-Methanol (3.32 ppm). Solution-state NMR experiments were done by Frank Yepez Castillo; a more detailed description will appear in his dissertation. Analysis of these data was done collaboratively with Frank Yepez Castillo. High-resolution magic-angle-spinning (HRMAS) NMR were collected with a Varian $^{13}C\{^{1}H\}$ HRMAS NanoProbe® and a Mercury VX 300 MHz NMR Spectrometer. VnmrJ 1.1D software (Varian, Inc.) was used for data collection and

processing. The ^{1}H chemical shift values were referenced to the residual water signal (HOD) at 4.8 ppm. Deuterium lock was maintained throughout data acquisition to control the field frequency ratio over the sample. Films of cross-linked PEI·HCl were soaked in D_2O for at least 1 hour prior to data collection and then loaded into a ceramic rotor. Subsequently, the rotor was filled with D_2O and spun at a rate of 2000 Hz. Sample spinning was achieved with a Torlon drive ring and dry air. The sample temperature was controlled at 25°C. Solid-state NMR experiments were done by Christopher Burba (Ph.D 2006, University of Oklahoma). Data analysis was done collaboratively with Frank Yepez Castillo; these results will also appear in his dissertation.

3.3 Results and Discussion

Glatzhofer and coworkers previously described the likely mechanism for the cross-linking reaction that occurs in this system.[18] Three possible product species may be found in the cross-linked membranes, as represented in Figure 3.1.

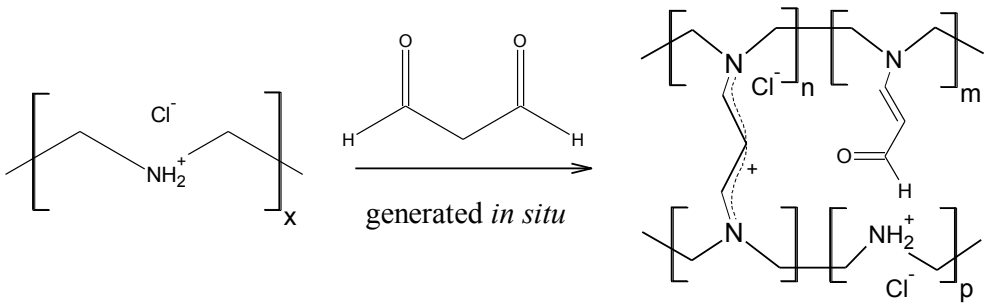

Figure 3.1. Reaction scheme - PEI·HCl with malonaldehyde. *n, m, p* represent the possible product species found.

Some of the protonated amine sites may remain, designated by *p*, in addition to the new cross-linked moieties, designated by *n*. However, at high cross-linker concentration, it is likely that there are β-aminoacrolein branching units, designated by *m*, due to a malonaldehyde molecule reacting with only one nitrogen site, because there are no other accessible sites.

3.3.1 Rate of Cross-linking Reaction

The cross-linking reaction shown in Figure 3.1 progresses rapidly early in the reaction and gradually slows as the number of cross-linker molecules and protonated amine sites decreases. The reaction rate can be controlled to some extent by varying the concentration of the polymer in water; this control allows the rate and the total time to be adjusted such that the reaction progress can be tracked using Raman spectroscopy. The sample is prepared as described in Section 3.1.1, except the mixed

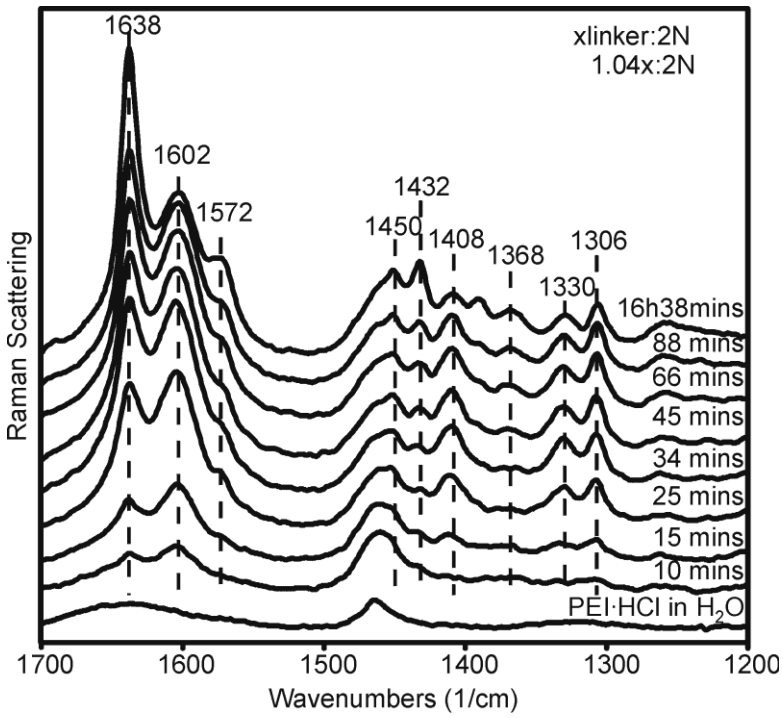

Figure 3.2 – Progress of cross-linking reaction tracked by Raman spectroscopy, 1700-1200 cm^{-1}.

reactants are immediately placed in a sealed glass tube. Spectra, which resulted from 100 averaged scans, are collected at approximately five minute intervals at a spectral resolution of 3 cm^{-1}. These parameters are chosen so the spectral changes that occur as the reaction progresses can be minimized within each sampling period.

Raman spectroscopy confirms that the reaction rate is faster early in the reaction. This can be seen in both Figures 3.2 and 3.3. In both cases the difference between consecutive spectra decreases as the time increases. In Figure 3.2, bands at 1638 and 1602 cm^{-1} appear as soon as the reaction can be monitored and continue to grow in intensity to become the strongest bands in the spectrum. These bands are attributed to CC and CO stretching motions in the cross-linker, as in moieties *n* and *m* in Figure 3.1. Few bands are present in the spectrum of PEI·HCl dissolved in H_2O, unlike the spectrum of solid PEI·HCl which has several bands in this region. In solution, any ordering of the polymer has essentially been removed, resulting in decreased intensity and significant broadening, such that most bands

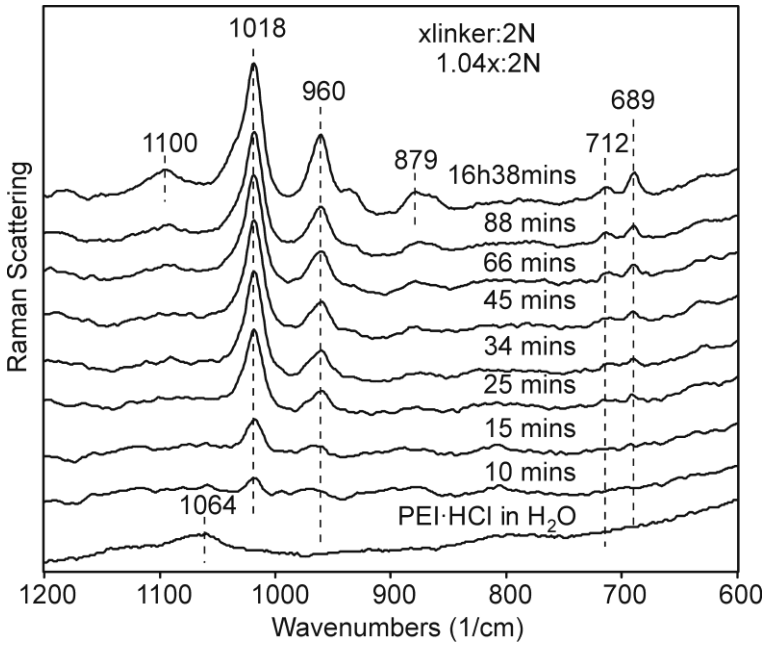

Figure 3.3 – Progress of cross-linking reaction tracked by Raman spectroscopy, 1200-600 cm^{-1}.

may not be discerned from the background. In Figure 3.2, only the band at 1463 cm^{-1} remains upon dissolution of the polymer. This band is attributed to the CH_2 deformation of the polymer backbone. This band shifts to lower frequencies and gains a low frequency component as the cross-linking reaction progresses. Other band structure also appears between 1400 and 1300 cm^{-1}. These bands could arise from mixed modes associated with both the polymer backbone and the cross-link unit. As the cross-linking reaction progresses, the motion of the polymer decreases as cross-link units tie one chain to the next, or the chain to itself, and the intensities of bands originating in the backbone increase. In Figure 3.3, the band at 1064 cm^{-1} slowly shifts to 1100 cm^{-1} with increasing time of reaction. Several other bands appear and grow in intensity as the cross-linking reaction occurs. The origin of these bands and some of those in Figure 3.2 will be discussed in further detail later in this chapter. A qualitative rate experiment also was done using NMR spectrometry by Frank Yepez Castillo, who found similar results. This experiment will be described in his dissertation.

3.3.2 Determination of the Degree of Cross-linking via NMR Spectroscopy

In order to accurately characterize the cross-linked PEI·HCl membranes, it is necessary to know the degree of cross-linking. The degree of cross-linking is considered to be the fraction of cross-linker molecules that actually make a linkage between two nitrogen atoms. Due to the high volatility of malonaldehyde and the presence of branching units (noted with subscript *m* in Figure 3.1), the degree of cross-linking is found to be lower than expected. HRMAS spectra of the cross-linked

polymer are shown in Figure 3.4; similar spectra are seen with the gelled samples collected with solution-state NMR techniques. The degree of cross-linking can be estimated with NMR spectroscopy by determining the ratio of backbone hydrogens (δ, ~3.4-4.2 ppm) to cross-link hydrogens (δ (hydrogens on α-cross-link carbons), ~7.05-7.8 ppm and δ (hydrogens on β-cross-link carbons), ~5.2 ppm). A ratio of eight backbone hydrogens to three cross-link hydrogens would indicate a 100% degree of cross-linking. By comparing the measured ratio to the 100% value, the degree of cross-linking of a particular sample may be calculated. The chemical shifts of the hydrogens

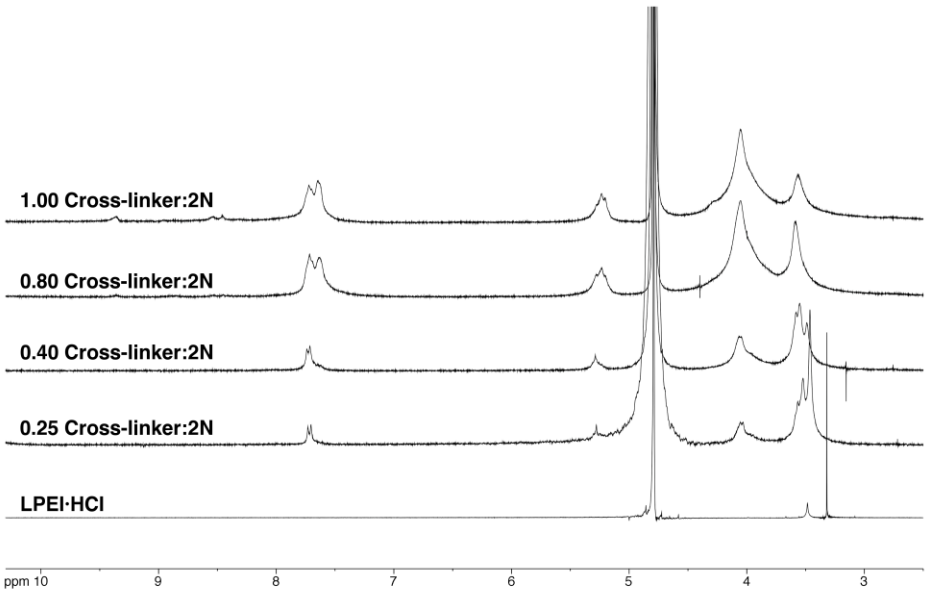

Figure 3.4 – HRMAS solid state ^{1}H NMR spectra of cross-linked PEI·HCl at various cross-linker concentrations and solution ^{1}H NMR of linear poly(ethylenimine) hydrochloride in d_2-water. Cross-link spectra collected by Christopher Burba. LPEI·HCl spectra collected by Mike Erikson. This figure will also appear in Frank Yepez Castillo's dissertation.

in the acrolein branches are similar to those of the cross-link hydrogens. However, it was noted that the peak for the proton on the β-cross-link carbon at 5.23 ppm in D_2O decreased in intensity relative to the other peaks over time, indicating exchange. The integration for this peak consequently was considered unreliable. Therefore, a ratio of eight backbone hydrogens to the two hydrogens on α-crosslink carbon was taken to indicate 100% degree of cross-linking and the degree of cross-linking was estimated by comparing the measured ratio to the theoretical maximum. The presence of these branches would increase the integrated area of the peaks in the region corresponding to

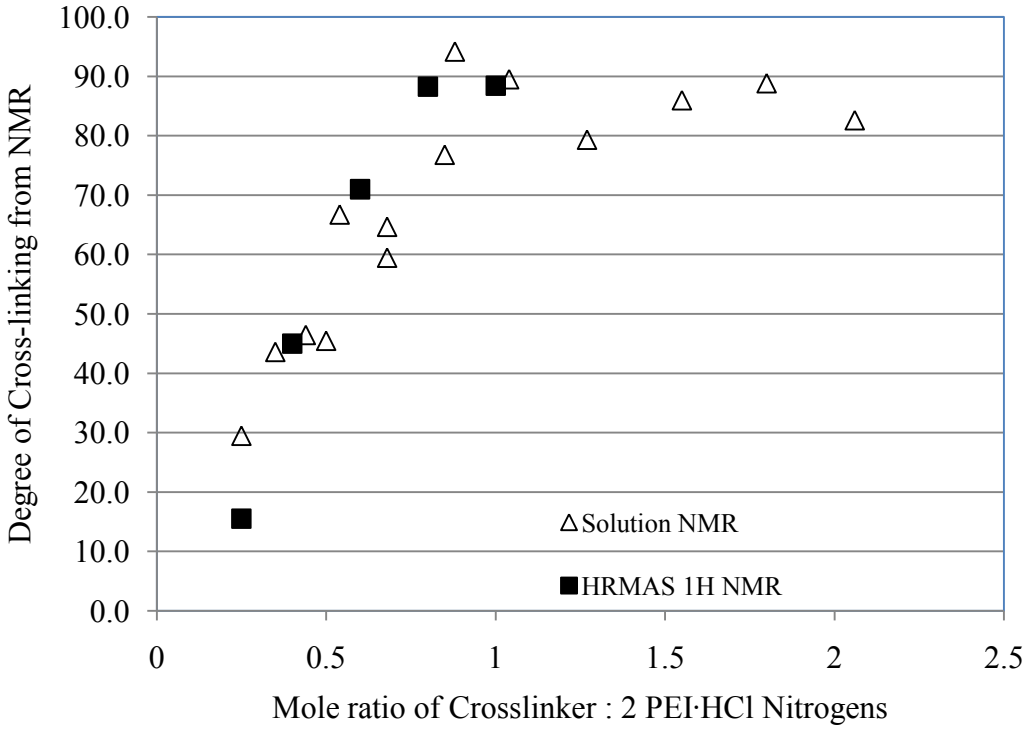

Figure 3.5 – Calibration curve for degree of cross-linking as determined from NMR data. As determined from: (♦) Solution NMR collected by Frank Yepez Castillo, (▲) Solid-State NMR collected by Christopher Burba. Data analysis was done in collaboration with Frank Yepez Castillo. This figure will also appear in his dissertation.

the cross-link hydrogens. This can be corrected by subtracting branching unit from the integrated values, as indicated by the number of aldehyde end groups (δ, 9.04 ppm).

A plot of the corrected degree of cross-linking, as determined from these NMR values versus the number of moles of cross-linker per two moles of PEI·HCl nitrogen atoms, is shown in Figure 3.5. The degree of cross-linking increases roughly linearly with an increase in the number of moles of cross-linker at low cross-linker concentrations. However, at higher cross-linker concentrations, the degree of cross-linking plateaus between approximately 0.8 and 0.9. It seems that the maximum degree of cross-linking that can be attained is about 90%. Higher cross-linker concentrations promote substantial branching.

Solid-state NMR is also used to examine the same peaks as described above to determine the degree of cross-linking. Data points from the solid-state experiments are also shown in Figure 3.5 and agree well with solution-state data points. Therefore, the plot shown in Figure 3.5 can be used as a calibration curve to estimate the degree of cross-linking for samples simply from the amount of cross-linker used in sample preparation.

3.2.3 Spectroscopic Identification of Cross-linker.

IR and Raman spectroscopy are used to identify the vibrational signatures of the cross-linker unit in the network. The cross-linker unit contains a run of three conjugated carbons capped with two nitrogen atoms of the PEI·HCl polymer backbone on adjacent chains or within the same chain. Its presence can be identified through a

series of bands between 1570 and 1640 cm^{-1} that are seen to grow in intensity throughout the course of the reaction, as shown in Figure 3.2 and Figure 3.6. In the Raman spectra shown in Figure 3.6, two bands at 1572 and 1638 cm^{-1} can be seen at lower cross-linker concentrations, with a third peak at 1602 cm^{-1} appearing at higher concentrations. This third peak is attributed to the presence of acrolein branching units that are only found at the higher cross-linker concentrations. The branching unit can be modeled with DMAA, which has two bands in this region at 1651 and 1602 cm^{-1}. The bands at 1602 cm^{-1} in both the DMAA model compound and the cross-linked membrane are attributed here to the CO stretching motion from the aldehyde group. The 1638 and 1572 cm^{-1} bands in the cross-linked membrane are primarily the result of the cross-link CC stretching motion.[21]

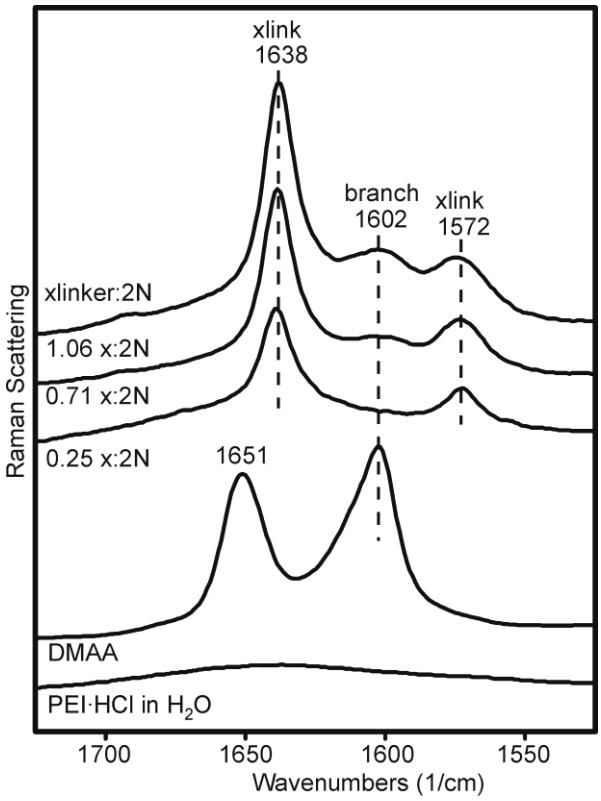

Figure 3.6 – Raman spectra of cross-linker stretching region. The notation xlinker:2N designates the ratio of the cross-linker molecules added to the solution to every 2 PEI-HCl nitrogen atoms.

Figure 3.7 shows the IR spectra of this region; the bands in the IR spectra are more complex than in the Raman spectra. Three bands at 1638, 1608 and 1572 cm^{-1} are

seen at all cross-linker concentrations. A significant broadening is seen in the middle peak as the cross-linker concentration increases. This broadening is accompanied by a slight frequency shift from 1608 to 1610 cm^{-1}. In the IR spectrum of the model compound there is one broad asymmetric band located at 1616 cm^{-1} that contains coupled CO stretching modes.[22] The mixing of these modes would lead to the broadening and slight frequency shift seen in the membrane at high cross-linker concentrations.

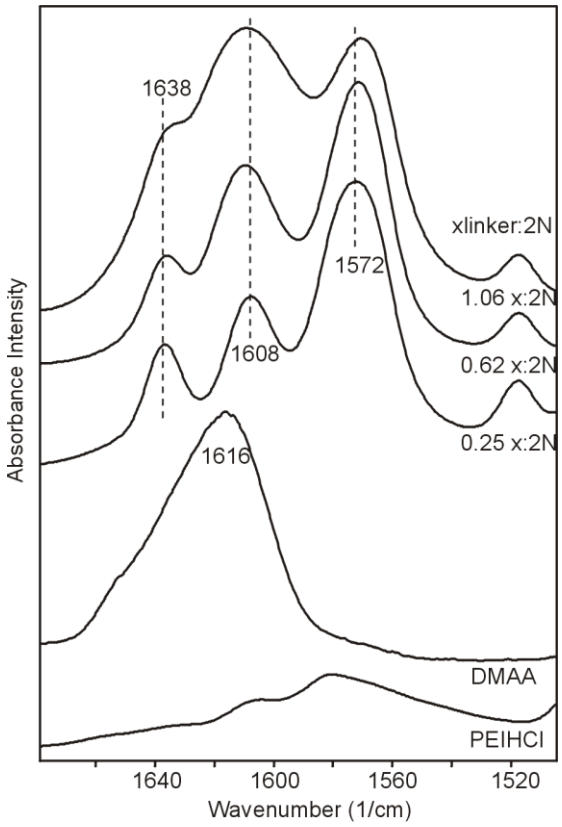

Figure 3.7 – Infrared spectra of cross-linker stretching region. The notation xlinker:2N designates the ratio of the cross-linker molecules added to the solution to every 2 PEI-HCl nitrogen atoms.

The above text describes the branching unit as consisting of only the β-unsaturated aldehyde. However, there is acid present in this system, and as a result, protonation of the branching unit can occur. Protonation can occur in a number of atoms, as shown in Figure 3.8: at the carbonyl oxygen to form an enol, species 2, at the enamine nitrogen, species 3 or at the carbon α to the carbonyl (data not shown). The rate constant for the formation of the enol is four times larger than that for protonation

at the enamine and seven orders of magnitude larger than that for protonation at the α-carbon.[17] All three of these protonated species exist in equilibrium with the unprotonated species.

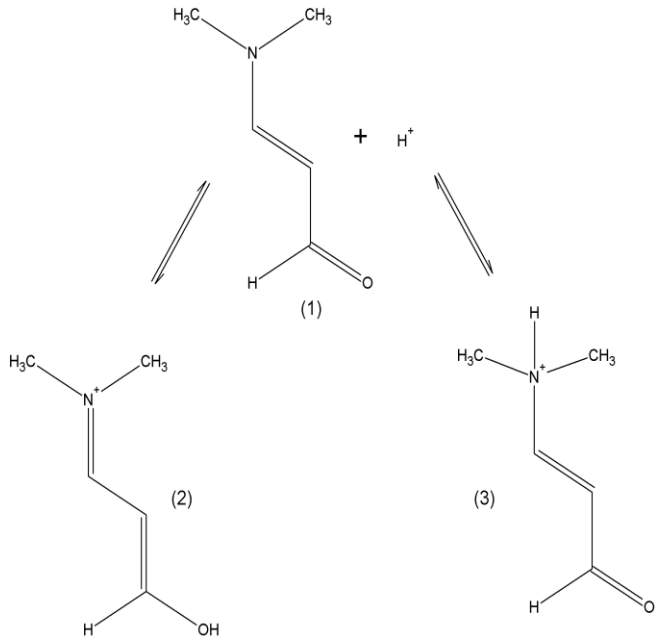

Figure 3.8 – Species which may occur in DMAA-acid solutions. Protonation can also occur at the α-carbon, but this is a very minor product. rate constant for protonation($sec^{-1}mol^{-1}$), oxygen=5-10*10^4, k(nitrogen)=7.6 [17]

A spectroscopic study of the model compound DMAA with increasing acid concentrations is shown in Figure 3.9. The Raman spectrum of DMAA shows two large peaks at 1651 and 1602 cm^{-1}. These peaks are assigned to the cis coupled CO stretching mode and the trans coupled CO stretch mode, respectively.[22] As hydrochloric acid is added to the system, both of these bands decrease in intensity and new features appear at 1661 and ~1630 cm^{-1}. These bands are attributed primarily to CN and CC stretching modes, respectively, in species 2, Figure 3.8. Even if there was a significant amount of CC stretching motion from species 3 present, it would be underlying these broad bands. Evidence for the equilibrium can be seen in the remnants of the 1602 cm^{-1} band that exist even at a N:HCl ratio of 1:1. Similar assignments can be made in the infrared

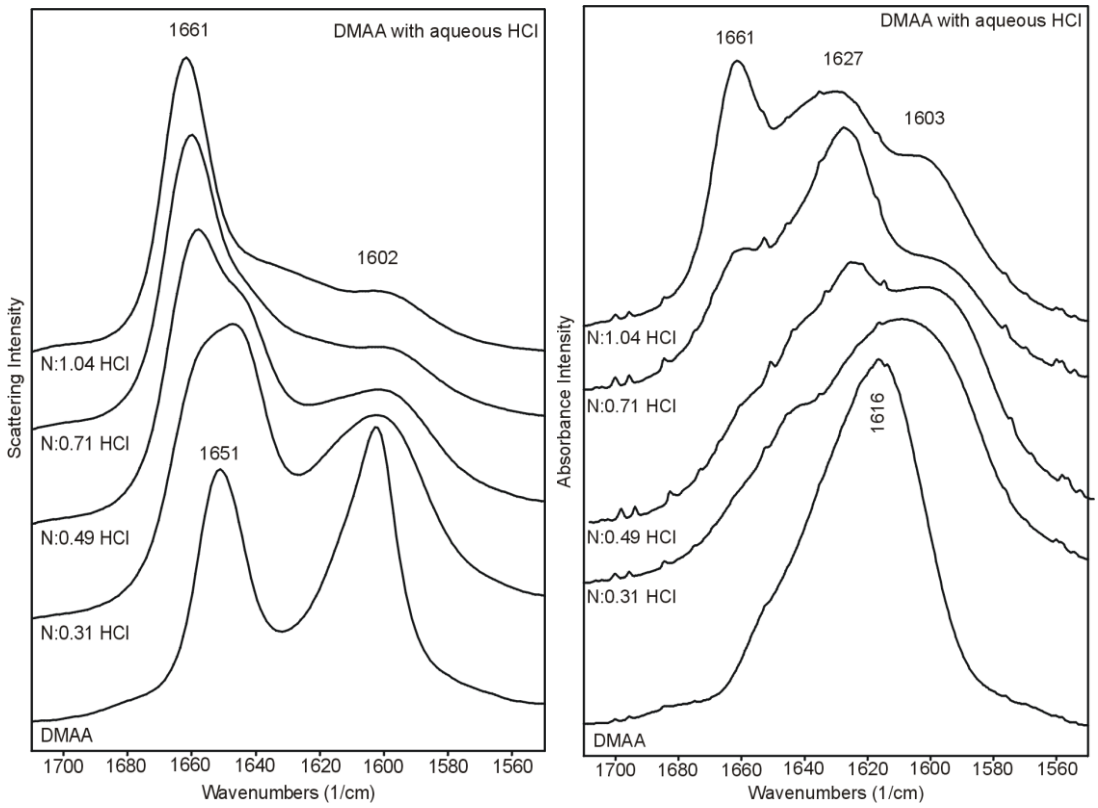

Figure 3.9 – Raman and infrared spectra of DMAA with increasing HCl. The notation N: x.xx HCl designates the ratio of the DMAA nitrogen atoms to the number of HCl molecules.

spectrum. The broad band in the neat DMAA contains contributions from the CO stretching mode of both the cis and trans conformers.[22] As the amount of acid present increases, the IR band structure begins to resemble that of the Raman spectra and can be similarly assigned.

3.2.4 Spectral Changes with Varying Degrees of Cross-linking

The stretching bands directly associated with the cross-link unit can be clearly identified in the region between 1570 and 1640 cm^{-1}. However, the lower frequency

regions are more complicated, because they contain bands that are associated with both the polymer backbone and the cross-link unit. Raman and IR spectra from 1500 to 1100 cm^{-1} can be found in Figures 3.10 and 3.11, respectively. This region contains bands arising from mixed modes that are associated with both the polymer backbone and the cross-link unit. Figure 3.10 shows a very simple spectrum for PEI·HCl in H_2O; the only band of significant intensity present appears at 1464 cm^{-1}. This band can be attributed to the CH_2 deformation or scissors mode. When cross-linker is added, another feature appears on the low frequency side of the 1464 cm^{-1} band at 1432 cm^{-1}. This band can also be attributed to the CH_2 group deformation or scissors mode. A CH_2 that is now next to a cross-linked amine site will have a different local environment than one that is next to a protonated amine site. The intensity of the low frequency component increases and the high frequency component shifts to lower frequency as the amount of cross-linker increases. This may occur because the CH_2 group found between a protonated amine nitrogen and a cross-link nitrogen would have a frequency intermediate to one that is between two protonated nitrogens or two

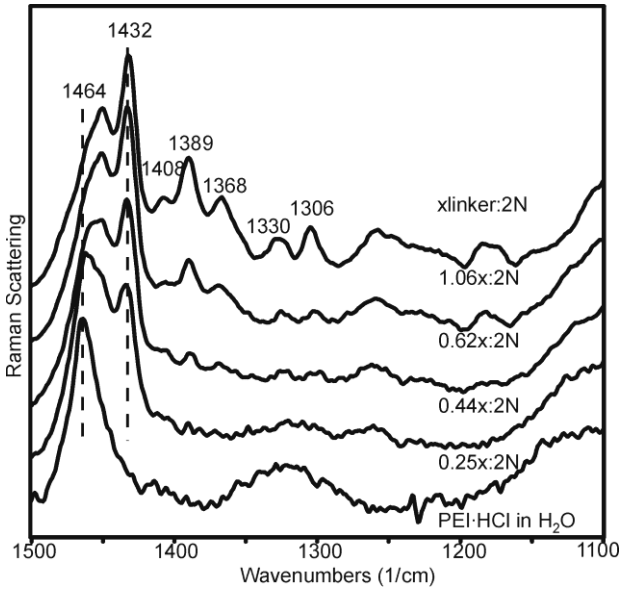

Figure 3.10 – Raman spectra of lower frequency region. The notation xlinker:2N designates the ratio of the cross-linker molecules added to the solution to every 2 PEI-HCl nitrogen atoms.

cross-linked nitrogens. The intensity of the highest frequency component decreases rapidly because the number of adjacent protonated amine sites also rapidly decreases as the amount of cross-linker increases. As the amount of cross-linker increases, other low intensity bands appear between approximately 1400 and 1300 cm^{-1}. These bands can be attributed to CH_2 twisting or wagging modes on the polymer backbone[23,24] or also to CH out-of-plane bending modes on the cross-linked unit. The CH out-of-plane bending modes were found to occur in 2,4-hexadiene, a conjugated alkene, from 1307 to 1238 cm^{-1}. The range in frequencies is the result of varying conformations around the conjugated segment. All *E* (trans) conformations have frequencies on the high end of this range and the *Z* (cis) conformations are on the low end.[25,26] The cross-link unit here is structurally different than 2,4-hexadiene in that the conjugated unit is capped by two nitrogen atoms from the polymer backbone and has a net positive charge spread over the length of the cross-link. Despite the differences in the system, the frequency range of the CH bending modes should be comparable. The bands between approximately 1400 and 1300 cm^{-1} do not appear until the 0.62:2N xlinker:2N spectrum. Below this point, there is little ordering of the polymer resulting in decreased intensity and significant broadening such that most bands may not be discerned from the background. It is only when the cross-link ties cause an increase in ordering that the intensity of the bands becomes large enough for them to be clearly discerned from the baseline.

Figure 3.11 shows the IR spectra of the same region as the Raman spectra in Figure 3.10. The PEI·HCl spectrum shown here is a solid state spectrum; therefore there are more bands of significant intensity throughout the region, in comparison to the

Raman spectrum, due to the increased order in the solid state. Similar trends are seen in the bands attributed to the CH_2 deformation mode as shown in Figure 3.10. As the amount of cross-linker increases, the higher frequency bands decrease in intensity, while a new band appears on the low frequency side. In general, as the amount of cross-linker increases, bands in this region of the spectra that were present in the pure polymer gain a lower frequency component and the high frequency component disappears. New bands appear at 1337, 1240 and ~1150 cm^{-1}. These bands are attributed to new modes that arise from the cross-linker unit or from mixed backbone and cross-linker modes. In particular, the band at 1240 cm^{-1} could have a significant contribution from the CH out-of-plane bending mode of the cross-link unit. As discussed in conjunction with Figure 3.10, these modes were seen in the spectra of the conjugated dienes. In these diene molecules, the out-of-plane bend occurred at lower frequencies in the IR than in the Raman spectra.[25,26] Bands in this region could also contain contributions from backbone CN and CC stretching modes.

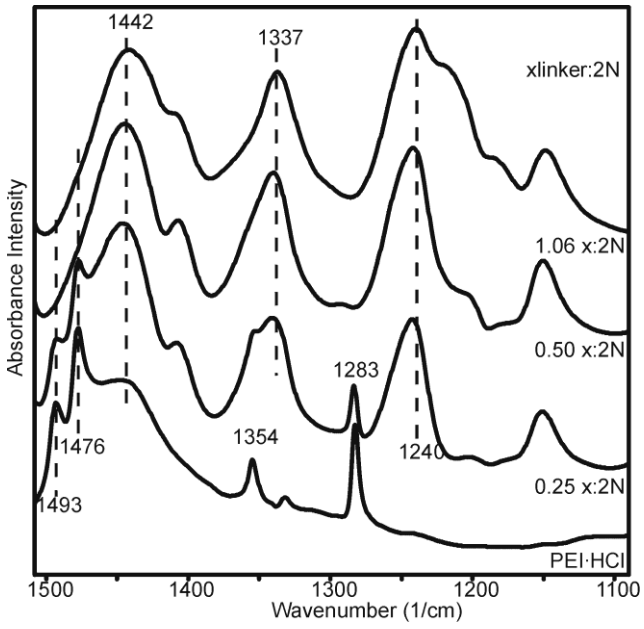

Figure 3.11 – IR spectra of lower frequency region. The notation xlinker:2N designates the ratio of the cross-linker molecules added to the solution to every 2 PEI-HCl nitrogen atoms.

Figure 3.12 shows the Raman spectra between approximately 1100 and 600 cm^{-1}. Bands in this region contain mixed modes that are sensitive to the conformation of the polymer backbone.[23,24] There are three bands at 1018, 960 and 689 cm^{-1} that appear even at low cross-linker concentrations. These bands are most likely associated with the cross-link unit itself and are mixed modes containing contributions from the CH in-plane bending mode and the CCC bending mode.[25] In contrast, the band at 1064 cm^{-1} in the PEI·HCl spectrum shifts to 1100 cm^{-1} as the cross-linker concentration increases. The bands at 863 and 934 cm^{-1} appear only at high cross-linker concentrations and therefore are attributed to the acrolein branching units.

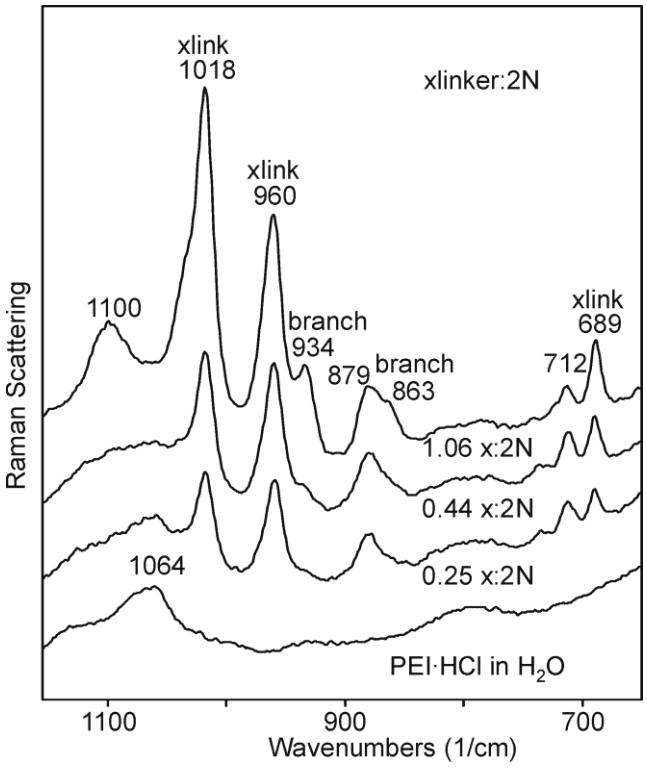

Figure 3.12 - Raman spectra of lower frequency region. The notation xlinker:2N designates the ratio of the cross-linker molecules added to the solution to every 2 PEI-HCl nitrogen atoms.

Similar trends can be seen in the IR spectra as in Figure 3.13. Bands at 1010, 620 and 564 cm^{-1} most likely are associated directly with the cross-link unit, whereas the bands at 1064 and 1010 cm^{-1} are attributed to the polymer backbone. Bands from 1000 to 1100 cm^{-1} contain contributions from ν(CN) and ν(CC) stretching motions. As

the cross-linking reaction occurs, the nitrogen atoms of the polymer backbone become covalently bonded to the cross-linker molecule. This results in a redistribution of electron density around the nitrogen and adjacent carbon atoms on the polymer backbone, changing both the effective force constants of the backbone CN and CC bonds and the dipole moment and polarizability derivatives for these modes. Those changes will appear as frequency shifts and intensity changes in the corresponding IR and Raman bands. Therefore, as the amount of cross-linker increases, the intensity of the 1062 cm^{-1} band decreases and the related band at 1010 cm^{-1} increases. The band at 835 cm^{-1} may be attributed to the acrolein branching units, consistent with the assignment of the 863 cm^{-1} band in the Raman spectrum. Finally, it is interesting to note that the spectrum labeled 0.25:1 resembles a superposition of pure PEI·HCl and the 0.50:1 spectra. This would indicate that membranes with mole ratios less than 0.25:2N contain domains of pure PEI·HCl in addition to the cross-linked moieties.

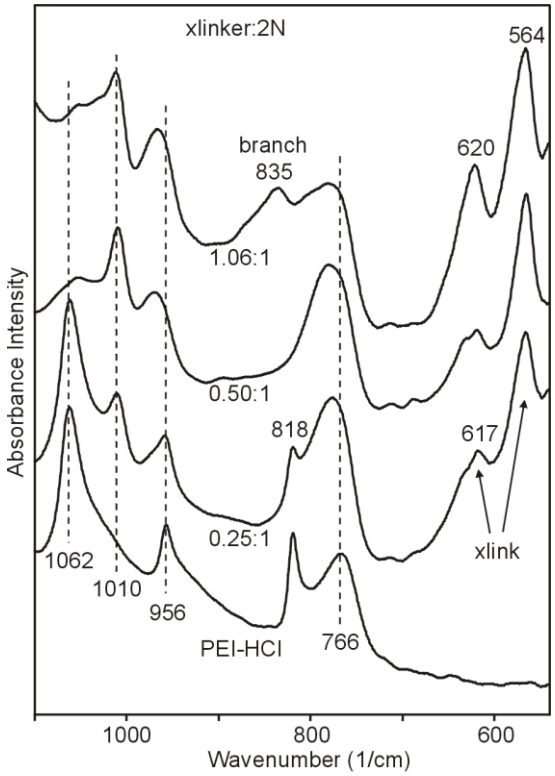

Figure 3.13 – Infrared spectra of lower frequency region. The notation xlinker:2N designates the ratio of the cross-linker molecules added to the solution to every 2 PEI-HCl nitrogen atoms.

3.4 Summary and Conclusions

Membranes made of cross-linked PEI·HCl have been investigated as a function of the degree of cross-linking with a number of different spectroscopic techniques. The degree of cross-linking was determined from NMR spectroscopy. The maximum degree of cross-linking attained is approximately 90%. Above this cross-linking level, most of the amine sites already have reacted, and the few remaining sites are not sufficiently close together to allow the cross-link molecules to react with two nitrogen atoms. This situation results in an acrolein branching unit whose presence is inferred from spectroscopic data. Vibrational modes associated with the cross-link unit can be identified in both the IR and Raman spectra from bands that are present even at low cross-linker concentrations but are not present in the pure polymer. In comparison, bands that are present in pure PEI·HCl, but exhibit shifts in frequency and intensity as the amount of cross-linker increases, are attributed to the polymer backbone. These shifts are associated with a redistribution of electron density along the backbone as the cross-linker molecule reacts with the polymer backbone. The bands associated with the acrolein branching units can be distinguished from those associated with both the cross-linker and the polymer backbone, as they are present only at high cross-linker concentrations.

3.5 References

(1) Smitha, B.; Sridhar, S.; Khan, A. A. *J. Membr. Sci.* **2005**, *259*, 10-26.

(2) Mehta, V.; Cooper, J. S. *J. Power Sources* **2003**, *114*, 32-53.

(3) Mauritz, K. A.; Moore, R. B. *Chem. Rev.* **2004**, *104*, 4535-4585.

(4) Basnayake, R.; Peterson, G. R.; Casadonte, D. J., Jr.; Korzeniewski, C. *J. Phys. Chem. B* **2006**, *110*, 23938-23943.

(5) Carretta, N.; Tricoli, V.; Picchioni, F. *J. Membr. Sci.* **2000**, *166*, 189-197.

(6) Sankir, M.; Kim, Y. S.; Pivovar, B. S.; McGrath, J. E. *J. Membr. Sci.* **2007**, *299*, 8-18.

(7) Cho, C. G.; Kim, Y. S.; Yu, X.; Hill, M.; McGrath, J. E. *J. Polym. Sci., Part A: Polym. Chem.* **2006**, *44*, 6007-6014.

(8) Hofmann, M. A.; Ambler, C. M.; Maher, A. E.; Chalkova, E.; Zhou, X. Y.; Lvov, S. N.; Allcock, H. R. *Macromolecules* **2002**, *35*, 6490-6493.

(9) Lee, H.-S.; Badami, A. S.; Roy, A.; McGrath, J. E. *J. Polym. Sci., Part A: Polym. Chem.* **2007**, *45*, 4879-4890.

(10) Yang, Y.; Holdcroft, S. *Fuel Cells* **2005**, *5*, 171-186.

(11) Asensio, J. A.; Borros, S.; Gomez-Romero, P. *J. Electrochem. Soc.* **2004**, *151*, A304-A310.

(12) Bouchet, R.; Siebert, E. *Solid State Ionics* **1999**, *118*, 287-299.

(13) Kim, H.-J.; Lim, T.-H. *J. Ind. Eng. Chem.* **2004**, *10*, 1081-1085.

(14) Lobato, J.; Canizares, P.; Rodrigo, M. A.; Linares, J. J.; Aguilar, J. A. *J. Membr. Sci.* **2007**, *306*, 47-55.

(15) Lobato, J.; Canizares, P.; Rodrigo, M. A.; Linares, J. J.; Manjavacas, G. *J. Membr. Sci.* **2006**, *280*, 351-362.

(16) Xiao, L.; Zhang, H.; Jana, T.; Scanlon, E.; Chen, R.; Choe, E. W.; Ramanathan, L. S.; Yu, S.; Benicewicz, B. C. *Fuel Cells* **2005**, *5*, 287-295.

(17) Kramer, H. E. A.; Gompper, R. *Tetrahedron Lett.* **1963**, 969-72.

(18) Glatzhofer, D. T.; Erickson, M. J.; Frech, R.; Yepez, F.; Furneaux, J. E. *Solid State Ionics* **2005**, *176*, 2861-2865.

(19) Tanaka, R.; Ueoka, I.; Takaki, Y.; Kataoka, K.; Saito, S. *Macromolecules* **1983**, *16*, 849-53.

(20) York, S.; Frech, R.; Snow, A.; Glatzhofer, D. *Electrochim. Acta* **2001**, *46*, 1533-1537.

(21) Socrates, G. *Infrared Characteristic Group Frequencies*; John Wiley & Sons: New York, 1980.

(22) Dabrowski, J.; Kamienska-Trela, K. *Roczniki Chemii* **1966**, *40*, 831-4.

(23) Boesch, S. E.; Yorek, S. S.; Frech, R.; Wheeler, R. A. *PhysChemComm* **2001**, Paper No 1.

(24) Matsuura, H.; Fukuhara, K. *J. Polym. Sci., Part B: Polym. Phys.* **1986**, *24*, 1383-400.

(25) Aly, M. M. A.; Baron, M. H.; Favrot, J.; Romain, F.; Revault, M. *Spectrochim. Acta, Part A* **1984**, *40A*, 1037-56.

(26) Panchenko, Y. N.; Rezvanova, D. R.; Pentin, Y. A.; Csaszar, A. G. *Acta Chim. Hung.* **1991**, *128*, 239-50.

CHAPTER IV

SPECTROSCOPIC INVESTIGATION OF SECONDARY AMINE HYDROHALIDES

Portions of this chapter have appeared in:

Giffin, G.A., Boesch, S., Bopege, D.N., Powell, D.R., Wheeler, R.A., Frech, R. "Vibrational Spectroscopy of Secondary Amine Salts: 1. Assignment of NH_2^+ Stretching Frequencies in Crystalline Phases." *J. Phys. Chem. B* (submitted, 2009)

Giffin, G.A., Boesch, S., Wheeler, R.A., Frech, R. "Vibrational Spectroscopy of Secondary Amine Salts: 2. Assignment of lower frequency NH_2^+ and other modes." *to be submitted* (2009).

4.1 Introduction

Amine salts have relevance in a wide variety of applications from materials science[1,2] to biological systems[3-5]. Small molecule amine hydrohalide salts make good models for both polyamine salts and other non-halide amine salts. Amine hydrohalides were studied in the 1950s and 1960s, primarily to examine the nature of hydrogen bonds, but the vibrational assignments of the NH_2^+ stretching frequencies in the literature are vague and inconsistent.[6-13] Furthermore, there have been no studies of secondary amine salts that directly correlate the vibrational spectra with a crystal structure. Chenon and Sandorfy stated that the stretching bands of protonated amino groups can be found between 2800 – 2400 cm^{-1}.[6] They compared the CH_2 group to the

NH_2^+ group and commented that two stretching bands should be expected. However, these authors also noted that there are many more than two bands present in the stretching region and attributed the "extra" bands in this region to combination bands.[6] Additionally, they concluded that the amino hydrogen atoms experienced hydrogen bonds of the form N^+H---X^-, as evidenced by a regular shift to lower wavenumbers with increasing anion size.[6] This description was reiterated by Brissette and Sandorfy, who emphasized the severe overlapping of the CH_3, CH_2 and NH_2^+ bands on the low frequency side of the CH stretching region.[7] Heacock and Marion also loosely correlated the complex series of bands between 2800 – 2000 cm^{-1} to the NH_2^+ stretching modes.[9] Stone, Craig and Thompson assigned bands at even higher frequencies to the protonated amine stretching modes (ν_{as} ~2920, ν_s ~2820 cm^{-1}). They supported their conclusions by assignment comparison with the ND stretching frequencies (ν_{as} ~2190, ν_s ~2100 cm^{-1}), which resulted in a very reasonable H to D isotopic shift $\left(\frac{\nu_D}{\nu_H} = 0.75\right)$.[12] Bellanato assigned bands at ~2980 cm^{-1} to overlapping CH and "free" N^+-H stretching modes and the peak at ~2430 cm^{-1} to the N^+H---X^- stretch. There have also been publications that examined diamines; the spectra of these compounds proved to be more complex than those of the simple secondary amines. Mureinik and Robb assigned peaks at 3135 and ~3000 cm^{-1} in N,N'-dimethylethylenediamine dihydrochloride and N,N'-diethylethylenediamine dihydrochloride as the NH_2^+ stretch. There were no peaks reported in the region around 2500 cm^{-1}.[8] In contrast, Baldwin briefly mentioned that in a variety of diamine salts the peaks around ~2500 cm^{-1} can be assigned as vibrations originating in the N^+H---X^- group.[10] Bands in other regions have also been examined

previously; these assignments primarily address the NH_2^+ deformation[6,7,9,11,12,14] or characteristic group frequencies of other lower frequency bands.[10] Mureinik and Robb have made assignments of the infrared active modes, but their assignments do not consider mixed modes that have been shown to occur in the unprotonated amines.[15,16]

This chapter will revisit these vibrational assignments in a variety of secondary amines salts and will include supporting computational results. Diamines such as N,N'-dimethylethylenediamine (DMEDA) or N,N'-dimethylpropylenediamine (DMPDA) are of particular interest because they make better models for the polyamine salts than simple secondary amines. However, the vibrations of DMEDA and DMPDA are complex, so starting with a simple amine such as dipropylamine (DPA) is useful to help understand the vibrational spectra. Crystal structures for four diamine salts will be presented here. Crystal structures for diisopropylamine hydrochloride and hydrobromide already have been reported.[17,18] It is reasonable to assume that the hydrogen-bonding environment around the protonated nitrogen atoms is similar in both DPA:HX and diisopropylamine:HX. It has been shown that the NH_2^+ stretching frequencies in amine salts are sensitive to the identity of the counter ion;[6,7,10] the sensitivity of other vibrational modes to the counter ion, particularly the CH stretching modes and the lower frequency modes, will be investigated. The low frequency vibrational assignments in several secondary amine salts are re-examined, complemented by supporting computational results. Complete vibrational assignments for DMEDA and DMPDA hydrochloride salts also will be presented.

4.2 Experimental Methods

4.2.1 Sample Preparation

Amine hydrohalide salts were prepared by adding concentrated hydrochloric acid, HCl, or hydrobromic acid, HBr, to the pure amine (dipropylamine, DPA, Aldrich; N,N'-dimethylethylenediamine, DMEDA, Aldrich; N,N'-dimethylpropylenediamine, DMPDA, Aldrich). Water was then removed from the samples by drying under vacuum until a powder was produced. Deuterium dilute samples were made by stirring the pure amine with deuterium oxide, D_2O (Cambridge Isotope Laboratories, inc.) for approximately 48 hours to allow isotopic exchange to occur. Deuterium-dilute hydrochloric or hydrobromic acid was added to the amine, and the resulting salt was dried as above. Crystals of DMEDA:2HBr and DMEDA:2HCl formed approximately 24 hours into the drying process. DMPDA:2HBr and DMPDA:2HCl crystals spontaneously formed shortly after mixing the amine and the acid.

4.2.2 Vibrational Spectroscopy

Samples were characterized using infrared and Raman spectroscopy. Samples for IR spectroscopic measurements were finely ground and prepared as KBr pellets. Infrared spectra were collected under vacuum (pressure = 13 mbar) using a Bruker IFS 66v spectrometer with a KBr beam splitter; 64 scans at a spectral resolution of 1 cm^{-1} were averaged for each spectrum. Samples for Raman spectroscopy were packed in capillary tubes. Raman spectra were collected on a Bruker Equinox 55 FRA 106/S with

a Nd:YAG laser (1064 nm; 300 mW) and a CCD detector; 1000 scans at a spectral resolution of 2 cm^{-1} were averaged for each spectrum.

4.2.3 X-Ray Crystallography

X-ray crystallographic data for these compounds were collected using a diffractometer with a Bruker APEX CCD area detector and graphite-monochromated MoKα radiation (λ = 0.71073 Å). The samples were cooled to 100(2) K. The structure was solved by direct methods and refined by full-matrix least-squares methods on F^2 [19,20]. Positions of hydrogen atoms bonded to the carbons were initially determined by geometry and refined by a riding model. The hydrogen atoms bonded to nitrogen were located on a difference map, and their positions were refined independently. Non-hydrogen atoms were refined with anisotropic displacement parameters. Hydrogen

Table 4.1 – Select crystallographic data.

	DMEDA:2HCl	**DMEDA:2HBr**	**DMPDA:2HBr***	**DMPDA:2HCl**
Final R1	0.0474	0.0232	0.0165	0.0260
Observed reflections, [I > 2σ(I)]	569	472	872	477
wR2	0.1242	0.0570	0.389	0.683
Unique reflections	624	484	976	507

*Refinement of the Flack parameter[21] suggested that the structure exhibited racemic twinning.

atom displacement parameters were set to 1.2 (1.5 for methyl) times the displacement parameters of the bonded atoms. Some of the crystallographic data are shown in Table 4.1.

4.2.4 Computations

The calculations were done by Scott Boesch. Analysis of the vibrational modes was done jointly with Scott Boesch. Experimental assignments were done solely by this author. The B3LYP hybrid Hartree-Fock/density functional method[22,23] and the 6-31G(d) split-valence plus polarization basis set[24] were used to perform complete geometry optimizations and vibrational frequency calculations for all molecules studied. The quantum chemistry program GAUSSIAN03[22] was used for the calculations. Berny's optimization algorithm[25] was utilized to perform full geometry optimizations in C_1 symmetry. Harmonic frequency calculations were performed at the optimized geometries without correcting for anharmonicity. Calculated frequencies are typically scaled to facilitate comparisons with experiment; the multiplicative scaling factors of Scott and Radom are used.[26] All frequencies less than 1000 cm^{-1} are multiplied by a factor of 1.0013, and those greater than 1000 cm^{-1} are multiplied by a factor of 0.9614. Vibrational mode assignments were performed by animating each mode using the program XMOL[27] and comparing the modes of one geometry to another using the program ViPA, an acronym for Vibrational Projection Analysis.[28-30] The ViPA program exploits the vector properties of vibrational normal modes to assess the similarity between modes of an object molecule and a structurally similar basis

molecule. The program first aligns the two molecules and calculates each molecule's normal modes and vibrational frequencies. Vibrational projection analysis has been used to compare normal modes modified by isotopic or chemical substitution, oxidation/reduction and non-covalent contacts.[15,16,28-31]

4.3 Results and Discussion

4.3.1 Crystal Structures

The crystal data for all four crystals in this study are summarized in Table 4.2. DMEDA:2HCl and DMEDA:2HBr crystallize in a monoclinic unit cell belonging to the C2/m space group. There are two molecules per asymmetric unit cell in both compounds. In the DMEDA-$2H^+$ cation, both nitrogen atoms are protonated and each ammonium hydrogen atom is hydrogen bonded to a halide ion, as shown in Figure 4.1 for DMEDA:2HCl. Additionally, each halide is hydrogen bonded to two ammonium hydrogen atoms. Both crystals pack in a one-dimensional polymeric chain along the crystallographic *c* axis, where the molecules are linked by the doubly-coordinated halide ions. The packing diagram for DMEDA:2HCl is shown in Figure 4.2. In comparing the chloride and the bromide crystals, it is interesting to note

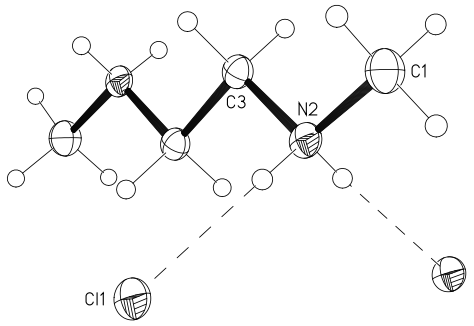

Figure 4.1 – Crystal structure of DMEDA:2HCl. In this structure, every ammonium proton is hydrogen bonded to a chloride ion.

Table 4.2 – Structural data for the DMEDA:HX and DMPDA:HX crystals.

Parameters	**DMEDA:2HCl**	**DMEDA:2HBr**	**DMPDA:2HBr**	**DMPDA:2HCl**
Crystal System	Monoclinic	Monoclinic	Orthorhombic	Orthorhombic
Space group	C2/m	C2/m	Pba2	Pbam
Temperature	100(2) K	100(2) K	100(2)	100(2)
a (Å)	18.08(2)	14.837(6)	9.6066(18)	9.4712(18)
b (Å)	5.121(3)	5.809(3)	10.4528(18)	10.091(2)
c (Å)	5.032(3)	5.352(2)	4.9959(10)	4.7840(10)
α	90º	90º	90º	90º
β	105.534(10)º	103.713(8)º	90º	90º
γ	90º	90º	90º	90º
Volume ($Å^3$)	448.8(6)	448.1(3)	501.67(16)	457.23(16)
Z	2	2	2	2
Density (Mg/m^3)	1.192	1.853	1.748	1.272
R1	0.0474	0.0203	0.0165	0.0260
Crystal size (mm^3)	0.36 x 0.17 x 0.02	0.60 x 0.42 x 0.02	0.20 x 0.10 x 0.05	0.26 x 0.14 x 0.10

that the *a* axis is significantly longer in the chloride than in the bromide, but the unit cell volumes are essentially the same.

DMPDA:2HCl and DMPDA:2HBr crystallize in an orthorhombic unit cell; the former crystal is in the Pbam space group, and the latter crystal is in the Pba2 space group. The hydrogen bonding arrangement within the two DMPDA-containing crystals is the same as that shown for DMEDA:2HCl in Figure 4.1. However, the crystal packing for the two DMPDA crystals exhibits a two-dimensional network that extends in a herring bone pattern in the *ab* plane, as shown in Figure 4.3. Unlike DMEDA:2HCl, the DMPDA:2HCl unit cell is smaller than the DMPDA:2HBr cell along all three crystallographic axes and, therefore, has a smaller unit cell volume. All

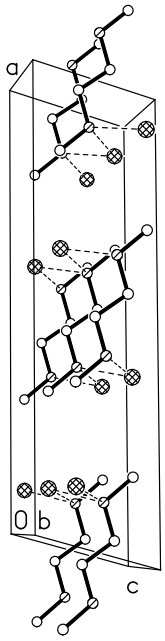

Figure 4.3 – Packing diagram of the DMEDA:2HCl crystal. This crystal and the DMEDA:2HBr crystal form a one-dimensional polymeric chain along the crystallographic *c* axis.

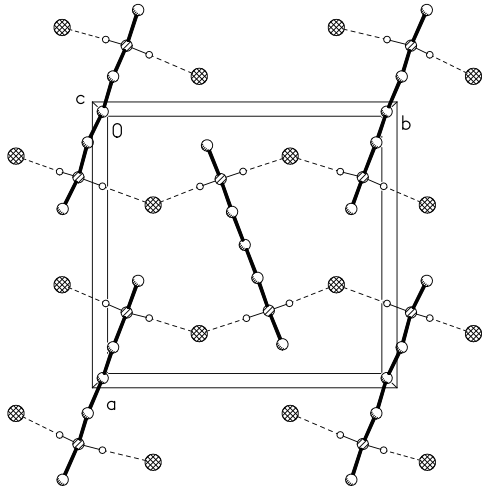

Figure 4.3 – Packing diagram of the DMPDA:2HCl crystal. This crystal and the DMPDA:2HBr crystal form a two-dimensional network that extends in a herring bone pattern in the *ab* plane.

four structures show a trans conformation for all torsional angles along the backbone. This conformation allows for the maximum separation between halide ions. These crystal structures confirm the "extended trans conformation" proposed by Baldwin in his 1962 spectroscopic studies.[10]

4.3.2 Vibrational Spectroscopic and Computational Study of NH_2^+ stretching region

4.3.2.1 DPA:HX in the NH_2^+ stretching region

DPA:HCl and DPA:HBr are the simplest secondary amine salts that were examined. Infrared spectra of both compounds are shown in Figure 4.4. In general, protonation of a secondary amine results in a change of the N-H stretching vibration from a single band[32] at 3289 cm^{-1} to a number of bands on the low frequency side of the CH stretching bands, between 2600 and 2300 cm^{-1}. Stretching modes for the NH_2^+ group are seen at 2530 and 2423 cm^{-1} for DPA:HCl and 2523 and 2409 cm^{-1} for DPA:HBr. The higher frequency band can be assigned as the symmetric NH_2^+ stretch and the lower frequency as the asymmetric NH_2^+ stretch. These bands also appear with reduced intensity in the Raman spectra of these compounds (data not shown). The small shift to lower frequencies that occurs when the anion size is increased can be attributed to the increased polarizability of the anion. This frequency shift occurs because the vibrationally-induced dipole in NH_2^+ group induces a dipole in the anion; the magnitude of the induced dipole is proportional to the polarizability of the anion. The vibrationally-induced dipole in the anion then

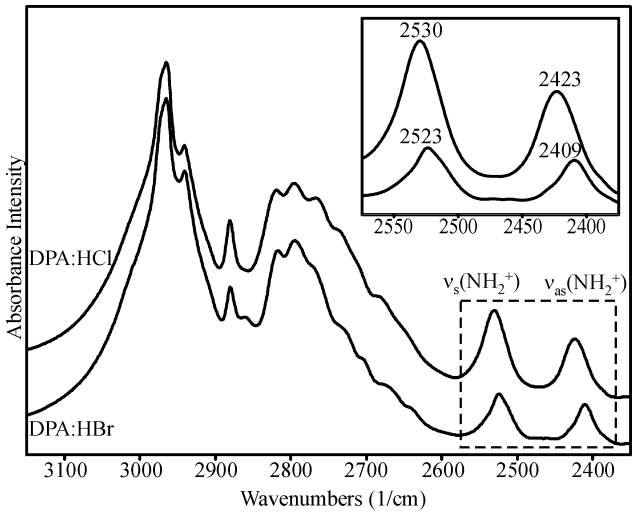

Figure 4.4 – IR spectra of DPA:HX in the CH and NH_2^+ stretching region. Inset expands NH_2^+ stretching region.

couples with the vibrationally-induced dipole of the NH_2^+ unit, shifting the vibrational mode to a lower frequency. Since the magnitude of the coupling is proportional to the polarizability of the anion, the frequency shift is lower for the bromide-containing amine salt than for the chloride-containing amine salt.

4.3.2.2 DMEDA:2HX in the NH_2^+ stretching region

The band structure in the diamine salts is more complex than in the single heteroatom amine salts, but the bands remain on the low frequency side of the CH stretching bands. Spectra of DMEDA:2HX are shown in Figure 4.5. There are four prominent features in the Raman spectra of both DMEDA:2HCl and DMEDA:2HBr. In DMEDA:2HBr, Raman bands at 2471, 2457, 2430, 2405 cm^{-1} correspond, within experimental error, to bands in the IR spectrum. There are also two weak IR bands at 2378 and 2356 cm^{-1} and a very weak Raman band 2354 cm^{-1}. These may be due to overtone or combination bands. In DMEDA:2HCl, Raman bands at 2500 and 2398 cm^{-1} correspond to

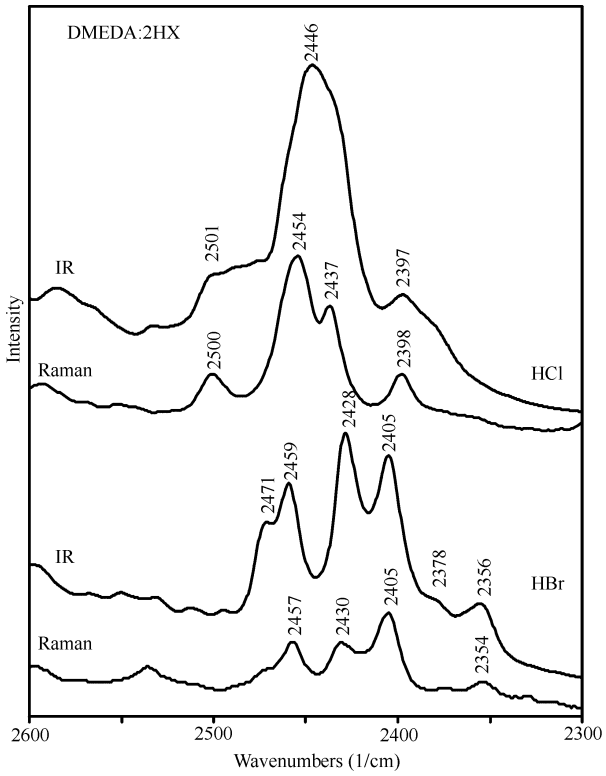

Figure 4.5 – IR and Raman spectra of DMEDA:2HX in the NH_2^+ stretching region.

bands in the IR spectrum. The Raman band at 2437 cm^{-1} is related to the low frequency shoulder of the strong IR band at 2446 cm^{-1}; the Raman band at 2454 cm^{-1} seems to correspond to the IR band at 2446 cm^{-1}.

The unit cells of both DMEDA:2HCl and DMEDA:2HBr contain two asymmetric units; each unit is comprised of a doubly protonated DMEDA molecule (with two NH_2^+ units and the two counter ions). Accordingly, there are eight N-H stretching vibrational degrees of freedom. A formal group theory analysis of the N-H stretching modes under the C2/m (C_{2h}^3) space group leads to the classification of the NH_2^+ stretching normal modes according to the irreducible representations of the C_{2h} unit cell group:

$$\Gamma(\nu(NH_2^+)) = 2A_g + 2B_g + 2A_u + 2B_u. \quad (4.1)$$

This analysis predicts four infrared-active N-H stretching modes (A_u and B_u) and four Raman-active N-H stretching modes (A_g and B_g). Given that the crystal structures of both DMEDA:2HCl and DMEDA:2HBr belong to the C_{2h}^3 space group, which has a crystallographic center of symmetry, one expects that the rule of mutual exclusion would be observed: *i.e.* modes that are infrared active are strictly Raman inactive, and conversely modes that are Raman active are strictly infrared inactive. In the DMEDA:2HCl spectra shown in Figure 4.5, only the Raman active mode at 2454 cm^{-1} and the IR active mode at 2446 cm^{-1} appear to obey the rule. All other NH stretching modes in both the HCl and HBr complexes appear to be simultaneously IR and Raman active, but have different intensities, as is expected.

It seems reasonable to suggest that the rule of mutual exclusion, although formally rigorous, is observed when intermolecular forces are present that are sufficiently strong to lead to the necessary vibrational coupling between the asymmetric units in a multiply occupied unit cell. If the vibrational coupling is very weak, then the vibrations of each asymmetric unit are essentially independent, *i.e.* each asymmetric unit is essentially isolated. In the case of sufficiently strong coupling forces, the factor group analysis (Equation 4.1) leads to four observed Raman active modes and four observed infrared active modes, which are usually shifted in frequency from each other.

This analysis suggests two possibilities to explain the NH stretching spectral data: (1) the intermolecular coupling forces are moderately weak, and although the intensities obey the mutual exclusion rule, the frequencies of pairs of factor group components (*e.g.* an A_g mode and the corresponding A_u mode) are either unshifted or only very slightly shifted, or (2) the intermolecular coupling forces are very weak so that the vibrations of the asymmetric unit ($CH_3NH_2^+CH_2CH_2NH_2^+CH_3$) are essentially independent and described by a site group approximation. The second approximation considers the NH stretching vibrations to originate in the symmetric NH_2^+ stretch, $\nu_s(NH_2^+)$, and the antisymmetric NH_2^+ stretch, $\nu_{as}(NH_2^+)$, of an isolated asymmetric unit. Since the middle of the C-C single bond lies on a two-fold rotation axis (Wyckoff g site in this space group), the asymmetric unit may be viewed as centered on the axis. Therefore, the vibrations are described in terms of the irreducible representations of the C_2 point group, which leads to the following irreducible representation structure:

$$\Gamma(\nu_s(NH_2^+)) = \Gamma(\nu_{as}(NH_2^+)) = 2A + 2B \qquad (4.2)$$

In this case, all four normal modes are simultaneously IR and Raman active.

It is important to note that the IR band at 2446 cm^{-1} is the strongest IR band in this spectral region and therefore has the largest dipole moment derivative of all the NH stretching modes. Consequently, the vibrations underlying this mode in each asymmetric unit are coupled, leading to the observed frequency difference of 8 cm^{-1} and adherence to the mutual exclusion rule. An important conclusion drawn from this interpretation is that the nature and degree of factor group coupling in a multiply occupied unit cell is dependent on the strength of the intermolecular forces responsible for the coupling of the vibrating units. In particular, if a crystal has a crystallographic center of symmetry, different normal modes may exhibit different degrees of adherence to the rule of mutual exclusion if the asymmetric unit itself does not possess a center of symmetry.

Calculated vibrational frequencies, assignments and IR intensities are summarized in Table 4.2 for a single asymmetric unit containing a DMEDA molecule, with its two NH_2^+ units, and two chloride ions. The second column describes the symmetry of the mode under the C_2 site group approximation, and the phase refers to the relative vibrational phase of the two NH_2^+ units. The factor group correlation method[33] allows the irreducible representations of the C_2 site group to be correlated to the irreducible representations of the C_{2h} unit cell group, which describes the Brillouin zone center vibrations of a crystal belonging the C_{2h}^3 factor group. This results in the following correlations:

{in-phase symmetric stretch, out-of-phase asymmetric stretch} $A \rightarrow A_g + A_u$ (4.3)

{out-of-phase symmetric stretch, in-phase asymmetric stretch} $B \rightarrow B_g + B_u$ (4.4)

The physical interpretation of Equations 4.3 and 4.4 is straightforward. A particular vibrational mode of an asymmetric unit (*e.g.* the in-phase symmetric stretching motion of an asymmetric unit, A symmetry in the C_2 site group) yields two factor group modes (A_g and A_u symmetry, respectively) when intermolecular forces couple the vibrational motions of the two asymmetric units in the cell.

The computational results summarized in Table 4.3 suggest that the two higher frequency bands in Figure 4.5 might be assigned as symmetric stretching modes coupled within a single asymmetric unit and the two lower frequency bands can be

Table 4.3 – Calculated vibrational frequencies, assigned modes and IR intensities of DMEDA:2HCl and DMPDA:2HCl.

DMEDA:2HCl

Assignment	Site Symmetry (C_2 Site Group)	Scaled Frequency (cm^{-1})	IR Intensity
$\nu_{as}(NH_2)^+$ (out-of-phase)	A	2596	1200
$\nu_{as}(NH_2)^+$ (in-phase)	B	2602	3300
$\nu_s(NH_2)^+$ (out-of-phase)	B	2634	1600
$\nu_s(NH_2)^+$ (in-phase)	A	2645	170

DMPDA:2HCl – Coupling between NH_2^+ units is weak.

Assignment	Site Symmetry (C_2 Site Group)	Scaled Frequency (cm^{-1})	IR Intensity
$\nu_{as}(NH_2)^+$ (in-phase)	B	2580	1400
$\nu_{as}(NH_2)^+$ (out-of-phase)	A	2589	2100
$\nu_s(NH_2)^+$ (out-of-phase)	B	2788	1800
$\nu_s(NH_2)^+$ (in-phase)	A	2788	54

assigned as similarly coupled antisymmetric stretching modes. This assignment is reasonable when the intermolecular coupling between the asymmetric units is very weak. In that case, Equation 4.2 predicts four modes that are simultaneously Raman and IR active. Each of these modes is each a mixture of $\nu_s(NH_2^+)$ and $\nu_{as}(NH_2^+)$ motions, although the computational results inform us that the two higher frequency bands (2471 and 2459 cm^{-1}) are predominantly due to coupled $\nu_s(NH_2^+)$ motions, while the two lower frequency bands (2428 and 2405 cm^{-1}) are predominantly due to coupled $\nu_{as}(NH_2^+)$ motions. It is interesting to note, as shown in Table 4.3, that the coupling between the two NH_2^+ units in a single DMPDA:2HCl unit is considerably smaller than that calculated for a single DMEDA:2HCl unit. This may occur because the additional methylene group in DMPDA leads to greater separation between the two NH_2^+ units and weaker through-bond coupling of the stretching modes.

4.3.2.3 DMPDA:2HX in the NH_2^+ stretching region

The unit cells of DMPDA:2HCl and DMPDA:2HBr also contain two asymmetric units, as in the case of the DMEDA salts described earlier. The space group of DMPDA:2HBr is Pba2 (C_{2v}^8); consequently, the N-H stretching modes can be classified according to the irreducible representations of the C_{2v} unit cell group as:

$$\Gamma(\nu(NH_2^+)) = 2A_1 + 2A_2 + 2B_1 + 2B_2. \quad (4.5)$$

This analysis predicts six modes that are simultaneously IR and Raman active ($2A_1 + 2B_1 + 2B_2$) and two modes that are only Raman active ($2A_2$). The A_2 mode is expected to be very weak. Thus, the spectra of DMPDA:2HBr in the N-H stretching region

should be interpreted in terms of the six modes that are simultaneously Raman and IR active. Four IR bands occur at 2501, 2493, 2451 and 2404 cm^{-1}, with corresponding bands in the Raman spectrum at 2503, 2495, 2452 and 2406 cm^{-1}. There is a weak IR band at 2529 cm^{-1}.

A similar distribution of bands in both IR and Raman spectra are also observed in the DMPDA:2HCl spectra in Figure 4.6. However, the presence of disorder in the crystal structure prevents a traditional group theory analysis. The computational results are given in Table 4.3. They are similar to the results obtained for the DMEDA:2HBr system in that the two higher frequency bands in the figure are assigned as coupled symmetric stretching modes and the two lower frequency bands are assigned as coupled antisymmetric stretching modes. The bands in the DMPDA:2HCl spectra generally occur at slightly higher frequencies than those in the DMPDA:2HBr spectra due to the decreased polarizability of the Cl^- anion.

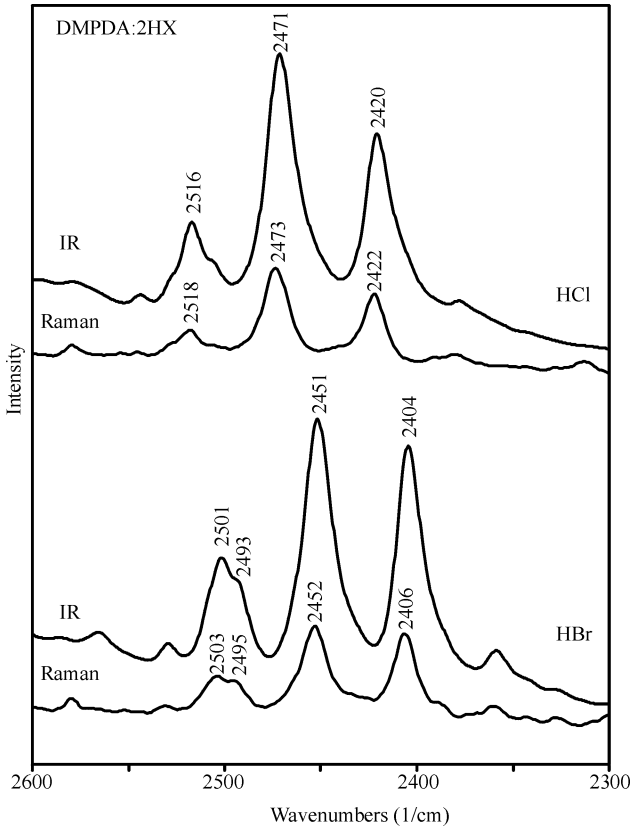

Figure 4.6 – IR and Raman spectra of DMPDA:2HX in the NH_2^+ stretching region.

4.3.3 Isotopic Dilution and the Effect on the NH^+ stretching region

Deuteration of the ammonium hydrogen atoms supports the assignment of the NH_2^+ stretching modes. In DMEDA:2HCl samples containing isotopically dilute deuterium, a band appears at 1865 cm^{-1} in the IR spectrum, as seen in Figure 4.7. This band is assigned to an ND_2^+ stretching mode. Comparing this band to the most intense NH_2^+ stretching band results in an average $\frac{\nu_D}{\nu_H}$ shift of 0.76. Similar results are observed in DMEDA:2HBr samples, where two bands are found in the IR spectrum at 1845 and 1832 cm^{-1}, also in Figure 4.7. The average deuterium shift ratio for the HBr spectrum also was approximately 0.76. These shifts are well within the accepted values.

There are a series of strong bands that appear between 2200 and 2100 cm^{-1}. Because the samples were partially substituted with deuterium, the deuterium atoms are assumed to be statistically distributed among the available

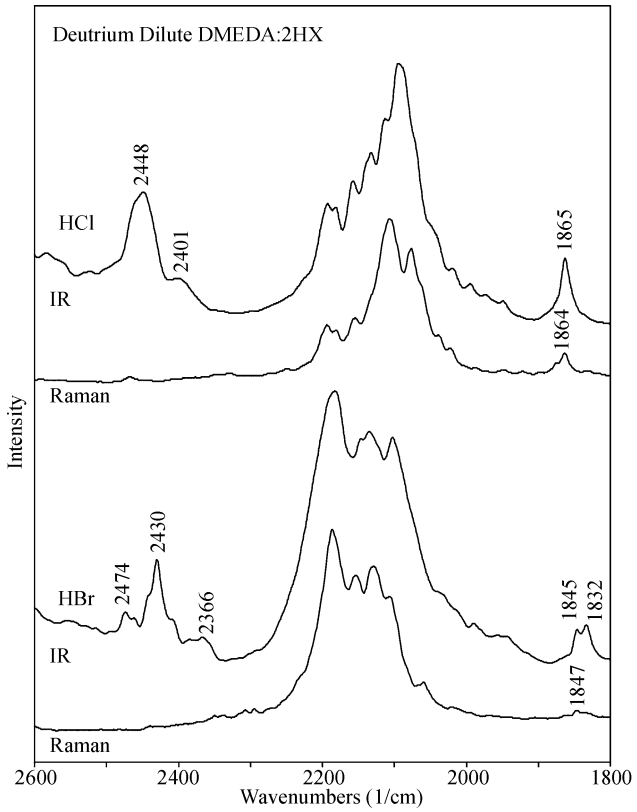

Figure 4.7 – IR and Raman spectra of deuterium-diluted DMEDA:2HX in the NH_2^+ and ND_2^+ stretching regions.

amine hydrogen atom sites in the unit cell. A single crystal of dilute deuterium-substituted DMEDA:2HCl was isolated and the crystal structure was determined by the single crystal X-ray diffraction techniques described in the Experimental section. The space group, unit cell parameters and Wyckoff site occupancy in the unit cell were identical to the non-deuterated DMEDA:2HCl crystal. This crystal structure eliminated the possibility of a hydrated compound. Consequently, the bands between 2200 and 2100 cm^{-1} are attributed to modes that contain contributions from coupled N-H and N-D stretching motions.

4.3.4 Vibrational Spectroscopic and Computational Study of Other Regions

4.3.4.1 NH_2^+ deformation region

In addition to the NH_2^+ stretching modes, the NH_2^+ deformation, sometimes described as a scissoring mode $\delta(NH_2^+)$, has a very characteristic vibrational signature. Protonation of the secondary amine produces a unit that is structurally analogous to a methylene group and, as such, has a scissoring motion that occurs from 70 to 100 cm^{-1} higher than the methylene mode. Each of the two asymmetric units in the unit cell of DMEDA:2HCl contains a single DMEDA molecule (with two NH_2^+ units). The resulting four NH_2^+ bending modes in the unit cell can be classified according to the irreducible representations appropriate to the C2/m (C_{2h}^3) space group:

$$\Gamma(\delta(NH_2^+)) = A_g + B_g + A_u + B_u. \quad (4.6)$$

This analysis predicts four scissoring modes, two infrared-active and two Raman-active. In DMEDA:2HCl two bands are observed at 1594 and 1630 cm^{-1} in the IR spectrum,

while in the Raman spectrum the corresponding bands are found at 1600 cm^{-1} and 1625 cm^{-1}, respectively, as shown in Figure 4.8. The scissoring region for DMPDA:2HCl also is shown in the figure; there is a single band at 1593 cm^{-1} in the IR spectrum and 1595 cm^{-1} in the Raman spectrum. A symmetry-based analysis of the $\delta(NH_2^+)$ mode in DMPDA:2HCl (space group Pba1) results in:

$$\Gamma(\delta(NH_2^+)) = A_1 + A_2 + B_1 + B_2. \quad (4.7)$$

The A_1, B_1 and B_2 modes are simultaneously IR and Raman active, whereas the A_2 mode is only Raman active. This analysis predicts three IR bands and four Raman bands. If the intermolecular coupling between the two asymmetric units is weak, then the vibrations of each asymmetric unit are essentially independent, and one would observe two $\delta(NH_2^+)$ modes that are simultaneously IR and Raman active. This appears to be the case (within experimental error) for these vibrations. This results from the lack of a crystallographic inversion center, which is a necessary

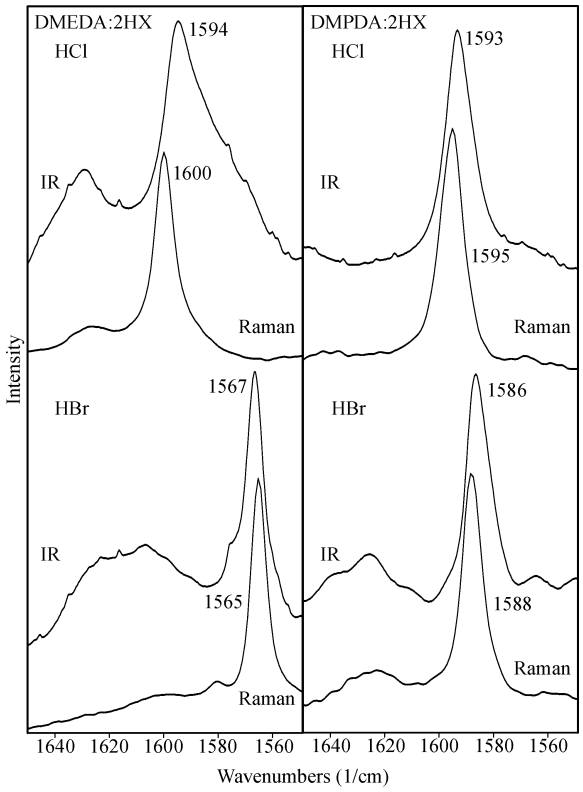

Figure 4.8 - IR and Raman spectra of DMEDA:2HX and DMPDA:2HX in the NH_2^+ bending region.

requirement for the rule of mutual exclusion to be valid: modes that are infrared active are strictly Raman inactive, and conversely, modes that are Raman active are strictly infrared inactive. In systems lacking an inversion center, bands that are strong in the Raman spectrum are often weak in the infrared spectrum, and vice versa.

The computational results show that there is a small amount of mixing between the NH_2^+ and the CH_2 deformations in DMEDA:2HCl. Such mixing was not seen in the computational results of DMPDA:2HCl. In both diamine salts, the NH_2^+ deformation shifts to lower frequencies when the counter ion is changed from chloride to bromide. The shift to lower frequencies that occurs can be attributed to the increased polarizability of the anion. This shift is analogous to the shift that occurs in the NH_2^+ stretching modes, and the reasoning for this shift is detailed above. The N-----X distances in DMEDA:2HX are 3.083(2) Å and 3.2727(19) Å for the chloride and bromide salts, respectively. The averages of the same distances in DMPDA:2HX are 3.177 Å and 3.282 Å for the chloride and bromide salts, respectively. The N-----X distance is longer in the bromide salt than in the chloride salt in both DMEDA:2HX and DMPDA:2HX. This implies that the hydrogen bond strength is somewhat weaker in both bromide salts. It has been shown that the NH_2 deformation modes in neutral amines shift to higher frequency with increasing hydrogen bond strength.[34,35] It is reasonable that the same trend would be seen in the NH_2^+ unit. Therefore, in addition to the polarizability, the decrease in the hydrogen bond strength in the bromide salt, as compared to the chloride salt, also contributes to the decrease in frequency. The differences in the bond lengths is greater in DMEDA:2HX (0.190 Å) than in

DMPDA:2HX (0.005 Å) which leads to a larger decrease in hydrogen bond strength in DMEDA:2HX. This may account for most of the shift of approximately 30 cm^{-1} in DMEDA complexes, in comparison to a shift of slightly less than 10 cm^{-1} observed in DMPDA complexes.

4.3.4.2 CH stretching region

The CH stretching modes of the protonated amines cover a frequency range significantly larger than expected in comparison to the unprotonated amines. This region of the IR spectra is shown in Figure 4.9. In each spectrum, the bands split into two groups; one from approximately 3020 to 2850 cm^{-1} and another from 2850 to 2670 cm^{-1}. The higher frequency group can be assigned to both CH_3 and CH_2 asymmetric stretching modes. The asymmetric frequency range is a bit wider than usual, but it is reasonable for methyl and methylene groups next to a nitrogen atom.[34,35] The frequencies of the symmetric modes in the protonated amine (2850 – 2670 cm^{-1}) are lower than expected in comparison to the unprotonated amine.

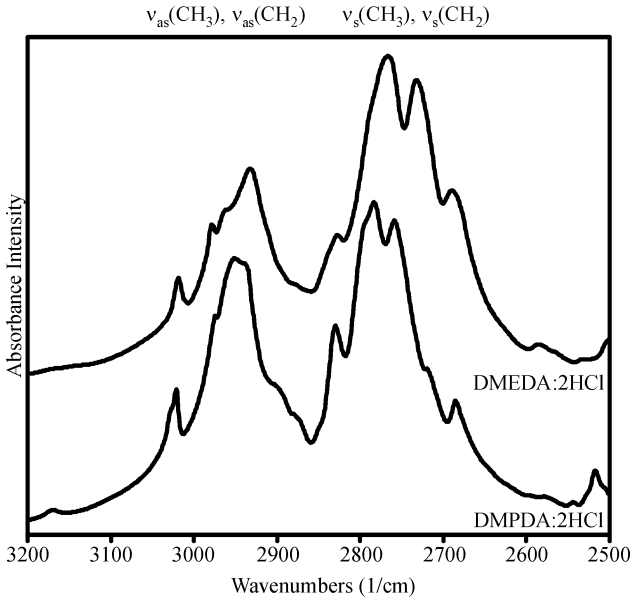

Figure 4.9 – IR spectra of DMEDA:2HCl and DMPDA:2HCl in the CH stretching region.

Table 4.4 – Sum of Mulliken charges calculated for methyl and methylene units in DMEDA and DMEDA:2HCl.

	Methyl	Methylene
DMEDA	0.120	0.132
DMEDA:2HCl	0.235	0.239

Protonation of the amine nitrogen results in electron density being pulled away from these alkyl groups, consequently shifting the CH stretching modes to lower frequencies. However, this effect is more dramatic in the symmetric modes, as the asymmetric stretching modes are relatively insensitive to neighboring groups.[35] The sum of the atomic charges on the alkyl groups, as determined by the computational results in Table 4.4, confirms a reduction of electron density compared to the neutral DMEDA molecule in both the methyl and methylene groups.

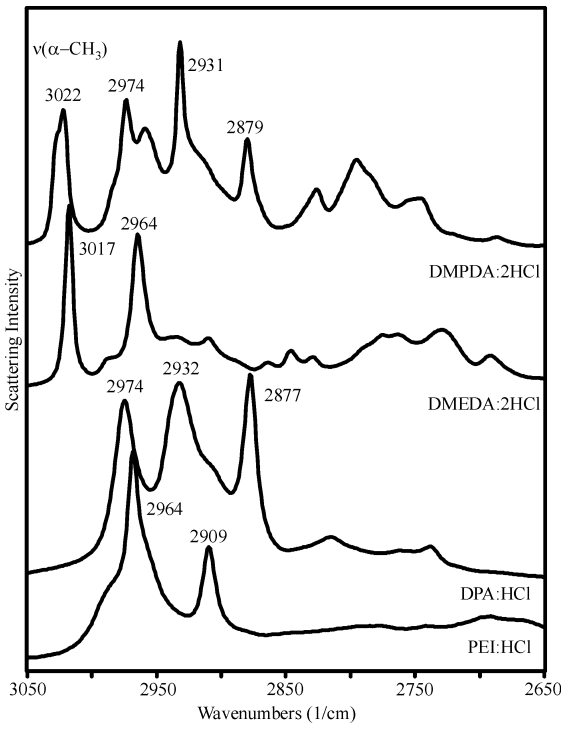

Figure 4.10 – Raman spectra of DMEDA:2HCl, DMPDA:2HCl, DPA:HCl and PEI:HCl in the CH stretching region.

In DMEDA:2HX and DMPDA:2HX, there is a band that is seen between 3017 and 3021 cm^{-1} in both the IR and Raman spectra. This

frequency is higher than expected for an aliphatic CH stretching mode. Figure 4.10 shows a comparison of several secondary amine salts in this region. This band does not appear in either dipropylamine hydrochloride or poly(ethylenimine) hydrochloride, neither of which have a methyl group alpha to the nitrogen atom. Lin-Vien *et al.* have reported a similar band in tetramethyl ammonium salts and have assigned this band to a methyl stretching motion.[34] Therefore, this band is assigned as the stretching motion of a methyl group that is alpha to a protonated nitrogen atom.

4.3.4.2 Low Frequency Regions

The frequency region below 1500 cm^{-1} contains many highly mixed bands, some of which are sensitive to the coordinating counter ion. Complete assignments of the vibrational spectra of DMEDA:2HCl and DMPDA:2HCl, based on the calculated vibrational modes, can be found in Tables 4.5 and 4.6, respectively. These tables show that the modes from the NH_2^+ units mix into many of the bands in

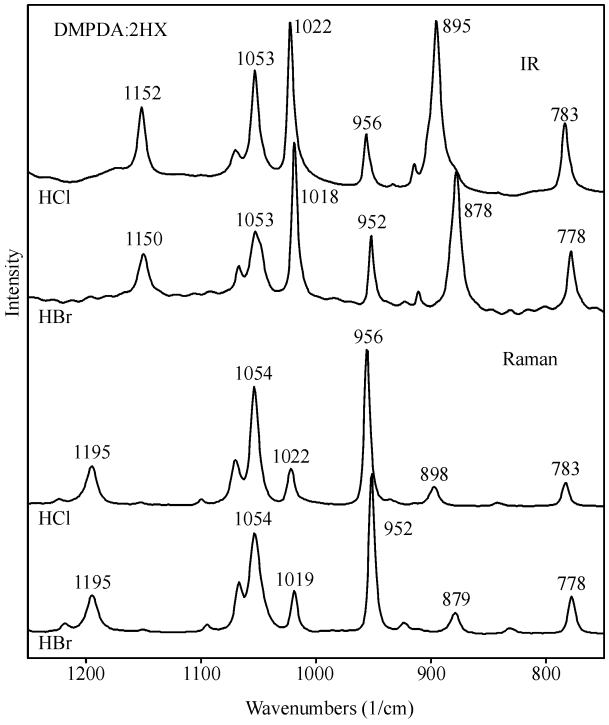

Figure 4.11 – IR and Raman spectra of lower frequency region of DMPDA:2HX.

this region, from the rocking modes around 800 cm^{-1} to the alkyl deformations at ca. 1500 cm^{-1}. This effect is particularly evident in DMPDA:2HX, as seen in Figure 4.11. The significance of the contribution of the NH_2^+ unit can be seen in the magnitude of

Table 4.4 – Experimental mode assignments of DMEDA:2HCl.

Mode Assignments	IR Freq	Raman Freq
τ CH_3		150
chain bend		281, 332
δ CNC + δ NCC		388
ρ CH_2 + ρ $(NH_2)^+$	797, 805	
ρ CH_2 + ν CN		885
ν CN + ω CH_3 + ρ $(NH_2)^+$ + ρ CH_2	907, 915	942, 977
ω CH_3 + ρ CH_2	1020	1016
ν CN + ν CC	1056	1046, 1065
ν CN + ω CH_3 + ρ $(NH_2)^+$ + τ CH_2	1100(sh), 1106	
ω CH_3	1138, 1155	1200
ω CH_3 + ρ $(NH_2)^+$ + ρ CH_2		1236
τ CH_2	1292, 1320, 1329	1288, 1326
ω CH_2 + $\delta_s CH_3$	1413(sh), 1430	1397
$\delta_s CH_3$		1407
$\delta_{as} CH_3$ + τ $(NH_2)^+$		1438
δ CH_2 + $\delta_{as} CH_3$ + τ $(NH_2)^+$	1458, 1467, 1478	1461, 1479, 1485
ω $(NH_2)^+$	1489, 1492	
δ $(NH_2)^+$	1594, 1629	1600, 1625
ν $(NH_2)^+$ asymmetric out-of-phase	2379(sh), 2397	2398
ν $(NH_2)^+$ asymmetric in-phase + symmetric out-of-phase	2433(sh), 2446, 2460	2437, 2455
ν $(NH_2)^+$ symmetric in-phase	2475(sh), 2486, 2501	2500
$\nu_s CH_2$ + $\nu_s CH_3$	2689, 2731, 2767, 2788(sh), 2828	2692, 2729, 2763, 2775, 2829, 2845, 2864
$\nu_{as} CH_2$ + $\nu_{as} CH_3$	2933, 2962, 2978, 3019	2910, 2935, 2964, 2988, 3018

Table 4.5 – Experimental mode assignments of DMPDA:2HCl.

Mode Assignments	IR Frequency	Raman Frequency
ω CH_3		135(sh), 149, 176, 238
chain bend		294, 319
δ CCC		435
δ CNC		500
ρ CH_2	783	783
ρ $(NH_2)^+$ + ρ CH_2 + τ CH_2	879(sh), 895, 902(sh)	843, 898
ω CH_3 + ρ $(NH_2)^+$ + ν CC	914	
ω CH_3 + ρ $(NH_2)^+$	956	936, 956
ω CH_3 + ρ CH_2	1022	1022
ν CC + ν CN	1053, 1070	1054, 1071
ω CH_3 + τ CH_2		1100
ω CH_3	1152	1195
ω CH_3 + ρ $(NH_2)^+$ + τ CH_2		1224
τ CH_2 + ω CH_2	1290	1279
ω CH_3 + ρ $(NH_2)^+$ + τ CH_2	1324	1327
ω CH_2 + $\delta_s CH_3$ + τ $(NH_2)^+$	1374	
$\delta_{as} CH_3$ + τ $(NH_2)^+$ + ω CH_2	1401, 1418, 1447	1401, 1418, 1433
δ CH_2 + $\delta_{as} CH_3$ + τ $(NH_2)^+$ + ω $(NH_2)^+$	1447, 1462, 1470, 1476, 1485(sh), 1490	1461, 1469, 1476, 1482, 1492
δ $(NH_2)^+$	1593	1595
ν $(NH_2)^+$	2378, 2421, 2472, 2505, 2517, 2544	2422, 2473, 2518
$\nu_s CH_2$ + $\nu_s CH_3$	2685, 2718(sh), 2759, 2783, 2829	2687, 2746, 2746, 2826
$\nu_{as} CH_2$ + $\nu_{as} CH_3$	2938, 2951, 2974, 3021, 3027(sh)	2879, 2912(sh), 2932, 2958, 2973, 2983(sh), 3022, 3027(sh)

the shift of the band when the counter ion is changed from chloride to bromide. In both the IR and the Raman spectra, shifts to lower frequencies can be seen in the DMPDA:2HCl bands at 956, 895, and 783 cm^{-1}. However, the shift in the 895 cm^{-1} band is almost four times larger than the shift of the other two bands. The 895 cm^{-1} band has contributions from both NH_2^+ and CH_2 rocking modes.

The large shift occurs because coupling between the NH_2^+ rocking motion and the rocking motion of the CH_2 modes results in what is essentially an extended chain rocking mode. Similar coupled rocking modes are seen in straight chain alkanes.[34] Various motions of the NH_2^+ unit mix with the other modes, but to a much smaller degree. A comparison of the Raman and IR spectrum for both DMPDA:2HCl and DMPDA:2HBr (Figure 4.11) shows that almost all bands are simultaneously IR and Raman active in each crystal.

Figure 4.12 shows IR and Raman spectra for DMEDA:2HCl and DMEDA:2HBr in a comparison similar to that for the DMPDA:2HX salts illustrated in Figure 4.11. The shifts due to the counter ion in the DMEDA:2HX bands are more pronounced in modes containing contributions from the CN stretching modes, as in the Raman peak at 885 cm^{-1} and the IR peak at 1056 cm^{-1}. In comparison, the band in DMPDA:2HX at 1053 cm^{-1} in the IR spectrum and 1054 cm^{-1} in the Raman spectrum, shown in Figure 4.11, which contains contributions from the CN stretching mode, does not shift in frequency. The sum of the Mulliken charges on the backbone differs by only 5%, but the charge is spread over two methylene units in DMEDA:2HCl, while it is spread over three methylene units in DMPDA:2HCl. Therefore, the difference in the spectra could

be accounted for by the fact that the electron density along the backbone of DMPDA:2HX is greater, and therefore less affected by protonation, than in DMEDA:2HX because of the additional methylene unit present in the propylene backbone. When the counter ion is changed from chloride to bromide in DMEDA:2HX, there is a switch in the relative intensities of the two bands at 915 and 906 cm^{-1}. In the chloride spectra, the higher frequency feature is more intense, while the lower frequency feature is more intense in the bromide. This intensity switch is also seen in the two bands at 807 and 797 cm^{-1}. The computational results predict only one mode in each of these two regions, but they describe the vibrations of a single asymmetric unit. The splitting is attributed to factor-group splitting due to the presence of two asymmetric units in the unit cell. Both of these modes contain contributions from the NH_2^+ rocking motion, so the shift in intensity may be due a change in the interaction with the counter ion. A comparison of the Raman and IR spectrum for both DMEDA:2HCl and DMEDA:2HBr (Figure 4.12)

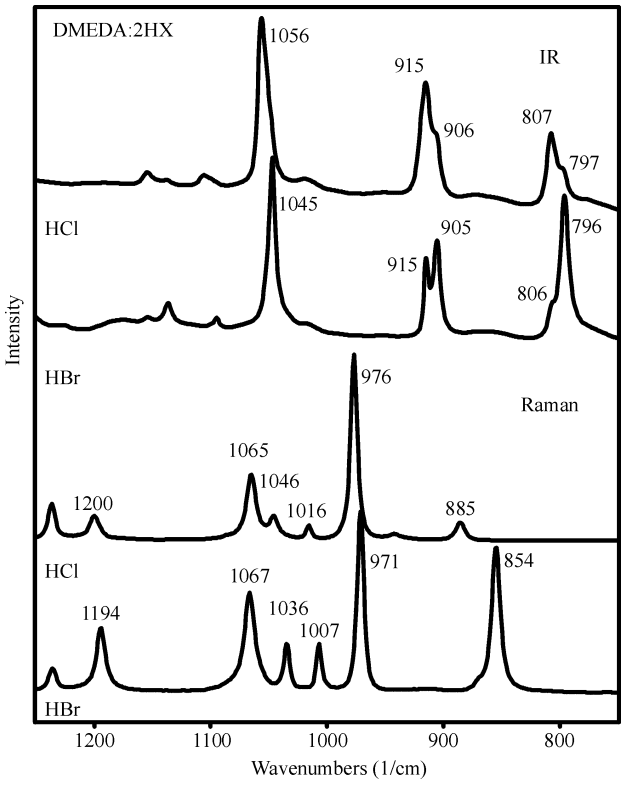

Figure 4.12 – IR and Raman spectra of lower frequency region of DMEDA:2HX.

shows that the rule of mutual exclusion is observed in this spectral region, *i.e.* no mode is simultaneously IR and Raman active. This is expected because the C_{2h}^3 space group possesses an inversion center, which is necessary for the rule of mutual exclusion to hold. The bands in Figure 4.12 are in sharp contrast to the NH stretching vibrations in these two systems where the four prominent NH stretching bands in the DMEDA:2HCl spectra seem to obey the mutual exclusion rule in the observed intensities, but the intermolecular coupling is too weak to result in a frequency shift. It was suggested above that the nature and degree of factor group coupling in a unit cell containing more than one asymmetric unit might depend on the strength of the interaction responsible for the coupling of the vibrating units. In a crystal with a crystallographic inversion center, different normal modes may exhibit different degrees of adherence to the rule of mutual exclusion if the asymmetric unit itself does not possess a center of symmetry, as is the case here.

4.3.5 Isotopic Dilution and the Effect on the Lower Frequency region

The deuterium dilution experiments result in spectra that contain a number of multi-featured bands and some new bands, as shown in Figure 4.13 for DMEDA:2HBr. Deconvolution of these bands is somewhat difficult due to the mix of isotopes and the mixing of the modes as seen above and in Table 4.5. The mutual exclusion rule is observed in the spectra of the undeuterated DMEDA:2HBr sample, as seen in Figure 4.12. However, in a crystal partially substituted with deuterium, the statistical distribution of deuterium atoms in the unit cell destroys the inversion center and breaks

the symmetry-based rule of mutual exclusion. Therefore, coincident bands appear in the IR and Raman spectra, *e.g.* 1224/1221, 1185/1886, 1169, 1101, 1002, 1093, 1055/1053, 909/911, 808/809, 795/796, 742/745, 696/695 cm^{-1}. The bands at 695 and 745 cm^{-1} in the Raman spectrum of the dilute deuterium sample appear to be isotopically shifted $\left(\frac{\nu_D}{\nu_H} = 0.76\right)$ from the 915/905 cm^{-1} IR band and the 971 cm^{-1} Raman band, respectively, in the undeuterated sample. These bands contain contributions from the NH_2^+ rocking modes and, therefore, would be expected to shift when deuterated. The series of new bands that appear between approximately 930 and 900 cm^{-1} could result from both the isotopic shifting of bands and the break-down of the mutual exclusion rule upon deuteration.

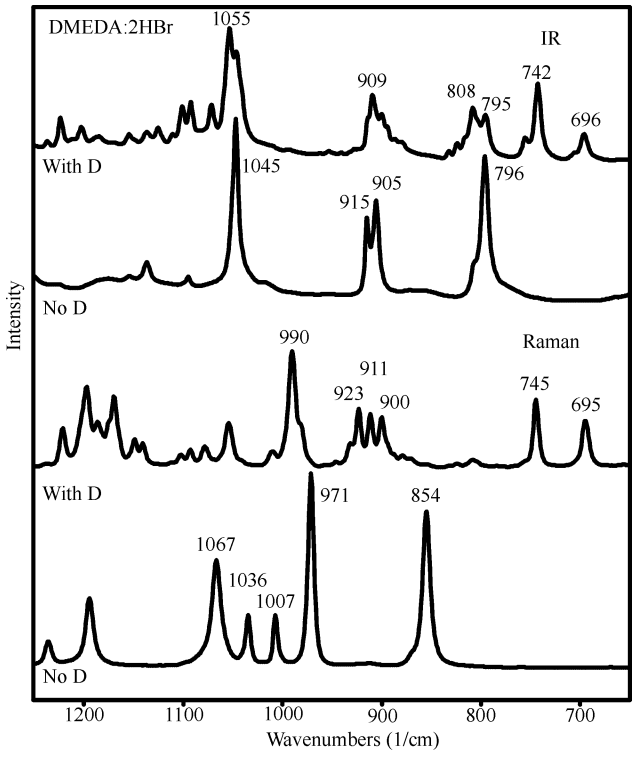

Figure 4.13 - IR and Raman spectra of deuterium dilute DMEDA:2HX in the lower frequency region.

4.4 Summary and Conclusions

The NH_2^+ stretching vibrations for several secondary amine halide salts are examined. The low frequencies of these modes (2530 – 2359 cm^{-1}) can be attributed to both the charge on the nitrogen atom and the strong hydrogen bonds formed with the chloride ions. It has been reported that the "free" N^+-H_x stretching frequency is approximately 3100 cm^{-1} in salts, $[(C_2H_5)_xNH_y]^+(BPh_4)^-$, where x + y = 4.[36] The N^+-H_x unit can be considered "free" or isolated due to the very weak interaction between the charge-protected tetraphenylborate $(BPH_4)^-$ anion and the cation.[36,37] A frequency near 3100 cm^{-1} was seen in the computational results of the protonated amine when the chloride counter ions were not present. The additional decrease in the NH_2^+ stretching frequencies can be attributed primarily to the strong hydrogen bonds with the chloride ions. A change in the anion from chloride to bromide results in an additional small frequency shift, $(NH_2^+)Cl^- \rightarrow (NH_2^+)Br^-$ = 7 – 25 cm^{-1}, from the increased polarizability of the Br^- anion.

The increase in the backbone carbon chain length in DMPDA, compared to DMEDA, leads to a relative decrease in the through-bond vibrational coupling between NH_2^+ units of the DMPDA molecule. The splitting between highest and lowest frequency bands is 66 cm^{-1} in the Raman spectrum of DMEDA:2HBr and 97 cm^{-1} in DMPDA:2HBr, with almost identical values in the IR spectrum. Similar results are obtained in comparisons of the IR and Raman spectra of the HCl complexes. Further, the separation between bands is clearly wider in DMPDA:2HX (with the exception of the two highest frequency bands) in all spectra shown in Figures 4.5 and 4.6. The

reduced coupling in the DMPDA complexes is also illustrated in the computational results. In Table 4.2, the difference between the highest and lowest NH_2^+ stretching frequencies is 49 cm^{-1} in DMEDA:2HCl and 208 cm^{-1} in DMPDA:2HCl.

One of the more interesting results is the role of intermolecular coupling in determining the nature of the factor group vibrations. This is particularly striking because of the presence of a crystallographic inversion center in the DMEDA:2HX crystals. The presence of a crystallographic inversion center rather than a molecular inversion center formally leads to vibrational modes that obey the rule of mutual exclusion: modes that are IR active are symmetry-forbidden in the Raman spectrum, and conversely, modes that are Raman active are symmetry-forbidden in the IR spectrum. However, the extent to which this exclusion rule is observed is highly dependent on the strength of the intermolecular forces that couple the vibrations of asymmetric units in the unit cell. This study shows that it is possible to have strongly coupled modes that appear to follow the exclusion rule and weakly coupled modes whose vibrations appear to be those of "independent" units and whose intensities, which are simultaneously IR and Raman active, do not follow the exclusion rule. However, another interpretation in this latter case may also be that the coupling is too weak to shift the frequencies but does lead to the rule of mutual exclusion in the observed intensities. In the latter interpretation, a Raman active and infrared active mode resulting from the coupling of the same normal mode in each asymmetric unit will be observed at a coincident frequency in both the Raman and IR spectrum.

Vibrations of the NH_2^+ unit in the protonated secondary amine mix into modes throughout the whole lower frequency, much as the NH unit does in the unprotonated amines.[15] This is evident in both the shifting of bands observed in the experimentally measured spectra and the mixed modes present in the computational results, which show that the sensitivity of CN stretching modes in DMEDA:2HX accounts for the most dramatic shifts upon changing the counter ion. In comparison, the mixing of the NH_2^+ unit in DMPDA largely accounts for the same effect. While the isotopic dilution experiments simplified some assignments in the NH_2^+ stretching region, the presence of deuterium complicated the spectrum in the lower frequency region. The distribution of deuterium and hydrogen atoms in the unit cell cause a break-down of the mutual exclusion rule in DMEDA:2HBr. This effect, combined with the isotopic shift of the NH_2^+ rocking motion, accounts for the new bands present below approximately 950 cm^{-1}.

The findings reported here can be useful in interpreting the results seen in protonated polyamine systems, which may have an important role as electrolytes in fuel cells. Determining the characteristic NH_2^+ and other group frequencies of protonated amines provides an important basis for understanding the nature of protonated sites in polyamine systems.

4.5 References

(1) Lee, S. B.; Koepsel, R.; Stolz, D. B.; Warriner, H. E.; Russell, A. J. *J. Am. Chem. Soc.* 2004, *126*, 13400-13405.

(2) Lin, J.-J.; Chu, C.-C.; Chiang, M.-L.; Tsai, W.-C. *Adv. Mater.* 2006, *18*, 3248-3252.

(3) Alpoz, A. R.; Tosun, N.; Eronat, C.; Delen, N.; Sen, B. H. *Environ. Int.* 2001, *26*, 137-142.

(4) Chattopadhyay, A.; Adhikari, S.; Adhikary, S. P.; Ayyappan, S. *Chem. Ecol.* 2007, *23*, 279-287.

(5) Li, S. N.; Kole, R. K. *Toxicol. Environ. Chem.* 2004, *86*, 237-243.

(6) Chenon, B.; Sandorfy, C. *Can. J. Chem.* 1958, *36*, 1181-206.

(7) Brissette, C.; Sandorfy, C. *Can. J. Chem.* 1960, *38*, 34-44.

(8) Mureinik, R. J.; Robb, W. *Spectrochim. Acta, Part A* 1968, *24*, 377-84.

(9) Heacock, R. A.; Marion, L. *Can. J. Chem.* 1956, *34*, 1782-95.

(10) Baldwin, M. E. *Spectrochim. Acta* 1962, *18*, 1455-61.

(11) Douse, C. S.; Tooke, P. B. *Can. J. Spectrosc.* 1973, *18*, 101-9.

(12) Stone, P. J.; Craig, J. C.; Thompson, H. W. *J. Chem. Soc.* 1958, 52-4.

(13) Bellanato, J. *Spectrochim. Acta* 1960, *16*, 1344-57.

(14) Cook, D. *Can. J. Chem.* 1964, *42*, 2292-9.

(15) Boesch, S. E.; York, S. S.; Frech, R.; Wheeler, R. A. *PhysChemComm* 2001.

(16) York, S. S.; Boesch, S. E.; Wheeler, R. A.; Frech, R. *PhysChemComm* 2002, *5*, 99-111.

(17) Kociok-Koehn, G.; Lungwitz, B.; Filippou, A. C. *Acta Crystallogr., Sect. C: Cryst. Struct. Commun.* 1996, *C52*, 2309-2311.

(18) Prince, P.; Miller, J. A.; Fronczek, F. R.; Gandour, R. D. *Acta Crystallogr., Sect. C: Cryst. Struct. Commun.* 1990, *46 (Pt 2)*, 336-8.

(19) Sheldrick, G. M. *SHELXTL Version 6.10 Reference Manual*; Bruker-AXS, 5465 E. Cheryl Parkway, Madison, WI 53711-5373 USA, 2000.

(20) Tables 6.1.1.4, and 4.2.4.2, Ed.; Kluwer: Boston, 1995.

(21) Flack, H. D. *Acta Crystallogr., Sect. A: Found. Crystallogr.* 1983, *A39*, 876-81.

(22) Frisch, M. J.; Trucks, G. W.; Schlegel, H. B.; Scuseria, G. E.; Robb, M. A.; Cheeseman, J. R.; Montgomery, J. A.; Vreven, T.; Kudin, K. N.; Burant, J. C.; Millam, J. M.; Iyengar, S. S.; Tomasi, J.; Barone, V.; Mennucci, B.; Cossi, M.; Scalmani, G.; Rega, N.; Petersson, G. A.; Nakatsuji, H.; Hada, M.; Ehara, M.; Toyota, K.; Fukuda, R.; Hasegawa, J.; Ishida, M.; Nakajima, T.; Honda, Y.; Kitao, O.; Nakai, H.; Klene, M.; Li, X.; Knox, J. E.; Hratchian, H. P.; Cross, J. B.; Bakken, V.; Adamo, C.; Jaramillo, J.; Gomperts, R.; Stratmann, R. E.; Yazyev, O.; Austin, A. J.; Cammi, R.; Pomelli, C.; Ochterski, J. W.; Ayala, P. Y.; Morokuma, K.; Voth, G. A.; Salvador, P.; Dannenberg, J. J.; Zakrzewski, V. G.; Dapprich, S.; Daniels, A. D.; Strain, M. C.; Farkas, O.; Malick, D. K.; Rabuck, A. D.; Raghavachari, K.; Foresman, J. B.; Ortiz, J. V.; Cui, Q.; Baboul, A. G.; Clifford, S.; Cioslowski, J.; Stefanov, B. B.; Liu, G.; Liashenko, A.; Piskorz, P.; Komaromi, I.; Martin, R. L.; Fox, D. J.; Keith, T.; Al-Laham, M. A.; Peng, C. Y.; Nanayakkara, A.; Challacombe, M.; Gill, P. M. W.; Johnson, B. G.; Chen, W.; Wong, M. W.; Gonzalez, C.; Pople, J. A.; Gaussian, Inc.: Wallingford, CT, 2004.

(23) Stephens, P. J.; Devlin, F. J.; Chabalowski, C. F.; Frisch, M. *J. Phys. Chem.* 1994, *98*, 11623-11627.

(24) Hehre, W. J.; Radom, L.; Schleyer, P. v. R.; Pople, J. A. *Ab initio Molecular Orbital Theory*; John Wiley & Sons: New York, 1986.

(25) Schlegel, H. B. *J. Comput. Chem.* 1986, *3*, 214-218.

(26) Scott, A. P.; Radom, L. *J. Phys. Chem.* 1996, *100*, 16502-16513.

(27) Wasikowski, C.; Klemm, S.; Research Equipment, Inc. d.b.a. Minnesota Supercomputer Center, Inc.: 1993.

(28) Grafton, A. K.; Wheeler, R. A. *J. Comput. Chem.* 1998, *19*, 1663-1674.

(29) Grafton, A. K.; Wheeler, R. A. *Comput. Phys. Commun.* 1998, *113*, 78-84.

(30) Wise, K. E.; Pate, J. B.; Wheeler, R. A. *J. Phys. Chem. B* 1999, *103*, 4764-4772.

(31) Razeghifard, M. R.; Kim, S.; Patzlaff, J. S.; Hutchison, R. S.; Krick, T.; Ayala, I.; Steenhuis, J. J.; Boesch, S. E.; Wheeler, R. A.; Barry, B. A. *J. Phys. Chem. B* 1999, *103*, 9790-9800.

(32) Rocher, N. M.; Frech, R.; Khan, M. *J. Phys. Chem. B* 2005, *109*, 20697-20706.

(33) Fately, W. G.; Dollish, F. R.; McDevitt, N. T.; Bentley, F. F. *Infrared and Raman Selection Rules For Molecular and Lattice Vibrations: The Correlation Method*; Wiley-Interscience: New York, 1972.

(34) Lin-Vien, D.; Colthup, N. B.; Fateley, W. G.; Grasselli, J. G. *The Handbook of Infrared and Raman Characteristic Frequencies of Organic Molecules*; Academic Press, Inc.: New York, 1991.

(35) Socrates, G. *Infrared and Raman Characteristic Group Frequencies*; 3rd ed.; John Wiley & Sons: New York, 2001.

(36) Nakamoto, K.; Margoshes, M.; Rundle, R. E. *J. Am. Chem. Soc.* 1955, *77*, 6480-6.

(37) Rocher, N. M.; Frech, R. *Macromolecules* 2005, *38*, 10561-10565.

CHAPTER V

SPECTROSCOPIC INVESTIGATION OF POLY(ETHYLENIMINE) HYDROCHLORIDE

5.1 Introduction

Linear poly(ethylenimine) hydrochloride, PEI·HCl is the base polymer for the entire poly(ethylenimine), PEI, family of compounds. PEI·HCl can be neutralized to PEI, which can synthetically modified to form the alkyl side-chain series of polymers that can be used in anhydrous applications, *e.g.* battery applications. Additionally, PEI·HCl itself can be modified by cross-linking and acid-doping for aqueous applications, *e.g.* fuel cell applications. PEI·HCl was studied by Chatani *et al.*[1] in the 1980s, and a crystal structure was determined from x-ray diffraction data. In the previous chapter, small molecule secondary amine salts are studied; crystal data and computational results are used to assign the peaks in the experimental spectra of secondary amine and diamine salts. The results from the secondary amine salts, combined with the vibrational assignments of the PEI spectra,[2] can be used to assign the vibrational spectra of PEI·HCl.

5.2 Experimental Methods

5.2.1 Polymer Synthesis

Linear poly(ethylenimine)-hydrochloride (PEI·HCl) was prepared by acidic

hydrolysis of poly(2-ethyl-2-oxazoline) (Aldrich, average M_w ca. 500,000).[3,4] Deuterium-dilute samples were made by dissolving neutral PEI in d-Methanol, MeOD (Cambridge Isotope Laboratories, inc.), and stirring for approximately 48 hours to allow isotopic exchange to occur. Deuterium-dilute hydrochloric acid was added to the solution and a white solid immediately precipitated. The water was then removed from the samples by drying under vacuum.

5.2.2 Vibrational Spectroscopy

Samples for IR spectroscopic measurements were finely ground and prepared as KBr pellets. Infrared spectra were collected under vacuum (pressure = 13 mbar) using a Bruker IFS 66v spectrometer with a KBr beam splitter; 64 scans at a spectral resolution of 1 cm^{-1} were averaged for each spectrum. Samples for Raman spectroscopy were packed in capillary tubes. Raman spectra were collected on a Bruker Equinox 55 FRA 106/S with a Nd:YAG laser (1064 nm; 300 mW) and a CCD detector; 1000 scans at a spectral resolution of 2 cm^{-1} were averaged for each spectrum.

5.3 Results and Discussion

5.3.1 Comparison of Crystal Structure of N,N'-DMEDA:2HCl Model Compound with PEI·HCl

The crystal structure for PEI·HCl was determined by Chatani *et al.*[1] The unit cell of the PEI·HCl powder sample was found to be metrically tetragonal. However, the authors found no tetragonal space groups that fit the data and contained only a single

chain.[1] As a result, they proposed that the unit cell really must be orthorhombic or monoclinic, not tetragonal. There are four possible space groups, one monoclinic and three orthorhombic, that have been proposed.[1] Selected parameters for the PEI·HCl crystal are given in Table 5.1. The parameters in the table for PEI·HCl appear to be for an orthorhombic crystal, but the unit cell could actually be monoclinic, considering the experimental error within the parameters.

N,N'-DMEDA has been previously used as a model compound for PEI.[2,5,6] Similarly, N,N'-DMEDA:2HCl can be used as a model compound for PEI·HCl. Selected parameters for the N,N'-DMEDA:2HCl crystal are compared to PEI·HCl in Table 5.1. In both cases, the molecular structure includes the molecule/polymer backbone lying in a nearly planar zigzag (*i.e.* all trans) conformation. Every nitrogen atom is bonded to two hydrogen atoms and every ammonium hydrogen atom is hydrogen-bonded to a chloride ion. In both cases, the N-H···Cl angle is nearly 180 degrees. However, unlike in N,N'-DMEDA:2HCl where no special positions are occupied, the two nitrogen atoms and two chloride ions all occupy special sites.[1] In PEI·HCl, there are two repeat units contained within the unit cell.[1] The polymer chain extends along the crystallographic *c* axis and the hydrogen bonding arrangement is exhibited along the *a* and *b* axes. The magnitude of these axes can be compared to the *b* and *c* axes in N,N'-DMEDA:2HCl. The difference in these axes is about 1%. In comparing the N·····Cl distance, this difference is also approximately 1%. The similarities in the structural conformation and the small differences in parameters affected by hydrogen bonding imply that N,N'-DMEDA:2HCl is a good structural

model for PEI·HCl. This also implies that the vibrational spectrum of PEI·HCl should be similar to that N,N'-DMEDA:2HCl.

Table 5.1 – Comparison of select parameters for N,N'-DMEDA:2HCl complex and PEI·HCl[1].

Parameters	**N,N'-DMEDA:2HCl**	**PEI·HCl[1]**
Crystal System	Monoclinic	Orthorhombic / Monoclinic
Space group	C2/m (C_{2h}^3)	$P222_1$ (D_2^2), $Pcm2_1$ (C_{2v}^2), $Pc2m$ (C_{2v}^4) / $P2_1/m$ (C_{2h}^2)
a (Å)	18.08(2)	5.06
b (Å)	5.121(3)	5.06
c (Å)	5.032(3)	7.57
d(N·····Cl)	3.083(2)	3.05

5.3.2 Assignment of Vibrational Spectra by Comparison with PEI and N,N'-DMEDA:2HCl.

Small molecule model compounds have been particularly useful in assigning the vibrational spectra of polymers.[2,7,8] N,N'-DMEDA:2HCl is a good model compound for PEI·HCl, as discussed above. Vibrational assignments have been previously made for the experimental spectra of neutral PEI.[2] These assignments also will be useful in assigning the vibrational spectra of PEI·HCl, as even with rearrangement of the electron density about the nitrogen atom due to protonation, there are many similarities between the two sets of spectra. Therefore, to make the best assignments for PEI·HCl, comparisons with both N,N'-DMEDA:2HCl and PEI will be made. The complete vibrational assignments can be found in Table 5.2.

Table 5.2 – Experimental vibrational assignments for PEI·HCl.

Mode Assignments	IR Frequencies	Raman Frequencies
δ CNC		559
ρ CH_2 + ρ $(NH_2)^+$	766, 818	
ν CN + ρ CH_2		885
ν CC	955	
ν CN + ν CC	1062	1042
τ CH_2 + ρ $(NH_2)^+$		1147
τ CH_2	1282	1224, 1298
ω CH_2	1330, 1354	1285
τ $(NH_2)^+$	1440	1430, 1440
ω $(NH_2)^+$ + ρ $(NH_2)^+$ + δ CH_2	1477, 1492	1480, 1489
δ $(NH_2)^+$ + δ CH_2	1580, 1605	1592
$\nu_{as}(NH_2)^+$	2384	2384
$\nu_s(NH_2)^+$	2436	2442
$\nu_s CH_2$	2616, 2670, 2728	2669, 2691, 2741, 2778
$\nu_{as} CH_2$	2914, 2953, 2981	2909, 2968, 2990

Significant differences between the spectra of PEI and PEI·HCl are expected in the NH stretching region, due to the protonation of the nitrogen atom. Spectra of this region can be found in Figure 5.1. In this region of the spectrum, there is more similarity between N,N'-DMEDA:2HCl and PEI·HCl than there is between PEI and PEI·HCl. There are only two bands for PEI·HCl in the NH_2^+ stretching region. The high frequency band at 2435 cm^{-1} in the IR spectrum (2441 cm^{-1} in the Raman spectrum) is assigned as the symmetric NH_2^+ stretching mode, while the low frequency band, 2383 cm^{-1} in the IR spectrum and 2385 cm^{-1} in the Raman spectrum, is assigned as the asymmetric NH_2^+ stretching mode. There are several features in the spectrum of N,N'-DMEDA:2HCl in both the IR and Raman spectra due to factor group splitting resulting from two asymmetric units in the crystal unit cell. In comparison, there are

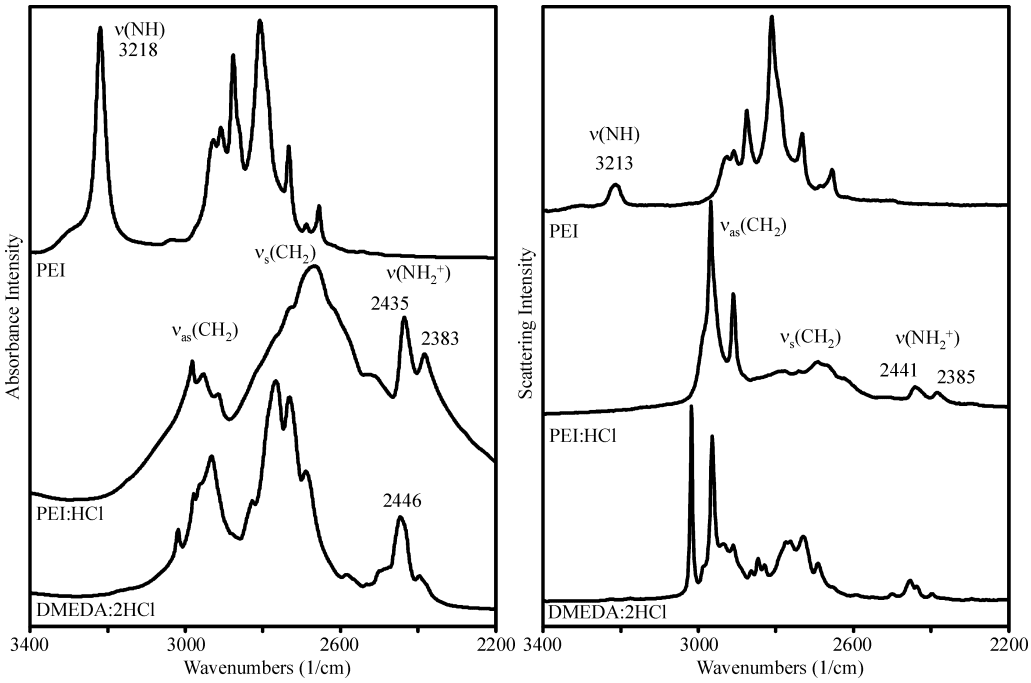

Figure 5.1 – IR and Raman spectra of PEI, PEI·HCl and DMEDA:2HCl in the NH and CH stretching regions.

only two features for PEI·HCl, as all of the N-H···Cl units in the PEI·HCl crystal structure are equivalent.

The CH stretching modes are also shown in Figure 5.1. The symmetric and asymmetric stretching modes are much more tightly grouped in PEI, while there are two distinct groups of bands in the protonated compounds. This separation occurs because the symmetric stretch is more sensitive to shifts in electron density of adjacent groups than the asymmetric stretch.[9] As a result, the symmetric CH stretching modes are shifted to lower frequencies, while the frequencies of the asymmetric stretching modes remain essentially the same.

In the lower frequency region, there are some bands in the PEI·HCl spectra that

are more similar to PEI and others that compare well with those of N,N'-DMEDA:2HCl. The bands that are more similar to N,N'-DMEDA:2HCl contain contributions from the nitrogen atom or the NH_2^+ group, while those bands originating in motions primarily from the ethylene backbone unit are more similar to PEI. As in the lower frequency region of N,N'-DMEDA:2HCl, *i.e.* below approximately 1400 cm^{-1}, there seems to be a mutual exclusion of bands between the IR and the Raman spectra. This would occur if there is an inversion center in the space group of crystal unit cell. Of the four proposed crystallographic space groups, only one (monoclinic, P21/m or C_{2h}^2) contains an inversion center.

A distinctive pair of bands appear in the IR spectrum of PEI·HCl, Figure 5.2, at

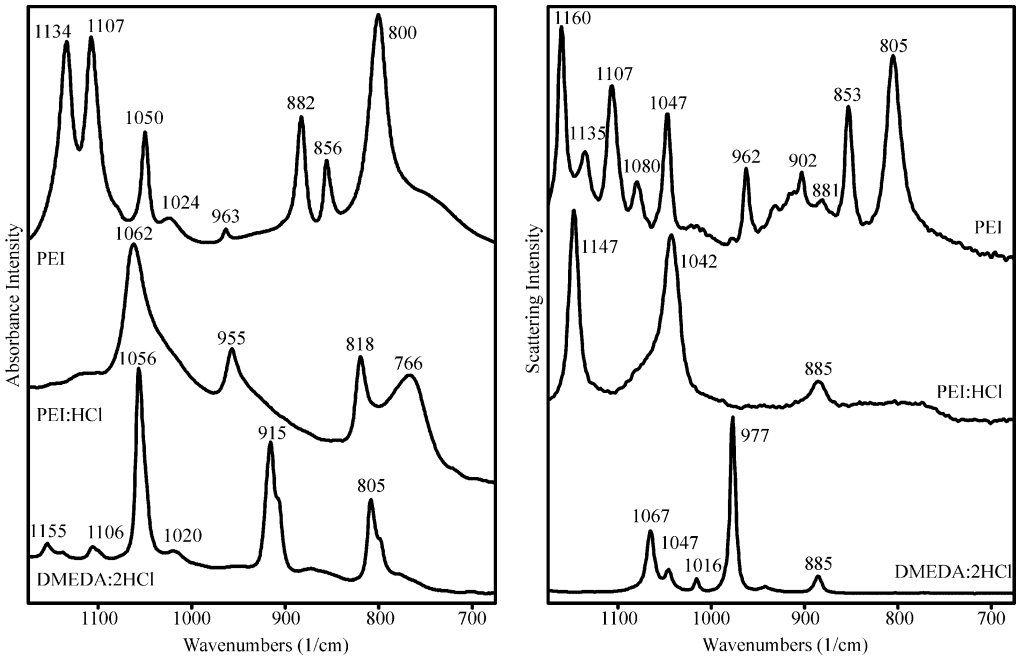

Figure 5.2 – IR and Raman spectra of PEI, PEI·HCl and DMEDA:2HCl in the region below 1200 cm^{-1}.

818 and 766 cm^{-1}. Bands in this region have been assigned to methylene rocking motions in n-alkanes, PEI and DMEDA.[2,5,10] It is reasonable to assign these bands, particularly the lower frequency band, to an extended chain rocking motion. In both PEI and N,N'-DMEDA:2HCl, there is a significant intensity difference between the high and low frequency modes. The NH_2^+ unit is structurally analogous to the methylene unit. Therefore, when the NH_2^+ and the methylene rocking modes couple, the vibrations of this extended chain could be compared to those of n-alkanes. In n-alkanes, as the number of methylene units increases, the frequency of the methylene rocking mode decreases.[10] The intensity difference between the low frequency bands in PEI·HCl and N,N'-DMEDA:2HCl can be accounted for by the length of the chain, as the chain is truncated at four units in the model compound, two NH_2^+ and two

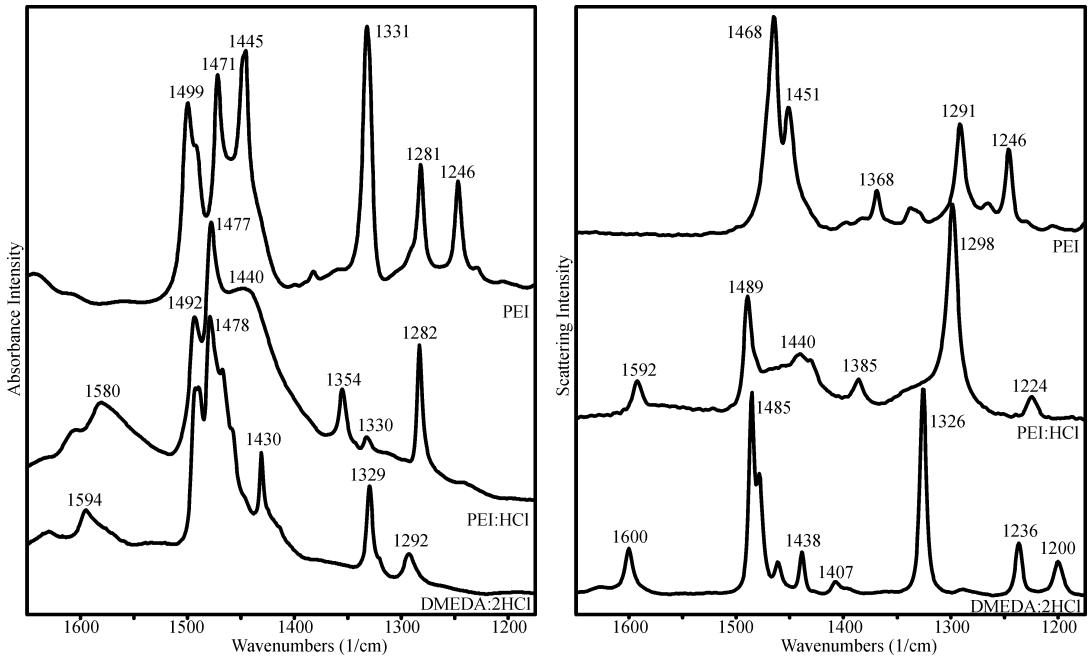

Figure 5.3 – IR and Raman spectra of PEI, PEI·HCl and DMEDA:2HCl.

methylene units. In PEI, the methylene units are coupled to a NH group. This coupling between the methylene rocking motion and the NH out-of-plane bending mode results in a lower frequency mode, but it does not have the intensity that results from coupling the structurally analogous NH_2^+ rocking mode.

The NH_2^+ unit mixes into many modes throughout the region below approximately 1500 cm^{-1}. The band shape is similar in the methylene deformation region (1430 – 1500 cm^{-1}) for both N,N'-DMEDA:2HCl and PEI·HCl, as seen in Figure 5.3. The NH_2^+ deformation, wagging and twisting modes are all found in this region and mix into the methylene modes. In comparison, the band shape of PEI in the methylene deformation region is quite different. There are several bands in PEI·HCl that are similar to those of PEI. Bands at 1282 cm^{-1} in the IR spectrum and 1298 and 1147 cm^{-1} in the Raman spectrum of PEI·HCl occur at 1281 cm^{-1} in the IR spectrum and 1291 and 1160 cm^{-1} in the Raman spectrum of PEI. These frequencies are so similar because these modes all contain significant contributions from the ethylene backbone and only minor contributions from the NH_2^+ units.

5.3.2 Isotopic Dilution experiments.

Deuterium-dilute samples were made to help identify bands that contain contributions from the NH_2^+ units. The ND_2^+ stretching modes were easily identified at 1862 and 1860 cm^{-1} in the IR and Raman spectra and resulted in an isotopic shift of $\frac{\nu_D}{\nu_H} \approx 0.76$. As with the secondary amine salts, there is a broad but sharp-featured band centered between 2100 and 2000 cm^{-1}. This band is attributed to coupled NH and ND

stretching modes. The breadth and multi-featured nature of the band is due to the distribution of deuterium throughout the various sites of the PEI·HCl unit cell.

The deuterium-dilution experiments are particularly helpful in understanding the lower frequency modes. Several striking differences exist in the deuterium-dilute and the undeuterated spectra shown in Figure 5.4. One of the most striking differences is a breakdown of the mutual exclusion rule as the symmetry of the unit cell is broken by the deuterium substitution. Equally noteworthy is the disappearance of the NH_2^+ deformation band in the Raman spectra, although some of the band intensity remains in the IR spectrum. The ND_2^+ deformation is assigned to the new band that appears at 1178 cm^{-1} in the Raman spectrum and 1161 cm^{-1} in the IR spectrum. This assignment would result in a very reasonable isotopic shift of $\frac{\nu_D}{\nu_H} \approx 0.73$. Several new bands appear

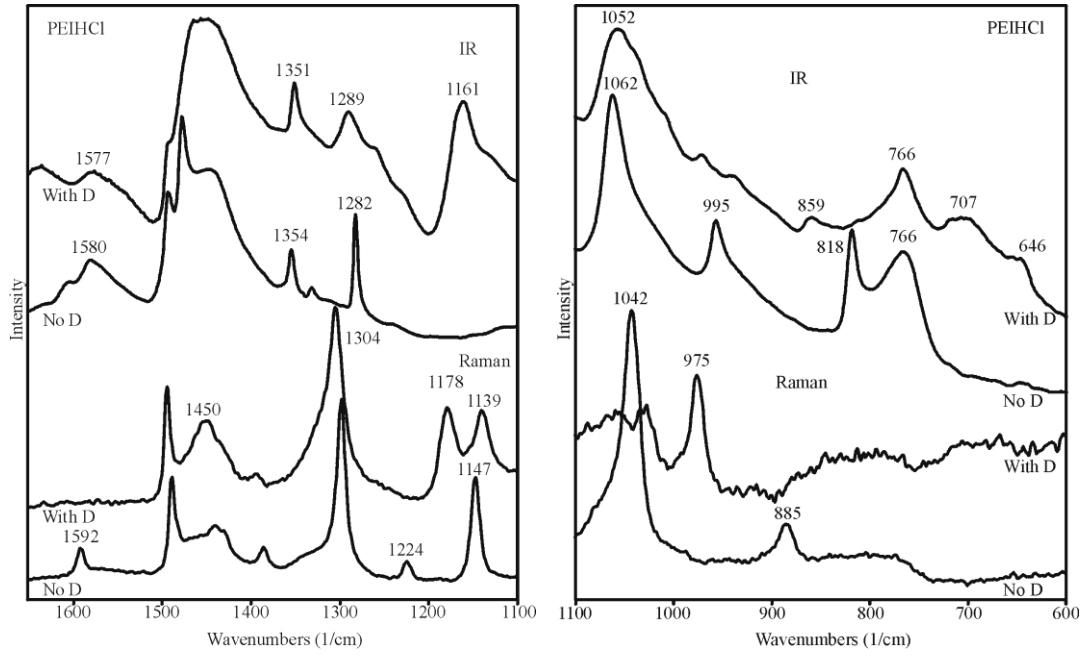

Figure 5.4 – IR and Raman spectra of deuterium-dilute and undeuterated PEI·HCl.

in the IR spectrum. The new band at 859 cm^{-1}, which would contain contributions from an ND_2^+ rocking motions, is most likely associated with the 1147 cm^{-1} Raman band. Bands at 707 and 646 cm^{-1} can also be related to the 955 cm^{-1} IR band and the 855 cm^{-1} Raman band, respectively, based on isotopic shift ratios.

5.4 Summary and Conclusions

PEI·HCl has structural similarities with both PEI and N,N'-DMEDA:2HCl; therefore, both can be used to make the vibrational assignments. The crystal structure determined by Chatani *et al.*[1] has many similarities with the crystal structure for N,N'-DMEDA:2HCl, particularly in the structural parameters which are dictated by the local hydrogen bonding environment. There appears to be a mutual exclusion of bands in the spectra below about 1400 cm^{-1} in PEI·HCl, as in N,N'-DMEDA:2HCl. This implies that there must be an inversion center in the unit cell of the crystal structure. Chatani reported four possible space groups for the crystal unit cell based on the x-ray diffraction results.[1] However, only the monoclinic crystal lattice (P21/m or C_{2h}^2 in Schönflies notation) includes an inversion center in the symmetry operations for that space group. Therefore, the spectroscopic results support the monoclinic lattice over the alternative three orthorhombic lattices for the PEI·HCl crystal structure. Motions involving the NH_2^+ units mix into many modes throughout the spectrum; evidence for mixing lies in the number of bands that shift in the spectrum during the deuterium-dilution experiments. Knowing the vibrational signatures of PEI·HCl can be useful in understanding the more complex systems where PEI·HCl is used as the base polymer,

such as the cross-linked PEI·HCl membranes described in Chapter III.

5.5 References

(1) Chatani, Y.; Irie, T. *Polymer* **1988**, *29*, 2126-2129.

(2) York, S.; Boesch, S. E.; Wheeler, R. A.; Frech, R. *Macromolecules* **2003**, *36*, 7348-7351.

(3) Tanaka, R.; Ueoka, I.; Takaki, Y.; Kataoka, K.; Saito, S. *Macromolecules* **1983**, *16*, 849-53.

(4) York, S.; Frech, R.; Snow, A.; Glatzhofer, D. *Electrochim. Acta* **2001**, *46*, 1533-1537.

(5) Boesch, S. E.; York, S. S.; Frech, R.; Wheeler, R. A. *PhysChemComm* **2001**.

(6) York, S. S.; Boesch, S. E.; Wheeler, R. A.; Frech, R. *PhysChemComm* **2002**, *5*, 99-111.

(7) Sanders, R. A.; Frech, R.; Khan, M. A. *J. Phys. Chem. B* **2003**, *107*, 8310-8315.

(8) Sanders, R. A.; Snow, A. G.; Frech, R.; Glatzhofer, D. T. *Electrochim. Acta* **2003**, *48*, 2247-2253.

(9) Socrates, G. *Infrared and Raman Characteristic Group Frequencies*; 3rd ed.; John Wiley & Sons: New York, 2001.

(10) Lin-Vien, D.; Colthup, N. B.; Fateley, W. G.; Grasselli, J. G. *The Handbook of Infrared and Raman Characteristic Frequencies of Organic Molecules*; Academic Press, Inc.: New York, 1991.

CHAPTER VI

AN UNUSUAL N,N-DMEDA HYDROBROMIDE CRYSTAL CONTAINING NH_3^+, NH_2 AND NH^+ MOIETIES

Portions of this chapter have appeared in Giffin, G.A., Powell, D.R., Frech, R. "An Unusual N,N-DMEDA Hydrobromide Crystal Containing NH_3^+, NH_2 And NH^+ Moieties." *to be submitted* (2009).

6.1 Introduction

In the process of characterizing samples for the N,N-DMEDA:2HX system, an unusual crystal was found. The crystal is very complex, with several different types of NH moieties in different hydrogen-bonding environments. The vibrational spectra are complicated, with many overlapping bands, and would be exceedingly difficult to understand without a crystal structure. However, a known structure can be combined with the spectral analysis of the secondary salts and two smaller amine salts to allow sufficient simplification of the spectra to understand the NH stretching and bending modes.

6.2 Experimental Methods

6.2.1 Sample Preparation

The N,N-dimethylethylenediamine hydrobromide salt, N,N-DMEDA:HBr, was prepared by adding concentrated hydrobromic acid, HBr, to the pure amine. Water was

then removed from the samples by drying under vacuum until a powder was produced. The crystal formed approximately 24 hours into the drying process.

6.2.2 X-Ray Crystallography

X-ray crystallographic data for this crystal were collected using a diffractometer with a Bruker APEX CCD area detector and graphite-monochromated MoKα radiation (λ = 0.71073 Å). The samples were cooled to 100(2) K. The structure was solved by direct methods and refined by full-matrix least-squares methods on F^2[3,4]. Hydrogen atom positions of hydrogen atoms bonded to the carbons were initially determined by geometry and refined by a riding model. The hydrogen atoms bonded to nitrogen were located on a difference map, and their positions were refined independently. Non-hydrogen atoms were refined with anisotropic displacement parameters. Hydrogen atom displacement parameters were set to 1.2 (1.5 for methyl) times the displacement parameters of the bonded atoms. The final R1 was found to be 0.0697 based on 2768 observed reflections, [$I > 2\sigma(I)$], and wR2 was 0.1954 based on 3095 unique reflections.

6.2.3 Vibrational Spectroscopy

The sample was characterized using infrared and Raman spectroscopy. The sample for IR spectroscopic measurements was finely ground and prepared as a KBr pellet. Infrared spectra were collected under vacuum (pressure = 13 mbar) using a Bruker IFS 66v spectrometer with a KBr beam splitter; 64 scans at a spectral resolution of 1 cm^{-1} were averaged for each spectrum. The sample for Raman spectroscopy was

packed in a capillary tube. Raman spectra were collected on a Bruker Equinox 55 FRA 106/S with a Nd:YAG laser (1064 nm; 300 mW) and a CCD detector; 1000 scans at a spectral resolution of 2 cm^{-1} were averaged for each spectrum.

6.3 Results and Discussion

6.3.1 Crystal Structure

The crystal data are summarized in Table 6.1. This sample crystallized in a monoclinic unit cell belonging to the $P2_1/n$ (C_{2h}^5) space group. A single asymmetric unit contains two N,N-DMEDA molecules and three HBr equivalents. This is one equivalent short of four fully protonated heteroatom sites. As a result, an intermolecular N–H···N hydrogen bond (N1B–H···N1A) is present to coordinate the lone pair of the remaining heteroatom site (N1A), as shown in Figure 6.1. Additionally, one of the bromide ions acts as a bridge between two heteroatom hydrogen atoms (N4B–H···Br3···H–N1B). The bridging counter ion forces the NCCN dihedral angle from a trans conformation, which seems to be favored for fully-protonated amine salts, to a dihedral angle of approximately 85 degrees. A trans conformation allows for the maximum separation between halide ions. An "extended trans

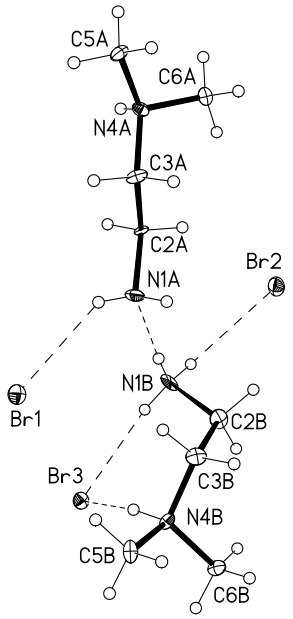

Figure 6.1 – Crystal structure of N,N-DMEDA:HBr. The ratio of N heteroatoms to equivalents of HBr is 4:3.

conformation" was proposed by Baldwin in 1962 spectroscopic studies[5] and was confirmed by the crystal structures presented in Chapter IV. There are seven NH units in the asymmetric unit, in four different types of amino moieties, *i.e.* NH_3^+, NH_2, and two NH^+ moieties. These are summarized in Table 6.2. The NH_3^+ unit is comprised of nitrogen atom N1B and hydrogen atoms H1B1, H1B2, and H1B3. H1B1 and H1B2 are associated with bromide ions Br2 and Br3, respectively, while H1B3 is hydrogen bonded to N1A. The NH_2 group is made up of nitrogen atom N1A and hydrogen atoms H1A1 and H1A2, both of which are coordinated with bromide ions (H1A1···Br1 and H1A2···Br2#1). One NH^+ unit is present on each molecule, at nitrogen atoms N4A and N4B. Each NH^+ hydrogen is coordinated to a bromide ion; one bromide ion bridges two N–H bonds within a single molecule (N4B–H···Br3···H–N1B), and the other makes a connection from a molecule in one unit cell to a molecule in the adjacent unit cell (N4A–H···Br1#2). The hydrogen bonding parameters are given in Table 6.2. Using the classifications by Jeffery,[6] only the N1A–H···N1B and the N4B–H···Br3 interactions would be considered moderate, mostly electrostatic interactions based on the H···A distance. The rest would be considered weak, with interactions that would be considered somewhere between electrostatic and dispersion. This mix of hydrogen-bonding environments further complicates the vibrational spectra.

Table 6.1 – Structural data for the N,N-DMEDA:HBr crystal.

Parameters	**N,N-DMEDA:HBr**
Crystal System	Monoclinic
Space group	$P2_1/n$
Temperature	100(2) K
a (Å)	8.7050(11)
b (Å)	7.2640(9)
c (Å)	25.236(3)
α	90º
β	95.772(2)º
γ	90º
Volume ($Å^3$)	1587.7(3)
Z	4
Density (Mg/m^3)	1.753
R1	0.0697
Crystal size (mm^3)	0.53 x 0.49 x 0.08

Table 6.2 – Hydrogen bonding parameters for the N,N-DMEDA:HBr crystal, d in Å and < in degrees.

Moiety	X–H···A	d(H···A)	d(X···A)	<(XHA)
NH_2	N1A–H1A1···Br1	2.74(9)	3.506(10)	147(11)
	N1A–H1A2···Br2#1	2.69(8)	3.539(10)	165(12)
NH^+	N4A–H4A···Br1#2	2.49(15)	3.235(10)	168(13)
NH_3^+	N1B–H1B1···Br2	2.59(10)	3.325(10)	142(12)
	N1B–H1B2···Br3	2.53(7)	3.396(9)	165(12)
	N1B–H1B3···N1A	1.90(7)	2.761(14)	174(13)
NH^+	N4B–H4B···Br3	2.33(14)	3.207(10)	157(11)

6.3.2 Vibrational Spectroscopy

The spectra of this crystal are complex, because of the variety of NH moieties present, but each of the NH_3^+, NH_2 and NH^+ groups will have its own distinct

vibrational signature in both the NH stretching and bending regions. The NH stretching region is shown in Figure 6.2. Vibrations of the NH^+ units can be compared to vibrations in triethylamine hydrobromide (TEA:HBr), which can be written as $Et_3NH^+:Br^-$. The NH^+ stretch in TEA:HBr is assigned as 2492 cm^{-1}. There are other lower-intensity bands in this region that could be associated with the NH^+ and have been done so by other authors.[7] However, most of these authors do not account for the shift of the methylene symmetric stretching mode to significantly lower frequencies when it is next to a protonated nitrogen atom. These CH modes can be seen at frequencies as low as 2600 cm^{-1} in protonated secondary amines, as shown in Chapter IV and previously cited.[8,9] The other bands in TEA:HBr at 2528, 2432 and 2353 cm^{-1} certainly could be associated with the NH stretch, but the most intense feature at 2492 cm^{-1} seems to be the main NH^+ stretching band. This same feature appears at 2498 cm^{-1} in TEA:HCl, showing the typical shift to lower frequency with increasing anion polarizability.

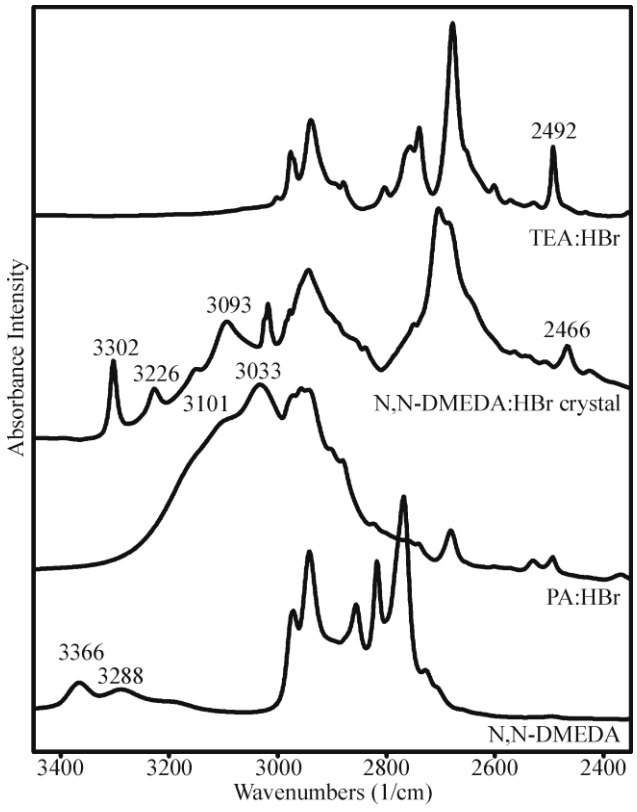

Figure 6.2 – IR spectrum of N,N-DMEDA:HBr crystal compared to IR spectra of TEA:HBr, PA:HBr and N,N-DMEDA[1,2].

The 2492 cm^{-1} band in TEA:HBr can be compared to the 2466 cm^{-1} band in the crystal. The frequency is lower, despite the fact the H···A distances of the TEA:HBr crystal and the N4B hydrogen bond are similar. The H···A distance in TEA:HBr has been reported as 2.24(3)Å,[7] while the distance in the crystal is 2.33(14) Å (N4B···Br3) or 2.49(15) Å (N4A···Br1#2). As these distances are close, within experimental error, something else must account for the frequency shift. A decrease in frequency can be accounted for by a decrease in electron density. TEA:HBr has three ethyl groups attached to the protonated nitrogen atom, which have more electron density to donate to the single nitrogen atom than two methyl groups and the methylene backbone of the N,N-DMEDA:HBr crystal, which is shared between two protonated nitrogen atoms. Therefore, the 2466 cm^{-1} band is assigned as the NH^+ stretching modes associated with nitrogen atoms N4A and N4B. The two NH^+ units within a single asymmetric unit are amply separated so no coupling between these units occurs, and the potential energy environments are sufficiently similar that NH^+ stretching modes are observed at the same frequency.

Vibrations of the NH_3^+ group, containing the protonated primary amine N1B, can be compared to the modes in propylamine hydrobromide (PA:HBr), which can be written as $PrNH_3^+:Br^-$. The NH_3^+ group in PA:HBr is seen as a broad feature with distinct bands at 3033 and 3101 cm^{-1}. These bands correspond to the symmetric and asymmetric stretching modes. In ethylene diamine hydrochloride, another protonated primary amine, the higher frequency band is assigned as the asymmetric stretch and the lower frequency band as the symmetric stretch based on computational results.[10]

Similar assignments are made here, assigning the 3101 cm^{-1} band as the asymmetric stretching mode and the 3033 cm^{-1} band as the symmetric stretching mode. These frequencies are higher than the previously-reported frequencies of other protonated primary amines, *i.e.* ethylene diamine and cyclohexylamine.[10,11] The NH_3^+ modes for the crystal are assigned as the 3149 and 3093 cm^{-1} bands. The hydrogen bonds that involve the bromide ions are considered somewhat weak, based on the hydrogen bonding classifications by Jeffrey,[6] which could result in a shift to higher frequencies. However, the frequencies only can be compared loosely because all three hydrogen atoms are in different hydrogen-bonding environments. Hydrogen atom H1B2 is coordinated to a bromide ion that bridges two hydrogen bonds within the same molecule (N1B–H···Br3···H–N4B). Hydrogen atom H1B3 is hydrogen bonded to the nitrogen atom in the adjacent molecule (N1B–H···N1A) and hydrogen atom H1B1 is associated with a bromide ion that is also hydrogen bonded to a molecule in an adjacent unit cell. These different hydrogen bonding environments make it difficult to predict the frequency shift of the modes.

The final NH moiety is the neutral primary amine on nitrogen atom N1A. The NH_2 vibrational modes in this group can be compared to those of N,N-DMEDA. In pure liquid N,N-DMEDA, there are bands present at 3366 and 3288 cm^{-1} that have been assigned as the asymmetric and symmetric NH_2 stretching modes, respectively.[1,2] The corresponding frequencies in the crystal are 3302 and 3226 cm^{-1}. These bands are considerably narrower than those in the pure liquid, which can be attributed to the crystallinity of the sample. The shift of the modes to lower frequencies can be

accounted for by the stronger hydrogen bonds present in the solid than in the liquid.

The NH bending modes can be similarly assigned, as shown in Figure 6.3. NH^+ bending modes are found at frequencies lower than 1500 cm^{-1} in TEA:HBr and occur among the methyl and methylene deformations.[11] As a result, it is not possible to distinguish this mode in the crystal. The band at 1640 cm^{-1} in the N,N-DMEDA:HBr crystal compares well with the 1597 cm^{-1} band in N,N-DMEDA, both in intensity relative to the CH deformation modes and in band shape. The shape of this band is distinctive in these spectra; it is a bell shaped feature, with large band width relative to the rest of the spectra. Therefore, the 1640 cm^{-1} band is assigned to the NH_2 deformation mode. The NH_2 deformation mode has been shown to shift to higher frequencies with stronger hydrogen bonding,[8,9] which may account for the shift to higher frequency in the crystal. The two bands at 1603 and 1559/1561 cm^{-1} are assigned as NH_3^+ modes through comparison with the spectrum of PA:HBr. The Raman spectrum is more useful for this particular comparison because

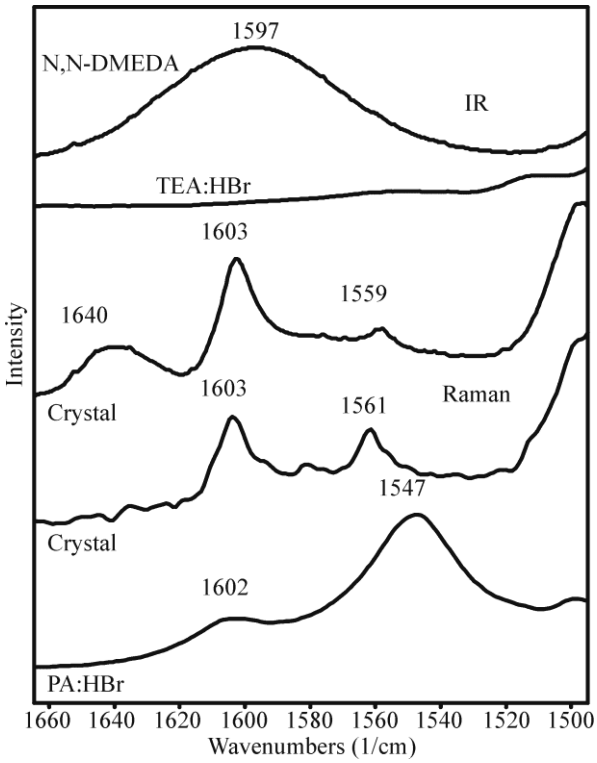

Figure 6.3 – IR and Raman spectra of N,N-DMEDA:HBr crystal compared to IR spectra of TEA:HBr and N,N-DMEDA[1] and Raman spectrum of PA:HBr.

good separation exists between the asymmetric and symmetric bending modes. In contrast, these modes are found as a single broad feature in the IR spectrum. In PA:HBr, the frequencies of these modes are 1602 and 1547 cm^{-1}. The frequency of the asymmetric mode in the crystal is the same, within experimental error, while the symmetric mode is 12-14 cm^{-1} lower.

6.4 Concluding Remarks

The spectra of this unusual N,N-DMEDA:HBr crystal are quite complicated, but can be understood by using simple molecules that model the NH_3^+, NH_2 and NH^+ portions of the crystallographic asymmetric unit. Upon comparison of the vibrations of these molecular analogs to the N,N-DMEDA:HBr crystal, the vibrational signatures of the various amine and protonated amine entities can be identified. This crystal is unique when compared to other members of the amine hydrohalide family. No other crystals have been solved that have not been fully protonated, and no other intramolecular bridging hydrogen bonds have been reported. This appears to be the only molecule with different types of amine and protonated amine heteroatom sites within a single molecule whose crystal structure has been elucidated.

6.5 References

(1) Rocher, N. M. Ph.D., University of Oklahoma, 2006.

(2) Rocher, N.; Frech, R. *J. Phys. Chem. A* **2007**, *111*, 2662-2669.

(3) International Tables for Crystallography, V. C.; Tables 6.1.1.4, and 4.2.4.2, Ed.; Kluwer: Boston, 1995.

(4) Sheldrick, G. M. *SHELXTL Version 6.10 Reference Manual*; Bruker-AXS, 5465 E. Cheryl Parkway, Madison, WI 53711-5373 USA, 2000.

(5) Baldwin, M. E. *Spectrochim. Acta* **1962**, *18*, 1455-61.

(6) Jeffery, G. A. *An Introduction to Hydrogen Bonding*; Oxford University Press: Oxford, 1997.

(7) James, M. A.; Cameron, T. S.; Knop, O.; Neuman, M.; Falk, M. *Can. J. Chem.* **1985**, *63*, 1750-1758.

(8) Lin-Vien, D.; Colthup, N. B.; Fateley, W. G.; Grasselli, J. G. *The Handbook of Infrared and Raman Characteristic Frequencies of Organic Molecules*; Academic Press, Inc.: New York, 1991.

(9) Socrates, G. *Infrared and Raman Characteristic Group Frequencies*; 3rd ed.; John Wiley & Sons: New York, 2001.

(10) Amado, A. M.; Otero, J. C.; Marques, M. P. M.; Batista de Carvalho, L. A. E. *ChemPhysChem* **2004**, *5*, 1837-1847.

(11) Sauvageau, P.; Sandorfy, C. *Can. J. Chem.* **1960**, *38*, 1901-10.

CHAPTER VII

NEAR INFRARED SPECTROSCOPY OF AMINE HYDROHALIDE SALTS

7.1 Introduction

All the spectra shown in the preceding chapters are in the mid-infrared (MIR) region, and the samples examined were thin films or small amounts of sample ground and pressed with potassium bromide into pellets. A typical thin film giving reasonable absorbance intensities in the MIR is about ten μm thick. This type of sample is very different from the membranes found in a functioning fuel cell, which are substantially thicker, from about 50 to 150 μm. This sample thickness cannot be examined in the MIR because the spectrum would be severely overabsorbed. This film thickness is ideal for a near-infrared (NIR) investigation because the bands found in this region have much smaller absorption coefficients (on the order of 100 times smaller for the first overtone[1]) than those found in the MIR region.

The MIR is used to examine fundamental vibrational transitions. Fundamental transitions result from a mode in the ground vibrational state absorbing energy and moving to the first excited vibrational state. The intensity of a fundamental transition is proportional to the square of the dipole moment derivative:

$$I \sim \left| \left(\frac{\partial \mu}{\partial Q} \right)_o \right|^2 \tag{7.1}$$

where Q is the normal coordinate. An overtone transition results from a mode in the ground vibrational state absorbing enough energy to move directly to the second, or

higher, excited vibrational state, while a combination transition results from the simultaneous excitation of two modes in the ground state to the first excited state. The intensity of an overtone transition is:

$$I \sim \left| \left(\frac{\partial^2 \mu}{\partial Q^2} \right)_o \right|^2 \tag{7.2}$$

and the intensity of a combination transition is:

$$I \sim \left| \left(\frac{\partial^2 \mu}{\partial Q_1 \partial Q_2} \right)_o \right|^2 \tag{7.3}$$

where Q_1 and Q_2 are the normal coordinates of modes one and two. There is no necessary relationship between the intensity of a fundamental transition and that of an overtone transition. Hydrogen-stretching modes, which are of particular interest in fuel cells, have large fundamental absorption coefficients. However, the overtones and combination transitions of these same modes, which are primarily found in the NIR region, have much smaller absorption coefficients. The NIR region is considered to be 4000 to 10000 cm^{-1}, while the range for the MIR region is 500 to 4000 cm^{-1}. Figure 7.1 shows the NIR spectra of two cross-linked PEI·HCl films. In the ~10 μm film the fundamentals are clearly observed, while the overtones and combinations cannot be discerned from the

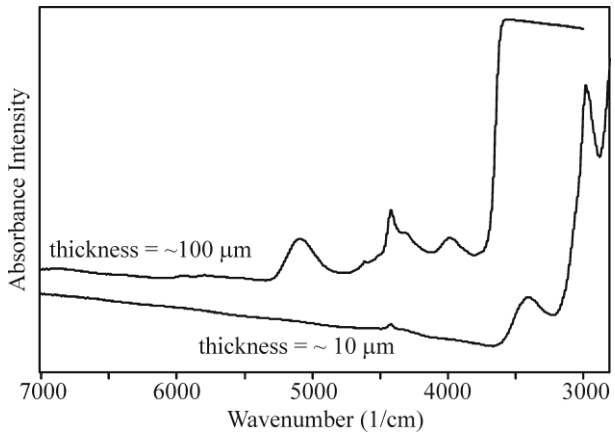

Figure 7.1 – NIR spectra of two cross-linked PEI·HCl films (xlinker:2N = 0.25x:2N).

background. Unlike the thin film, in the ~100 μm film the fundamentals are overabsorbed, while the overtones and combinations are easily observed.

Although there are some definite advantages to NIR spectroscopy with respect to the sample, there are also some disadvantages. Characteristic group frequencies are well known for many fundamental transitions, but they are not as well known for the NIR. Spectra of complex structures in the MIR can be understood by using small molecules to model portions of the structure, therefore allowing the spectroscopic signature of various parts of the network to be identified. This same strategy can be used in the NIR. Small molecule amines have been previously studied by a number of different groups,[2-7] but their hydrohalide salts have only been given a cursory glance.[1,8] Here, primary and secondary amines and their hydrohalide salts are examined to identify the hydrogen-stretching modes and the other predominant bands in the region.

7.2 Experimental Methods

7.2.1 Near Infrared Spectroscopy

NIR spectra were collected using a Bruker IFS 66v spectrometer with a quartz beam splitter; 64 scans, at a spectral resolution of 1 cm^{-1}, were averaged for each spectrum. Spectra of the amine salts were measured at 11 mbar, while those of the liquid amines were measured under a dry air purge. In the MIR, powders are suspended in media that have no peaks in the region being examined, such as KBr or fluorolube. The difference in refractive indices of the two media can cause reflective scattering, but this poses little problem in the MIR, where the particle is much smaller than the

wavelength. However, the shorter wavelengths found in the NIR are of the same order as the particle size produced from grinding the sample. This exacerbates the reflective scattering, resulting in an unusable spectrum. Sinsheimer and Keuhnelian provided the solution to this problem in their 1966 publication.[8] Pellets composed solely of the amine salts were made by grinding the pure salts and pressing them in a stainless steel die. This method resulted in pellets ranging in mass from 10-50 mg.

7.3 Results and Discussion

7.3.1 Secondary Amines and their Hydrohalide Salts

Dipropylamine (DPA) is the simplest secondary amine studied, and the fundamental vibrations of both DPA and its hydrochloride salt (DPA:HCl) are understood, making the NIR assignments easier. NIR spectra of both DPA and DPA:HCl can be seen in Figures 7.2 and 7.3. The first overtone of the NH stretch previously has been assigned as the peak at 6499 cm^{-1} and was noted to be a single band that includes both hydrogen-bonded and "free" amines.[3,7,9] In the fundamental region, there is a single IR band at 3289 cm^{-1}, which is NH units that are more

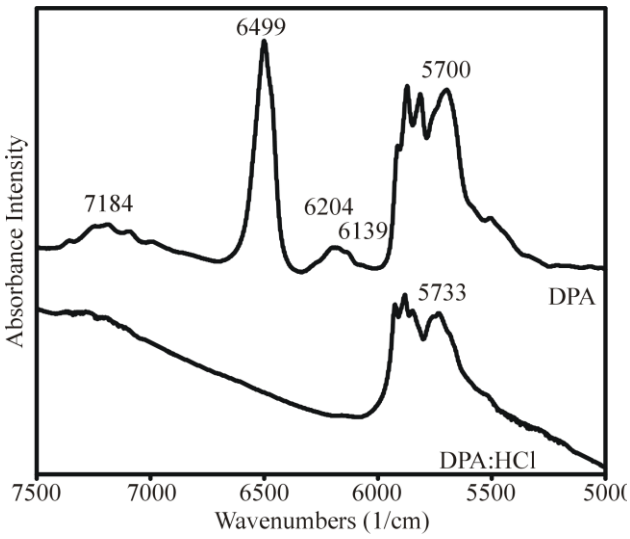

Figure 7.2 – NIR spectra of DPA and its hydrochloride salt (DPA:HCl).

strongly hydrogen bonded, and two overlapping Raman bands at 3327 and 3315 cm^{-1} that are weakly hydrogen bonded NH units.[10] Some asymmetry can be seen in the 6499 cm^{-1} NIR band that would imply that the more associated and the "free" components do not actually appear at the same frequency. Therefore, the higher frequency mode is assigned as the "free" species and the lower frequency mode at 6461 cm^{-1} should be assigned as the associated species.

There is a pair of overlapping bands present at 6204 and 6139 cm^{-1}. Bernard-Houplain and Sandorfy proposed that a similar feature in dimethylamine at 6150 cm^{-1} could be assigned as a combination of the fundamental NH stretching mode and the first overtone of the NH bending mode.[2] This assignment seems reasonable. In computational studies of N,N'DMEDA, it was found that the parallel NH bending mode mixed into many of the lower frequency modes, particularly the methyl and methylene deformations.[11] Therefore, these bands could be assigned as a combination of the NH stretching motions and the first overtone of a mode containing a contribution from the NH bending motion. There could be a single combination band as in dimethylamine,[2] or there may be more than one, as in DPA. The number of combination bands varies because the number of modes containing NH bending contributions varies.

The first overtone of the methyl and methylene stretching modes are contained in the group of peaks that run from approximately 5900 to 5600 cm^{-1}, as seen in Figure 7.2. The first overtones of the methyl asymmetric and symmetric modes could be assigned as the two highest frequency peaks, at 5913 and 5872 cm^{-1}. The methyl group is three carbon units away from the nitrogen atom, and, therefore, could reasonably be

compared to terminal aliphatic methyl frequencies, which have been reported at 5905 and 5876 cm^{-1}.[7] The frequencies of the methylene groups cannot be compared as easily to aliphatic CH frequencies because the former is more affected by the amino nitrogen atom. The rest of the features in this region can be assigned either as the first overtone of methylene stretching motions or as a combination of asymmetric and symmetric stretching modes, which appear at approximately 5800 cm^{-1} in a purely aliphatic molecule.[7] This frequency would be slightly lower in DPA:HCl because the fundamental modes shift to lower frequency upon protonation of the nitrogen. The group of peaks centered around 7184 cm^{-1} can be assigned as the combination of the first overtone of the CH stretching modes and the methyl or methylene deformation.[7]

In comparison to DPA, the spectrum of DPA:HCl shown in Figure 7.2 is relatively simple. The fundamental stretching frequencies of the NH_2^+ units are at 2530 and 2423 cm^{-1}, so the first overtone of these modes would occur at frequencies lower than the CH first overtones. The band shape of DPA:HCl in both the CH first overtone and the combination shown in Figure 7.2 is very similar to that of DPA, so the assignment of the methyl and methylene modes would not be drastically different from those discussed above.

The combination of the NH stretching and bending modes of DPA can be seen in Figure 7.3 at 4777 cm^{-1}. As discussed above, the NH bending motion contributes to many mixed modes in the lower frequency fundamental region. So more correctly, this band and some of the weak bands on the low frequency side of the 4777 cm^{-1} could be assigned as combinations of the NH stretching motion and mixed modes containing

contributions from the NH bending mode. Sauvageau and Sandorfy assigned a similar frequency band at 4762 cm^{-1} in piperidine.[1] They also assigned some of the lower intensity bands below the 4762 cm^{-1} band as combinations of NH and methylene modes.[1]

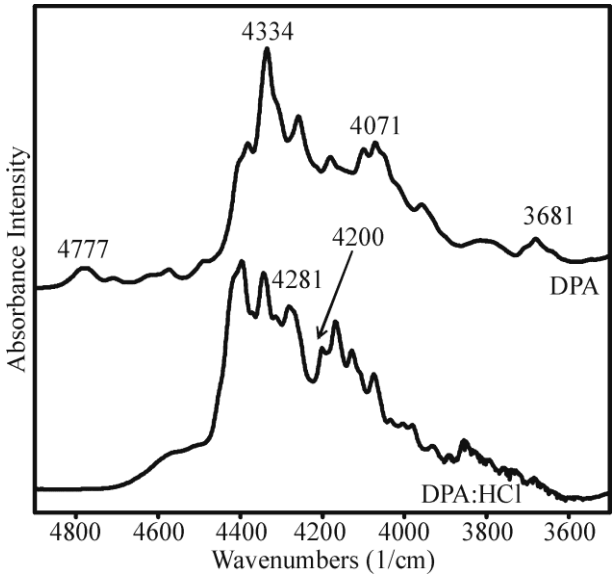

Figure 7.3 – NIR spectra of DPA and DPA:HCl.

The region below approximately 4450 cm^{-1} is a densely-packed group of overlapping bands, which makes precise assignments very difficult. The highest frequency and intensity bands can be attributed to combinations of the methyl and methylene asymmetric and symmetric stretching motions and their respective deformations. There seems to be some separation between the groups of peaks in DPA:HCl located between the 4281 and 4200 cm^{-1} peaks. As previously discussed, the symmetric shift of alkyl groups next to a protonated nitrogen atom tends to shift to frequencies that are lower than expected. This gap could result from separation of the symmetric methylene combination bands from the rest of the alkyl stretching/bending combination modes. The complexity of the bands in this region, particularly on the lower frequency side, can be attributed to combinations resulting from the alkyl stretching modes and the other vibrations such as bending, wagging, twisting or rocking motions that are typically found in the

fundamental "fingerprint" region, *i.e.* below 1500 cm^{-1}.[7] For example, the band at 3681 cm^{-1} in DPA could be assigned as a combination of the methylene stretching motions and the methylene rocking mode at 727 cm^{-1}. This region could also contain higher-order combinations or overtones of the alkyl deformation modes.[7]

Combinations of the NH_2^+ stretching and bending modes in DPA:HCl are significantly harder to distinguish because they are severely overlapped with the CH combination modes. However, based on their additive frequencies, they should be located between about 4100 and 4000 cm^{-1}. Comparing the spectra of salts with different counter ions makes discerning these bands from the rest of the peaks in this region much easier. This is illustrated in Figure 7.4 with N,N'-dimethylethylenediamine hydrochloride (DMEDA:2HCl) and N,N'-dimethylethylenediamine hydrobromide (DMEDA:2HBr). Bands at 4025 and 4015/4005 cm^{-1}, in DMEDA:2HCl and DMEDA:2HBr, respectively, show a low

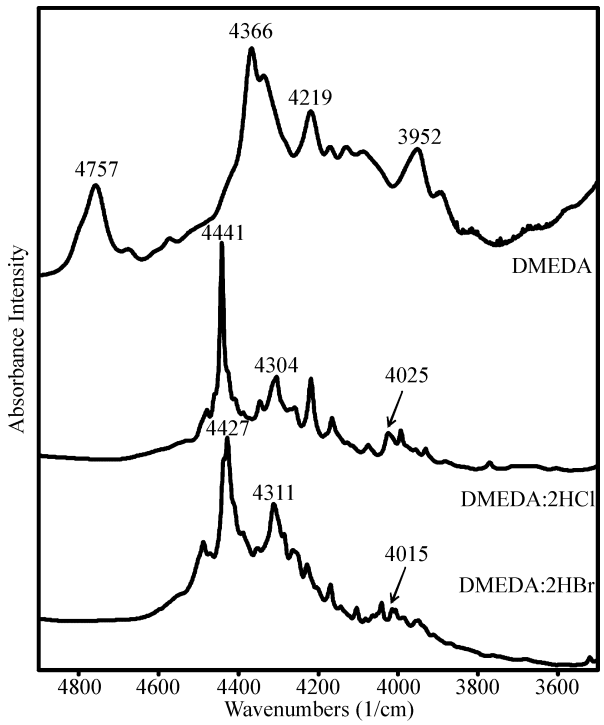

Figure 7.4 – NIR spectra of N,N' – dimethylethylenediamine (DMEDA) and its hydrochloride (DMEDA:2HCl) and hydrobromide (DMEDA:2HBr) salts.

frequency shift when changing the counter ion from chloride to bromide. The same is also true of the 3993 and 3985 cm^{-1} pair of bands. These pairs of bands are unique because they are essentially the only ones in the region below 4500 cm^{-1} in which the bromide salt has lower band frequencies than the chloride salt.

There are a couple of bands of particular interest in the first overtone region of the methyl and methylene stretching modes of DMEDA:2HX, as shown in Figure 7.5. The highest frequency peak of this group, at 6021 cm^{-1}, can be assigned as the first overtone of the methyl alpha to the protonated nitrogen atom. In comparison, the highest frequency band of this grouping in DPA:HCl, which does not have an alpha methyl group, is at 5925 cm^{-1}. The pair of bands at 5290 and 5107 cm^{-1} is also particularly interesting due to their low frequency as compared to the other alkyl overtones. The frequencies are too high to be first overtones of the NH_2^+ stretch, but they could be overtones of the symmetric methylene stretching mode that occurs in a range ending below 2700 cm^{-1} in the fundamental CH stretching region.

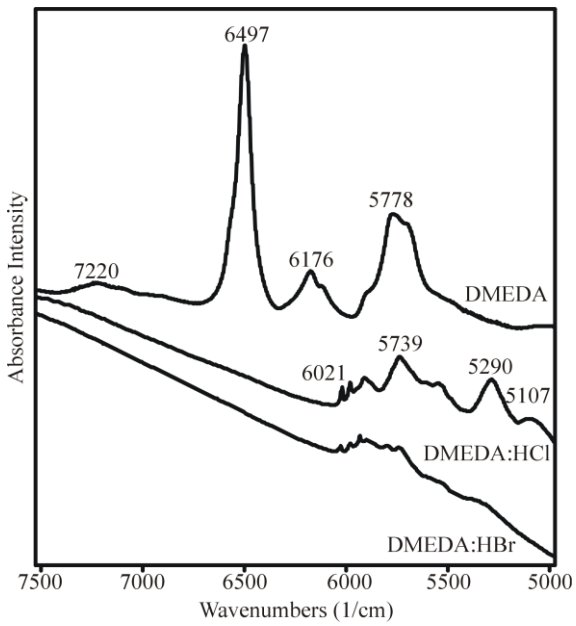

Figure 7.5 – NIR spectra of DMEDA, DMEDA:2HCl and DMEDA:2HBr.

7.3.2 Primary Amines and their Hydrohalide Salts

Propylamine (PA) was chosen as a representative simple primary amine. At a first glance, the spectrum of the unprotonated primary amine is similar to that of DPA due to similar length alkyl chains, but is different in modes involving the heteroatom shown, as is seen in Figure 7.6. The bands at 6715 and 6540 cm^{-1}, correspond to the first overtone of the asymmetric and symmetric NH_2 stretching modes, respectively. These bands correspond to bands at 3371 and 3293 cm^{-1} in the fundamental region. These NIR frequencies are in good agreement with the NH_2 stretching frequencies for other similar primary amines.[4] There is a small amount of asymmetry present in the 6540 cm^{-1} band. This asymmetry could be attributed to the presence of species in different hydrogen-bonding environments.

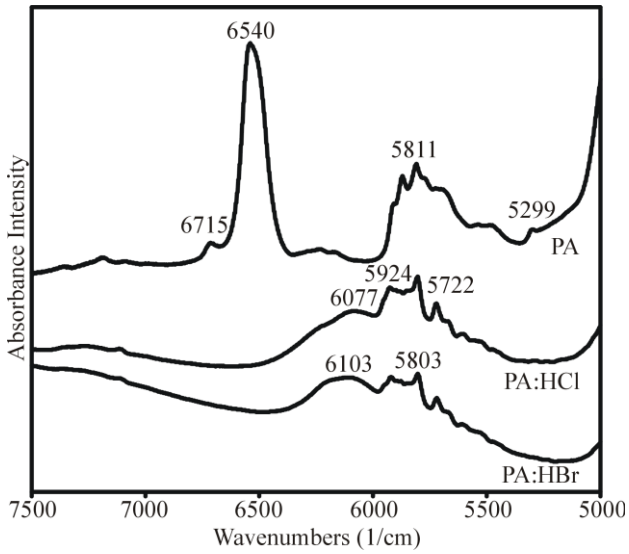

Figure 7.6 – NIR spectra of propylamine (PA), and its hydrochloride (PA:HCl) and hydrobromide (PA:HBr) salts.

The assignment of the CH stretching overtones and combinations is similar to those of DPA. There are large broad features at 6236 and 6077 cm^{-1} in PA:HCl and at 6193 and 6077 cm^{-1} in PA:HBr. These are most likely the first overtone of the broad feature at 3111 and 3026 cm^{-1} in PA:HCl and 3101 and 3033 cm^{-1} in PA:HBr. These features are

most likely associated with the NH_3^+ stretching motion. The fundamental frequencies are higher, but not unreasonable when compared with other NH_3^+ stretching frequencies previously published.[1,4,12] These fundamental modes also contribute to the bands at 4662 and 4632 cm^{-1} in PA:HCl and PA:HBr, respectively, as shown in Figure 7.7. These modes are assigned as a combination of the NH_3^+ stretch and the NH_3^+ deformation. Similar bands were seen in cyclohexylamine hydrohalide salts.[1] These bands around 4650 cm^{-1} are particularly valuable in distinguishing protonated primary amines from protonated secondary and tertiary amines.[1] The combination of the NH_2 stretching and deformation modes in the unprotonated PA occurs at higher frequencies than the NH_3^+ combination, at 4941 and 4966 cm^{-1}. The two components have been attributed to an associated NH_2 and a "free" NH_2 unit.[5]

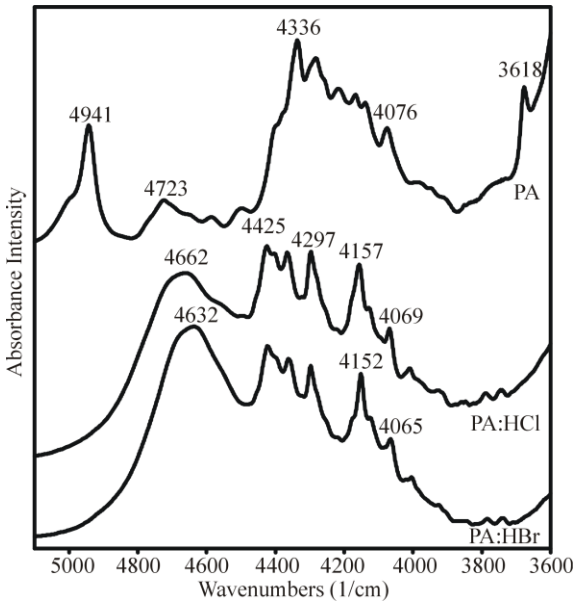

Figure 7.7 – NIR spectra of PA, PA:HCl and PA:HBr.

7.3.3 Tertiary Amines and its Hydrohalide Salts

Triethylamine (TEA) and its hydrohalide salts have been previously studied by Sauvageau and Sandorfy.[1] They determined that the amine salt NH^+ stretching overtones are weak and the NH+ combinations are in the same region as the CH

combinations and, therefore, are highly overlapped. Spectra of TEA and its hydrohalide salts were measured, but, upon examination of the data, nothing more definitive could be said than what already was published.

7.4 Concluding Remarks

NIR spectroscopy is becoming an increasingly important technique for spectroscopists and has been applied to many industrially relevant systems, as is evident from the over 20 chapters devoted to NIR applications in the most recent *Handbook of Near-Infrared Analysis*.[13] The weak intensity of overtones and combinations is actually an advantage because much thicker samples can be examined. As shown in this chapter, the overtones and combinations can be used to obtain data about the local environment of a functional group. Information such as hydrogen-bonding environment can be important, particularly if NIR is going to be applied to a research question like hydrogen transport through fuel cell membranes. The ideas presented above contribute to fundamental science. It is difficult for vibrational spectroscopic techniques to be widely used in new and challenging applications without understanding basic fundamentals, such as normal mode assignments.

7.5 References

(1) Sauvageau, P.; Sandorfy, C. *Can. J. Chem.* **1960**, *38*, 1901-10.

(2) Bernard-Houplain, M. C.; Sandorfy, C. *J. Chem. Phys.* **1972**, *56*, 3412-17.

(3) Berthomieu, C.; Sandorfy, C. *J. Mol. Spectrosc.* **1965**, *15*, 15-21.

(4) Rai, V. K.; Rai, S. B. *Indian J. Phys. B* **2003**, *77B*, 351-354.

(5) Sinsheimer, J. E.; Keuhnelian, A. M. *Anal. Chem.* **1974**, *46*, 89-93.

(6) Wolff, H.; Gamer, G. *Spectrochim. Acta, Part A* **1972**, *28*, 2121-9.

(7) Workman Jr., J.; Weyer, L. *Practical Guide to Interpretive Near-Infrared Spectroscopy*; CRC Press: Boca Raton, 2008.

(8) Sinsheimer, J. E.; Keuhnelian, A. M. *J. Pharm. Sci.* **1966**, *55*, 1240-4.

(9) Russell, R. A.; Thompson, H. W. *Proc. R. Soc. London, Ser. A* **1956**, *A234*, 318-326.

(10) Rocher, N.; Frech, R. *J. Phys. Chem. A* **2007**, *111*, 2662-2669.

(11) Boesch, S. E.; York, S. S.; Frech, R.; Wheeler, R. A. *PhysChemComm* **2001**.

(12) Amado, A. M.; Otero, J. C.; Marques, M. P. M.; Batista de Carvalho, L. A. E. *ChemPhysChem* **2004**, *5*, 1837-1847.

(13) *Handbook of Near-Infrared Analysis*; 3rd ed.; Burns, D. A.; Ciurczak, E. W., Eds.; CRC Press: Boca Raton, 2008.

LIST OF ABBREVIATIONS

$\delta(NH_2^+)$	NH_2^+ deformation mode
$\delta_s(CF_3)$	CF_3 symmetric deformation mode
DMEDA	N,N'-dimethylethylenediamine
DMPDA	N,N'-dimethylpropylenediamine
DMAA	3-(dimethylamino)-acrolein
DPA	dipropylamine
FTIR	Fourier transform infrared spectroscopy
HCl	hydrochloric acid
HBr	hydrobromic acid
HRMAS	high-resolution magic-angle-spinning
$LiCF_3SO_3$	lithium trifluoromethane sulfonate or lithium triflate
LPEI	linear poly(ethylenimine)
MIR	mid infrared
$\nu_{as}(NH_2^+)$	NH_2^+ antisymmetric stretching mode
$\nu_s(NH_2^+)$	NH_2^+ symmetric stretch mode
$\nu_{as}(SO_3)$	SO_3 antisymmetric stretching triflate mode
$\nu_s(SO_3)$	SO_3 symmetric stretching triflate mode
NIR	near infrared
NMR	nuclear magnetic resonance

N,N-DMEDA	N,N-dimethylethylenediamine
N,N'-DMEDA	N,N'-dimethylethylenediamine
PA	propylamine
PBEI	poly(N-butylethylenimine)
PEEI	poly(N-ethylethylenimine)
PEI	linear poly(ethylenimine)
PEI·HCl	polyethylenimine hydrochloride
PEM	proton exchange membrane
PEMFC	proton exchange membrane fuel cells
PMEI	poly(N-methylethylenimine)
PEO	polyethylene oxide
TEA	triethylamine
T_g	glass transition